The Institute of Paper Science and Technology

Atlanta, Georgia

Doctor's Dissertation

The Depletion of Nitric Oxide by Reaction with Molten Sodium Carbonate and Sodium Carbonate/Sodium Sulfide Mixtures

Laura M. Thompson

January 1995

THE DEPLETION OF NITRIC OXIDE BY REACTION WITH MOLTEN SODIUM
CARBONATE AND SODIUM CARBONATE/SODIUM SULFIDE MIXTURES

A Thesis Submitted by

Laura M. Thompson

B.S. 1988, University of New Hampshire

M.S. 1990, Institute of Paper Science and Technology

in partial fulfillment of the requirements
for the degree of Doctor of Philosophy
from the Institute of Paper Science and Technology
Atlanta, Georgia

January 1995

TABLE OF CONTENTS

ABSTRACT

This study was an investigation of the depletion of NO by reaction with sodium species that are present in a kraft recovery furnace. Thermodynamic calculations identified many reactions that could occur to form sodium nitrate ($NaNO_3$) as a product. Because $NaNO_3$ begins to thermally decompose at temperatures greater than 450°C, it is believed that $NaNO_3$ may not be a final product, but could play a role as an intermediate species in the depletion of NO.

The rate of depletion of NO by reaction with molten sodium carbonate and mixtures of sodium carbonate and sodium sulfide has been determined over the temperature range, T = 860 to 973°C. The heterogeneous reaction system has been shown to fit a mixed control reaction model where both mass transfer and chemical reaction kinetics play an important role.

The rate of depletion of NO has been shown to follow a pseudo first-order rate expression. Values for the rate constant have been determined experimentally for the depletion of NO by reaction with Na_2CO_3 and mixtures of Na_2CO_3/Na_2S.

Analysis of gaseous products indicated that all of the NO that is depleted by reaction with Na_2CO_3 is converted to oxygen (O_2) and nitrogen (N_2). For Na_2CO_3/Na_2S mixtures, no oxygen could be detected in the gas stream. It was shown that the oxygen formed by depletion of NO was consumed by the sodium sulfide to form sodium sulfate (Na_2SO_4).

Analysis of the nitrogen content of samples taken from industrial furnaces showed that approximately half of the nitrogen entering the furnace in black liquor could not be accounted for. It was therefore assumed that nitrogen leaves the furnace as a gas phase species, e.g., N_2 or

NH_3. As noted previously, reactions of NO with Na_2CO_3 or Na_2S have been shown to reduce NO

to N_2. Thus, nitrogen in black liquor could be reduced to N_2 by the following pathway:

$$\text{Fuel N} \xrightarrow[\text{Oxidation}]{} \text{NO} \xrightarrow[\substack{\text{Reduction by} \\ \text{Na Species}}]{} \tfrac{1}{2}\ N_2\ +\ \tfrac{1}{2}\ O_2.$$
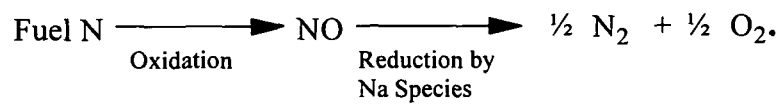
INTRODUCTION

Nitric oxide (NO) and nitrogen dioxide (NO_2) can be formed during the combustion of fuels in the presence of nitrogen. These oxides of nitrogen (collectively referred to as NO_x) have been shown to be key constituents in reactions leading to photochemical smog and acid rain.[1,2] For these reasons, the emission of NO_x from combustion sources is regulated by both state and federal government agencies.

In 1991, results of an analysis of the best available control technology (BACT) options for kraft recovery furnace NO_x emissions were published.[3] The authors evaluated several control methods including selective catalytic reduction, selective noncatalytic reduction, flue gas recirculation, and proper combustion control. The authors determined combustion control to be the BACT for NO_x emissions from a recovery furnace. Therefore, there is a great need to understand recovery furnace operating conditions as they relate to NO_x emissions.

It has been an ongoing project at the Institute of Paper Science and Technology to develop a three-dimensional, fundamental mathematical model of a kraft recovery furnace. It is intended that the model will predict gas flow patterns, temperature profiles, and species concentration profiles, and ultimately allow the user to predict the effect of changing operational parameters on such things as combustion efficiency, reduction efficiency, corrosion potential, air emissions, etc. To include predictions for NO_x emissions in the model, it is necessary to understand the rates of NO_x formation and depletion reactions in a recovery furnace environment.

NO_x emission models have been developed for many types of furnaces and fuels. However, due to the nature of the operation of recovery furnaces, other models would not be applicable for predicting NO_x emissions from a recovery furnace. This is primarily due to some of the unique features of black liquor: low fuel nitrogen content ($\sim 0.1\%$), high moisture content (15 to 35%), and high inorganic composition ($\sim 33\%$ of black liquor solids).

The impact of sodium species on NO_x emissions has essentially been ignored in the literature. However, black liquor solids are typically on the order of 15 to 20% sodium by weight. It is understood that sodium species react with SO_x in a recovery furnace; it was therefore hypothesized that analogous reactions could occur with NO_x species. This thesis is primarily a kinetic investigation of the reaction of nitric oxide with molten sodium species.

OBJECTIVES

The overall objective of this thesis was to provide a better understanding of the depletion of nitric oxide by reaction with sodium species that are present in a kraft recovery furnace. Specific objectives included:

* Determine the thermodynamic feasibility of reactions between NO_x and different sodium species.

* Determine the rate of depletion of NO by reaction with molten Na_2CO_3 and mixtures of Na_2CO_3/Na_2S over the temperature range, $T = 860$ to $973°C$.

* Identify a global mechanism for the depletion of NO by reaction with molten Na_2CO_3 and mixtures of Na_2CO_3/Na_2S.

ORGANIZATION

This dissertation has been written as a series of five articles that have been published and/or presented in a variety of sources. An introduction to the kraft pulping process and overviews of black liquor combustion, recovery boiler emissions, and fume formation chemistry are provided as background material. Each article is preceded by a summary and followed by a discussion of the results presented in the article.

The first article presents an overview of NO_x formation mechanisms as they relate to black liquor combustion. The article also identifies several research needs that were considered important to provide a better understanding of NO_x emissions from recovery furnaces. The concept of depletion of NO_x by reaction with sodium species was first introduced in this article. It was suggested that nitrogen in black liquor could be oxidized to form nitric oxide, a fraction of which undergoes further reactions (possibly with sodium species) which reduces NO to N_2.

The second article presents results of thermodynamic calculations which were made to illustrate the feasibility of reactions of NO_x with different sodium species. While thermodynamics predicted that reactions with sodium species could provide a potential mechanism for the depletion of NO, it was not clear if these reactions occur fast enough to have any effect on NO_x emissions from recovery furnaces. Thus, experiments were designed to investigate the rate of depletion of NO.

The third and fourth articles present the results of experimental work conducted to determine the rate of depletion of NO by reaction with molten Na_2CO_3 and Na_2CO_3/Na_2S

mixtures, respectively. The fourth article also includes experimental results which show that all of the nitrogen in NO that is depleted could be identified as N_2 in the gas phase.

The final article presents results of nitrogen analyses of samples taken from industrial recovery furnaces. The results of the nitrogen analyses support the concept that black liquor nitrogen can be oxidized to form NO and then subsequently reduced to N_2 by reaction with sodium species.

The five articles are followed by a list of conclusions and recommendations for future work. All of the experimental data and a complete list of nomenclature are included in the Appendix. Literature citations within each article are listed at the end of the article. Citations from all other sections are listed at the end of the thesis in the section titled, "Literature Cited," which begins on page 92.

BACKGROUND

THE KRAFT PULPING PROCESS

The kraft, or sulfate, process is the dominant method for processing wood pulp for papermaking. In 1993, approximately 80% of wood pulp manufactured in the United States was made using the kraft process.[4] Advantages of the kraft process include its ability to cook all types of wood, the high strength of the pulp, and the chemical recovery cycle. The recovery cycle is largely responsible for the success of the process as it makes the process essentially self-sufficient. Due to chemical recovery, very little makeup chemicals are needed, and enough process steam is produced to run the entire pulp mill.[5] A brief overview of the kraft process is presented below.

In the kraft pulping process, wood chips are digested under temperature and pressure in white liquor, a solution of sodium hydroxide ($NaOH$) and sodium sulfide (Na_2S), to fragment and dissolve lignin and hemicellulose. The cooking liquor and dissolved organic compounds are then separated from the cellulosic pulp fibers in a washing stage. The spent liquor is known as weak black liquor and contains the inorganic chemicals that were in the white liquor in addition to organic and inorganic solids extracted from the wood. Total solids in weak black liquor is typically on the order of 10 to 15%.

The weak liquor is concentrated in multiple-effect evaporators to 65-75% solids and is then fired as a fuel to a recovery furnace. The combustion of black liquor converts the thermal energy from the organic portion for steam production. Combustion of black liquor is described in greater detail in the next section. The inorganic fraction of the liquor is recovered as a molten

smelt (primarily sodium carbonate, sodium sulfide, and sodium sulfate) through the bottom of the furnace.

Molten smelt is dissolved in water to form green liquor. The green liquor is clarified to remove the insoluble dregs, and then fed to the slaker where it is mixed with calcium oxide to convert sodium carbonate to sodium hydroxide as follows:

$$Na_2CO_3 + CaO + H_2O \rightarrow 2\ NaOH + CaCO_3. \tag{Eq. 1}$$
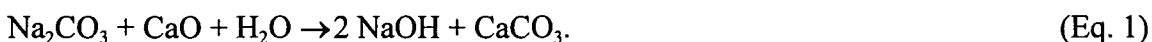
The reaction is continued in a series of mixed tank reactors known as causticizers.

Due to the low solubility of $CaCO_3$, it precipitates from solution and is separated by settling in a clarifier or by filtration in a pressure filter. The $CaCO_3$, or lime mud, is burned in a lime kiln to regenerate CaO as follows:

$$CaCO_3 + heat \rightarrow CaO + CO_2. \tag{Eq. 2}$$
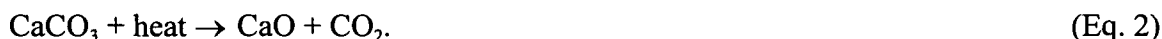
The clarified solution is the white liquor which is fed back to the digesters to complete the recovery cycle. A block diagram of the kraft pulping and recovery process is shown in Figure 1.
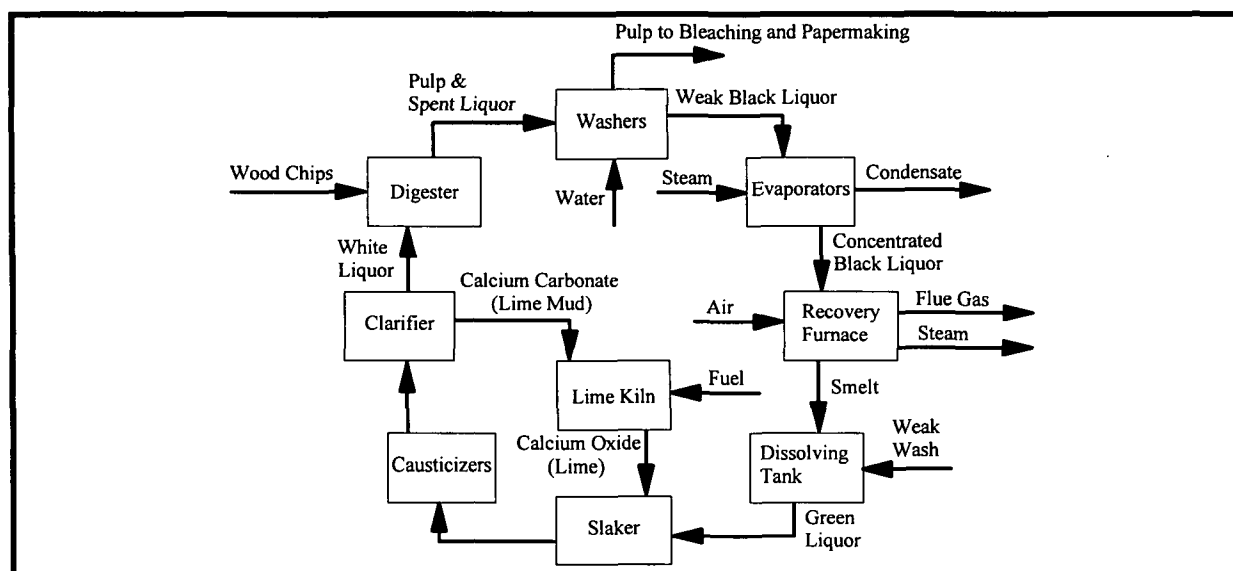
Figure 1. Schematic of the Kraft Pulping and Recovery Process.

BLACK LIQUOR COMBUSTION

The organic fraction of black liquor solids is composed of ligneous materials, saccharinic

acids, low molecular weight organic acids, and extractives. Inorganic constituents include

sodium hydroxide, sodium sulfide, sodium carbonate, sodium sulfate, sodium thiosulfate, sodium

chloride, and analogous potassium species (KOH, K_2CO_3, etc.). The actual composition of the

solids will vary considerably depending on wood species and pulping conditions. Examples of

elemental analyses of several kraft black liquors are reported below in Table 1.

Table 1. Elemental Analysis of Kraft Black Liquor Samples. Composition Is Reported as Percent by Weight of Black Liquor Solids. NM Indicates not Measured.

Element	Mill A (Pine)[6]	Mill A (Birch)[6]	Mill B[7]	Mill C[8]
Carbon, C	35.1	30.2	35.0	32.6
Hydrogen, H	3.8	3.5	3.43	3.8
Oxygen, O	35.3	37.9	35.4	35.9
Sodium, Na	19.5	22.4	18.0	20.8
Sulfur, S	4.3	3.8	5.47	5.0
Nitrogen, N	0.1	0.1	<0.1	0.05
Potassium, K	1.7	1.9	2.21	1.6
Chlorine, Cl	0.2	0.2	0.20	0.26
Total	100.0	100.0	99.7	100.0
HHV (kJ/kg)	14,770	13,200	14,680	13,890
NHV (kJ/kg)	12,590	11,240	NM	NM

Higher heating values (HHV) for black liquor solids are reported to be in the range of

13,400 to 15,500 kJ/kg of black liquor solids.[9] However, the measurement of HHV includes the

energy released from oxidation of all of the sulfur in the black liquor. In a recovery furnace, the

majority of the sulfur leaves the furnace in a reduced form as Na_2S. Thus, the net heating value

(NHV) which accounts for the reduction of sulfur more accurately reflects the amount of energy that is released during black liquor combustion. Net heating values can be as much as twenty percent less than higher heating values.[9]

In a recovery boiler, black liquor is sprayed into the lower furnace through nozzles which produce droplets in the range of 0.5 to 5 mm in diameter. The distribution of drop sizes has been measured over a broad range of conditions varying temperature, solids fraction, flow rate, and nozzle type.[10,11] While it is possible to affect the mean drop size, the overall distribution consistently follows a square root normal distribution. It is not possible to change this distribution with currently available commercial nozzles.[11]

Upon entering the furnace, black liquor drops burn in a series of stages which can be classified as drying, devolatilization (or pyrolysis), and char burning.[12] Because black liquor is a wet fuel (25 to 35% H_2O), most of the water must be removed before pyrolysis can begin. During the drying stage, black liquor drops will swell and collapse as the water escapes.

As the temperature of the drop rises, the organic material will start to decompose into light gases and hydrocarbons which will burn in an oxidative environment. Pyrolysis is typically characterized by the presence of a luminous flame and the drop can undergo swelling by as much as 10 to 30 times its original size.[13] At the end of devolatilization, the remaining char consists of organic carbon and the inorganic sodium species.

In an oxidizing environment, some of the reduced sulfur can be oxidized. During char burning the carbon is consumed by reaction with sodium sulfate to produce CO, CO_2, and Na_2S.

This process of sulfur reduction has been described by Grace and co-workers as the sulfate-sulfide cycle which is depicted below in Figure 2.[14] Char carbon may also be consumed by reactions with O_2, CO_2, and H_2O.[15,16]
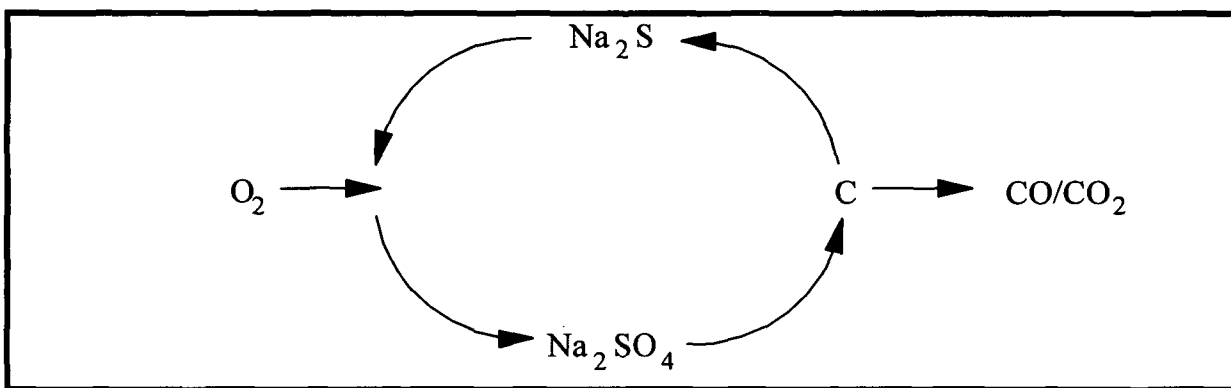
Figure 2. Schematic of the Sulfate-Sulfide Cycle.

A model for the three combustion stages was developed at IPST in the late 1980s. In the model, drying and volatilization were modeled as external heat transfer limited processes. Char burning was modeled as limited by oxygen mass transfer to the surface of the char.[17]

RECOVERY BOILER AIR EMISSIONS

Perfect combustion of a hydrocarbon with a sufficient amount of an oxidizer will give CO_2 and H_2O as the final products. If sulfur and nitrogen are present, these species can be oxidized to form SO_2 and NO_x. However, in real systems, combustion is never complete, and undesirable species can leave the furnace in the flue gas. In a recovery furnace, potential air emission problems include reduced sulfur gases, SO_2, carbon monoxide, particulates, and NO_x.

Reduced sulfur gases, also referred to as total reduced sulfur (TRS), include malodorous species such as hydrogen sulfide (H_2S), methyl mercaptan (CH_3SH), dimethyl sulfide (($CH_3)_2S$),

and dimethyl disulfide (CH_3SSCH_3). Emissions of these species are controlled by providing excess air and good mixing to promote oxidation of sulfur species to SO_2. Sulfur dioxide levels are controlled primarily by increasing the char bed temperature which promotes fuming. The reaction of SO_2 with fume acts as a scrubbing mechanism and essentially eliminates SO_2 from the flue gas. Fume formation and reactions with SO_2 are discussed further in the following section. Particulates are removed from the flue gas predominantly by the use of electrostatic precipitators (ESP). Like TRS, CO is controlled primarily by promoting oxidation to CO_2.

While TRS and CO are controlled by promoting oxidation, the oxidation of nitrogen species gives NO_x, an undesirable flue gas constituent. As noted previously, combustion control, or minimization of nitrogen oxidation, has been determined to be the best available control technology for NO_x. The trade-off between CO and NO_x has been cited as a problem in controlling air emissions.[18,19] This problem underscores the need for further understanding NO_x chemistry in a recovery furnace.

FUME FORMATION

One of the unique aspects of recovery furnace operation is the composition of the char. Black liquor char consists of carbon, sodium carbonate, sodium sulfide, and sodium sulfate. Volatilization of the sodium salts leads to the formation of fume in the upper part of the furnace. Fume particles collected from electrostatic precipitators are typically fine spherical particles consisting primarily of sodium sulfate (90 to 95%), sodium carbonate (1 to 3%), and sodium chloride (3 to 5%). Measurement of fume particle size shows a wide range of particle diameter (.01 to 70 μm) and mass distribution with a peak mass at 0.7 μm.[20]

Fume deposition on tube walls leads to plugging and fouling of heat transfer surfaces, and the large volume of particulates requires the use of electrostatic precipitators for particulate emission control. On the other hand, the reactions that form sodium sulfate act as a scrubbing mechanism for SO_2 and SO_3 and are in this sense, quite favorable. Approximately ten percent of the sodium entering the furnace forms fume.[21] While fume chemistry is not completely understood, mechanisms have been presented in the literature which explain the formation of the primary compounds: Na_2CO_3 and Na_2SO_4.

Because both Na_2CO_3 and Na_2SO_4 have very low vapor pressures, it is unlikely that fume is formed by direct volatilization of these species. It is believed that most fume is formed from sodium vapor which reacts with other species in the gas phase above the char bed. A reaction-enhanced vaporization mechanism has been proposed by Cameron,[22] who suggests that the reduction of Na_2CO_3 by Na_2S in the smelt bed enhances the volatilization of sodium from the molten smelt. As the sodium in the gas phase above the melt reacts, the volatilization is further enhanced by the reduction of the partial pressure of sodium in the gas phase. Grace postulated the following set of reactions for the formation of fume:[5]

$$Na_2CO_3 + 2\,C \rightarrow 2\,Na + 3\,CO \qquad\qquad (Eq.\ 3)$$

$$Na_2CO_3 + CO \rightarrow 2\,Na + 2\,CO_2 \qquad\qquad (Eq.\ 4)$$

$$2\,Na + \tfrac{1}{2}\,O_2 \rightarrow Na_2O \qquad\qquad (Eq.\ 5)$$

$$Na_2O + CO_2 \rightarrow Na_2CO_3 \qquad\qquad (Eq.\ 6)$$

$$Na_2O + SO_2 + \tfrac{1}{2}\,O_2 \rightarrow Na_2SO_4 \qquad\qquad (Eq.\ 7)$$

$$Na_2O + SO_3 \rightarrow Na_2SO_4 \qquad\qquad (Eq.\ 8)$$

This mechanism for fume formation has been criticized for the use of Na_2O as an intermediate. Blackwell and King[23] argue that Na_2O is not stable in a recovery furnace environment and that there are no data to support its presence in a furnace. However, if Na_2O is a highly reactive intermediate, its presence may be difficult to detect.

Blackwell and King propose that most of the material that ultimately forms fume is present as Na_2CO_3 and NaOH gas in the lower furnace. Then, in the upper furnace, Na_2SO_4 can be formed by the following reactions:[23]

$$Na_2CO_3 \ (s,l) + SO_2 \ (g) + \tfrac{1}{2} \ O_2 \ (g) \rightarrow Na_2SO_4 \ (s,l) + CO_2 \ (g) \qquad \text{(Eq. 9)}$$

$$Na_2CO_3 \ (s,l) + SO_3 \ (g) \rightarrow Na_2SO_4 \ (s,l) + CO_2 \ (g) \qquad \text{(Eq. 10)}$$

$$2 \ NaOH + SO_2 + \tfrac{1}{2} \ O_2 \rightarrow Na_2SO_4 \ (s,l) + H_2O \ (g) \qquad \text{(Eq. 11)}$$

$$2 \ NaOH \ (g) + SO_3 \rightarrow Na_2SO_4 \ (s,l) + H_2O \ (g) \qquad \text{(Eq. 12)}$$
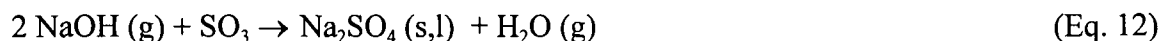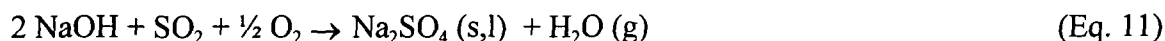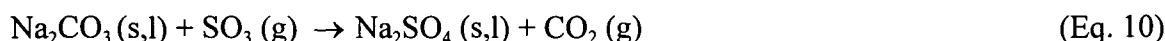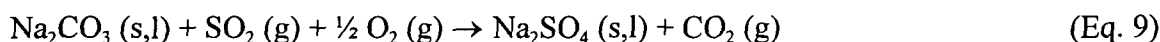
NaOH can also react to form sodium carbonate:

$$2 \ NaOH \ (g) + CO_2 \ (g) \rightarrow Na_2CO_3 \ (l) + H_2O \ (g) \qquad \text{(Eq. 13)}$$
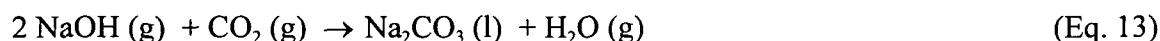
The sulfation of sodium carbonate as it relates to fume formation has been the subject of many studies.[24,25,26,27] A recent review article concluded that the reaction of SO_2 with Na_2CO_3 below its melting point (850°C) does not occur fast enough to account for the amount of SO_2 depletion that occurs in a recovery furnace.[27] The authors suggest that the reaction most likely occurs with molten sodium carbonate.

While the primary compounds of fume are Na_2CO_3 and Na_2SO_4, analysis of the chemical composition of fume has also identified Na_2SO_3, $Na_2S_2O_3$, and Na_2S.[28] The presence of Na_2SO_3

and $Na_2S_2O_3$ is particularly interesting to note as neither are thermodynamically stable at recovery furnace temperatures. Samples of fume taken at various points in a furnace have shown Na_2SO_3 and $Na_2S_2O_3$ compositions totaling as high as 18%.[28] Blackwell and King propose that the compounds exist due to a kinetic limitation in their decomposition.[23]

Other compounds found in fume include sodium chloride and analogous potassium salts (KSO_4, KCO_3, KCl). While potassium compounds are found in low quantities, their presence lowers the sticky temperature of the dust and can lead to greater fouling of tube surfaces.[29]

Because the chemistry of fume formation is not fully understood, modeling attempts have been limited. Work at Åbo Akademi (in Finland) has taken on an equilibrium-based approach.[30,31] While equilibrium calculations can provide useful, initial estimates for gas phase composition, the importance of reaction kinetics is not considered.

Researchers at the VTT Aerosol Technology Group (also in Finland) have developed an aerosol model which considers reactions in the gas phase, vapor condensation by homogeneous nucleation, heterogeneous condensation, and particle growth by coagulation.[20] The model assumes condensation of either Na_2SO_4 and/or $NaOH$. In cases where $NaOH$ is the condensing species, it is further assumed that it will react quickly to form Na_2CO_3 as an intermediate species or directly to Na_2SO_4. Again, due to the lack of kinetic data available, rates of formation of these species are not included in the model.

Results from VTT's model predict particle size distributions which resemble fume

samples collected from industrial furnaces. In general, the predicted particle sizes have a larger

mean particle size and a narrower distribution than measured values.

In general, fume is believed to be formed by sodium species reacting with CO_2 and SO_2

to form sodium carbonate and sodium sulfate. It thus seems likely that similar reactions could

occur between sodium species and NO_x to form sodium nitrate ($NaNO_3$). However, sodium

nitrate is not thermally stable at temperatures above 450°C.[32] It is possible, however, that nitrate

is formed as an intermediate species which then undergoes thermal decomposition. Thus,

decomposition of sodium nitrate is discussed further below.

DECOMPOSITION OF SODIUM NITRATE

The decomposition of sodium nitrate is a complex stepwise process. Gaseous products of

decomposition include NO, O_2, and N_2. The following mechanism for the decomposition has

been postulated based on a thermogravimetric study conducted over the temperature range of 300

to 850°C.[33]

Step 1: Formation of sodium nitrite and oxygen by the equilibrium reaction:

$$NaNO_3 \leftrightarrow NaNO_2 + \frac{1}{2} O_2 \qquad\qquad \text{(Eq. 14)}$$

Step 2: Nitrite is pyrolized according to the reaction:

$$2\,NaNO_2 \rightarrow Na_2O + 2\,NO + \frac{1}{2} O_2 \qquad\qquad \text{(Eq. 15)}$$

Step 3: The pyrolysis of nitrite according to reaction 15 above is accompanied by a

partial regeneration of the salts leading to the formation of nitrogen:

$$Na_2O + 3\,NO \rightarrow 2\,NaNO_2 + \frac{1}{2} N_2 \qquad\qquad \text{(Eq. 16)}$$

Step 4: Nitrite can be oxidized into nitrate by nitric oxide:

$$NaNO_2 + NO \rightarrow NaNO_3 + \tfrac{1}{2} N_2 \qquad\qquad (Eq.\ 17)$$

A similar study investigated the effects of several oxides on the decomposition of

$NaNO_3$.[32] Results of this study supported the above mechanism. The authors showed that the

decomposition started at about 450°C. The gases formed were NO, O_2, and N_2, where the

formation of N_2 was detected only above 680°C. The authors investigated the behavior of gas

formation in the decomposition of the following binary systems: $NaNO_3 + SiO_2$, $NaNO_3 + TiO_2$,

$NaNO_3 + ZrO_2$, $NaNO_3 + AlO_3$, and $NaNO_3 + MgO$. Their results showed that the formation of

N_2 as a decomposition product could be blocked or enhanced by the presence of different

oxides.[32]

A REVIEW OF NO$_x$ FORMATION MECHANISMS IN RECOVERY FURNACES[34]

SUMMARY

This paper was the first publication to give an overview of NO$_x$ formation mechanisms as they relate to black liquor combustion in a recovery furnace. A fundamental review of the thermal NO$_x$ and the fuel NO$_x$ mechanisms was presented. Also, a brief survey of nitrogen content in black liquor and NO$_x$ emissions from recovery furnaces was included. In addition to the literature review, theoretical calculations were presented to estimate the amount of thermal NO$_x$ that could potentially be formed in a recovery boiler. Several general research needs were also identified to further understand NO$_x$ emissions from kraft recovery furnaces.

A review of NO$_x$ formation mechanisms in recovery furnaces

Kenneth M. Nichols, Laura M. Thompson, and H. Jeff Empie

Abstract: Review of NO$_x$ formation studies shows that NO forms in recovery furnaces primarily by two independent mechanisms, thermal and fuel. Thermal NO formation is extremely temperature-sensitive. However, theoretical predictions indicate that recovery furnace temperatures are not high enough to form significant thermal NO. Fuel NO formation is less temperature-sensitive, and is related to fuel nitrogen content. Black liquors are shown to contain 0.05 to 0.24 weight percent fuel nitrogen. Conversion of just 20% of this would yield approximately 25-120 ppm NO$_x$ (at 8% O$_2$) in the flue gas, enough to represent the majority of the total NO$_x$. Data from operating recovery furnaces show NO$_x$ emissions ranging from near zero to over 100 ppm at 8% O$_2$. An apparent increase in recovery furnace NO$_x$ emissions was observed with increasing solids. This increase is much less than predicted by thermal NO formation theory, indicating that other NO formation/destruction mechanisms, such as fuel NO formation, are important. No data are available to show the relative importance of thermal and fuel NO to total NO$_x$ during black liquor combustion.

Keywords: Bibliographies, Black liquors, Combustion, Emission, Nitrogen oxides, Reaction, Mechanisms, Recovery, Furnaces.

Nitric oxide (NO) and nitrogen dioxide (NO$_2$) are formed during combustion whenever nitrogen is present in the fuel or in the combustion air. These oxides of nitrogen (collectively referred to as NO$_x$) are considered to be key constituents in reactions associated with photochemical smog and acid rain (1). For protection of human health and vegetation from adverse effects, NO$_x$ emissions from stationary combustion sources have been regulated by local and federal agencies.

Traditionally, recovery furnaces have been operated such that NO$_x$ emission levels were below typical emission standards for coal- and residual oil-fired boilers. Surveys of NO$_x$ emissions from kraft recovery furnaces in the late '70s (2,3) showed emissions in the range of 0.05-0.14 lb/million Btu (26-71 ppm on an in-stack concentration basis). At the same time, the New Source Performance Standard for large new residual oil-fired steam generators built after 1971 was 0.30 lb/million Btu.

More recently, due to improved technologies for concentrating black liquors, recovery furnaces are operating at higher levels of liquor solids concentration. Decreases in liquor moisture will result in higher combustion temperatures, and there is some concern that increased temperatures will yield increases in NO$_x$ emissions. In several cases, observed increases in recovery furnace NO$_x$ emissions have been related to firing higher solids concentrations (4-8).

The purpose of this paper is to present basic information on the chemistry and formation of NO$_x$, most of which has been developed in other combustion fields (such as fossil fuel combustion), to discuss the implications for NO$_x$ emissions from recovery furnaces, and to identify several research needs relating to the subject of recovery furnace NO$_x$ emissions.

Mechanisms for NO$_x$ formation

Most of the NO$_x$ emitted by combustion sources is NO with only a small fraction (typically 5% or less) appearing as NO$_2$. The total NO emitted is formed by three independent mechanisms: thermal NO (the fixation of molecular nitrogen by oxygen atoms

Nichols, Thompson , and Empie are with The Institute of Paper Science & Technology, 575 14th Street, N. W., Atlanta, GA 30318

produced at high temperatures), fuel NO (the oxidation of nitrogen contained in the fuel during the combustion process), and prompt NO (the attack of hydrocarbon free radicals on molecular nitrogen producing NO precursors). Prompt NO is usually considered to be of minor importance for industrial furnaces *(9)*. The relative importance of each of the other two mechanisms in determining the total NO emission level is dependent on furnace temperatures and fuel nitrogen levels.

The kinetics involved in these NO formation mechanisms are generally rate limiting. Concentrations of NO measured in hot combustion gases are typically orders of magnitude less than equilibrium concentrations at hot gas temperatures. Conversely, NO levels are effectively frozen as the combustion gases are cooled, resulting in flue gas concentrations which are much greater than equilibrium concentrations at low temperatures.

Thermal NO

Thermal NO is the dominant source of NO_x emissions for combustion of fuels such as natural gas, which contain very low levels of chemically bound nitrogen. The mechanism for the formation of thermal NO was first described by Zeldovich *(10)* in 1946 as the following two reaction steps:

$$N_2 + O \leftrightarrow NO + N \qquad (1)$$

$$N + O_2 \leftrightarrow NO + O \qquad (2)$$
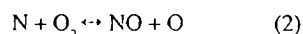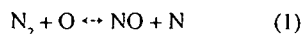
The first step (Reaction 1) is rate-limiting and has a very high activation energy (75 kcal/gmol). This high activation energy results in high temperature sensitivity, hence the designation "thermal" NO. The Zeldovich mechanism is frequently extended *(9)* to more accurately describe thermal NO formation under fuel-rich conditions by including a third reaction step:

$$N + OH \leftrightarrow NO + H \qquad (3)$$
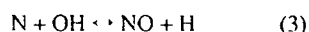
Because thermal NO is formed to some degree during the combustion of nearly all fuels with air, this mechanism has been studied extensively.

Kinetic rate coefficients for both the forward and reverse rates (of Reactions 1-3) have been reported over a wide range of temperatures *(11)*. The reactions involve primarily the oxygen-nitrogen system and can be considered, with reasonable accuracy, separately from the combustion process, since the time scale for NO formation reactions is generally greater than the time scale for combustion reactions. This fact enhances the utility of applying information derived from laboratory combustion studies on thermal NO to NO_x formation in industrial furnaces.

From the Zeldovich mechanism (Reactions 1 and 2) a simple expression can be derived to approximate the rate of thermal NO formation. In practical flames, NO concentrations are small compared to O_2 and N_2 concentrations, and the forward rates are greater than the reverse rates. Considering only the forward reactions, and invoking the steady state assumption for atomic nitrogen (i.e., d(N)/dt=0), the following expression is obtainable for the maximum NO formation rate:

$$d(N)/dt = 2k_1(O)(N_2) \qquad (4)$$

1. Approximate temperature and oxygen dependency of thermal NO, as determined by Eq. 7

2. Overall reaction pathway for formation of NO from fuel nitrogen.
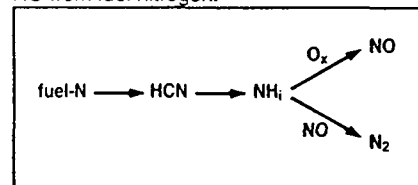
I. Nitrogen levels in 13 kraft black liquors

Mill	Wood	N, % of dry solids
1	mxd	0.05
2	swd	0.06
3	swd	0.06
4	mxd	0.06
5	swd	0.1
6	NA[a]	0.1
7	NA	0.14
8	NA	0.05
9	NA	0.14
10	NA	0.24,0.20,0.08[b]
11	NA	0.12,0.19,0.10[b]
12	NA	0.1
13	NA	0.1
Average		0.11
Standard dev.		0.06

[a] Not available
[b] Samples collected on different days

where

k_f = rate constant for the forward rate of Reaction 1.

By assuming equilibration of the combustion reactions, the concentration of atomic oxygen can be estimated from its equilibrium with O_2 as in Eq. 5.

$$(O) = 3.01 \cdot 10^5 \exp[-30,300/T] \quad (5)$$
$$(O2)^{1/2}[P/RT]^{1/2}$$

As shown by Bowman (11), a generally accepted expression for the forward rate constant is Eq. 6.

$$k_f = 1.8 \cdot 10^{11} \exp[-38,400/T], \quad (6)$$
$$m3/kgmol/s$$

Substitution of these expressions (Eqs. 5 and 6) into Eq. 4 yields Eq. 7:

$$d(NO)/dt = 3.79 \cdot 10^{15}/T^{1/2} \exp$$
$$[-68,700/T](O_2)^{1/2} (N_2), kgmol/m^3/s \quad (7)$$

where

T = gas temperature, Kelvin

t = reaction time, s

gas concentrations = $kgmol/m^3$

It is evident from this rate expression that thermal NO formation is highly temperature dependent, and is also dependent on oxygen concentration and residence time.

This is more clearly illustrated with **Fig. 1**, which is a graphical representation of Eq. 7. Figure 1 shows the potential for moderate increases in temperature to have a significant impact on thermal NO formation. Concentrations of thermal NO increase by an order of magnitude for each 100-140°F (55-80°C) increase in furnace temperature. The dependencies on oxygen concentration and residence time are less pronounced than the temperature dependency.

Considering the typical ranges of oxygen concentration and temperature

in the lower recovery furnace (indicated by the shaded box in Fig. 1), it appears that the thermal NO formation mechanism is unable to account for observed recovery furnace NO_x emission levels. This prediction does not account for local temperatures, which can be much higher (by 200 ^ C or more) than average temperatures due to exothermic combustion reactors at burning particle surfaces, and due to turbulent fluctuations. Actual concentrations of oxygen atoms may exceed equilibrium. Mixing in recovery furnaces is imperfect and may lead to local oxidizing and reducing zones. Properly accounting for these factors could lead to predicted thermal NO levels in recovery furnaces which are greater than those shown in Fig. 1. In spite of these simplifying assumptions, however, it seems unlikely that temperatures in recovery furnaces are sufficiently high to result in significant thermal NO concentrations.

Figure 1 and Eq. 7 also illustrate that strategies for reducing thermal NO formation must bring about reductions in one or more of the three parameters; viz., furnace temperature, oxygen concentration, or residence time at high temperature. As discussed by Anderson and Jackson (12), demonstrated strategies for conventional steam generating boilers include biased firing, off-stoichiometric combustion (or air staging), and low excess air firing.

Fuel NO

Fuel NO is formed during combustion as a result of the oxidation of nitrogen contained in the fuel. A great deal of research has been focused on understanding the elementary steps and reaction mechanisms leading from fuel nitrogen to fuel NO. General reviews of this research are available (13,14). A large number (hundreds) of reactions are involved, and many of these contain difficult-to-measure intermediates and radical species. Though an exact determination of the complete mechanism is presently not available, it is

generally accepted (11,14-16) that the fuel NO mechanism includes a rapid (not rate limiting) conversion of fuel nitrogen compounds into intermediate nitrogen compounds (HCN, CN, NH_2, NH, N) which can either be converted to NO by attack of oxygen-containing species or be converted to N_2 by reaction with NO itself. **Figure 2** shows an overall reaction pathway which is often used to represent this process (16).

Overall reaction rates of NO and N_2 formation from fuel nitrogen have been determined for laboratory hydrocarbon flames doped with simple nitrogen compounds such as ammonia, cyanogen, and pyridine (15,16). These overall reaction rates measured on simpler combustion systems have also been applied with encouraging success for the prediction of fuel NO formation during coal combustion (17).

Factors affecting fuel NO formation are fuel nitrogen content and concentration of oxygen in the gas. Unlike thermal NO, the formation of fuel NO is not highly sensitive to temperature changes caused by fuel heating value (18). Increased fuel nitrogen content can lead to higher emissions of fuel NO, although fuel NO cannot be correlated with nitrogen content alone. The relationship between weight percent of nitrogen in fuel, and the percent of fuel nitrogen conversion to NO in practical combustors has been reported for a variety of fossil and synthetic fuels with nitrogen contents up to 2% (1,11). On average, fractional conversion to NO increases with decreasing nitrogen content. The data, however, are widespread; for example, fuels containing less than 0.2% nitrogen showed conversions to NO ranging from a minimum of 20% to as high as 80%.

There are little to no data showing the fractional conversion of black liquor nitrogen to NO. Researchers investigating nitrogen dioxide pretreatment of pulp (the Prenox process) found that 5% or less of the nitrogen in nitrate added to black liquor was found as NO_x in the recovery boiler flue gases (19). This may not be representative, however, since the inorganic form of

the nitrogen bound in nitrate may behave very differently from the chemical forms of nitrogen found in black liquor.

Measurements of nitrogen content for a number of kraft black liquors are shown in **Table I**. Expressed as a weight percentage of the dry liquor solids, the values are in the range of 0.05-0.24 with the average being 0.11. Using the minimum fuel nitrogen to NO conversion value of 20% discussed above, a recovery furnace burning black liquor with the range of nitrogen contents in Table I would yield NO emission levels of approximately 25-120 ppm in the flue gas at 8% O_2. This estimate suggests that fuel nitrogen is an important source of recovery furnace NO_x.

In fuel oil combustion studies (20, 21), fuel NO was shown to be responsible for greater than 50% of total NO emissions during residual oil combustion at conditions of high air preheat (530°F) and about 80% of total NO without air preheat (because thermal NO was lower). The residual oil contained 0.20% nitrogen, which is within the range of black liquor nitrogen levels shown in Table I.

A question of importance to fuel NO formation is during which stage of combustion the fuel nitrogen is released (or converted) from its chemical form in the fuel to the gas phase intermediates in Fig. 2. This will affect when and where in the furnace the reaction of the intermediates will occur, and will affect the distribution of products formed (i.e., NO versus N_2). In combustion of coal, the release of fuel nitrogen occurs primarily during devolatilization, although additional nitrogen release occurs during char combustion (22). Thus, the majority of the coal nitrogen is chemically bound in a manner so as to be readily volatile.

For coals, the rate at which nitrogen is released is normally slightly more rapid (by a factor of 1.2-1.5) than the rate at which carbon is burned from the fuel (22). The chemical form of nitrogen in coal is thought to be

II. Summary of published NO_x flue gas concentrations from kraft and NSSC recovery furnaces

| Source	Solids, %	NO_x	NO_x, ppm at 8% O_2
Galeano and Leopold (1971)	NA[a]	0-53 ppm	33
Galeano and Leopold (1971)[b]	NA	13-65 ppm	35
Galeano, et al. (1973)[b]	62	10-50 ppm	30
Hood and Miner (1981)	NA	0.05-14 lb/10⁶ BTU (data from 10 furnaces)	
Bjorklund, et al. (1989)	64.6[d]	95 ppm	73
	76.5[d]	155 ppm	120
Brannland, et al. (1990)	65.0	57 mg/MJ	60
IPST data (1991)	67.6[d]	70 ppm[e]	59
IPST data (1991)	67.9[d]	110 pm[e]	91
Oscarsson, et al. (1991)	68	71 ppm	71
Netherton and Osborne (1991)	65	35 ppm	35
	80	90 ppm	90

[a] Not available
[b] NSSC liquor
[c] Based on approximate conversion factor of (390 ppm @ 8% O_2)/(lb/10⁶ BTU).
[d] Before salt cake addition
[e] Represents average of 6 to 10 one-day tests.

3. NOx emissions observed in flue gases from recovery furnaces, effect of increasing solids. All values normalized to a common basis of 8% O2 in flue gas. Sources of data as given in Table II.
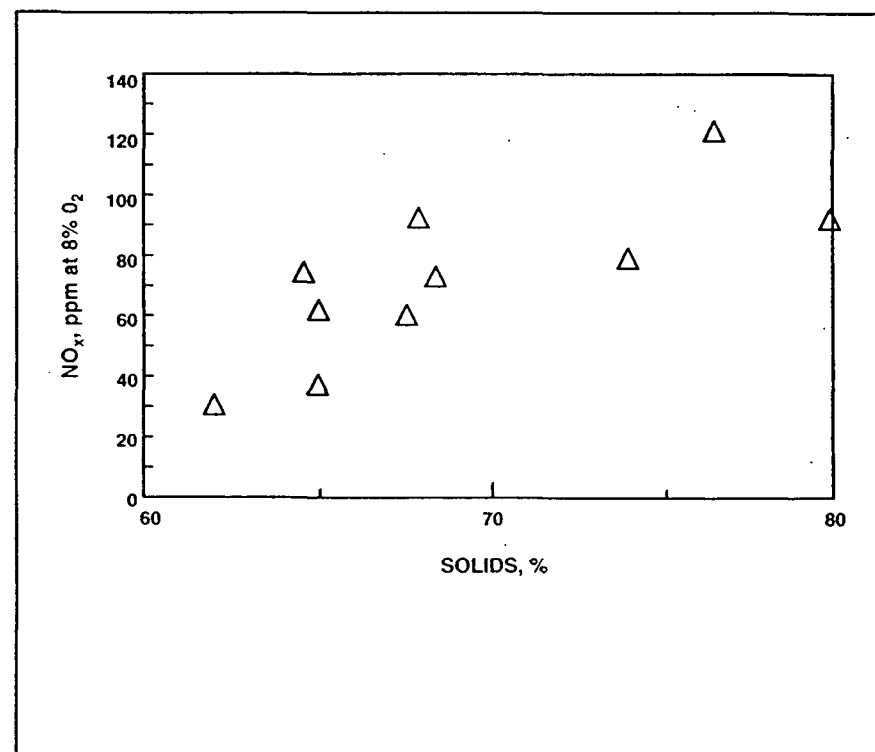
primarily heterocyclic aromatic ring structures such as pyridine, though this is difficult to ascertain because removal of the nitrogen-containing compounds from coal without their destruction is difficult. There are no data available for black liquor to show the chemical form of the fuel nitrogen, or to show how much is released during the respective stages of devolatilization and char burning.

Recovery furnace emissions

Published data on NO_x emissions from recovery furnaces are somewhat limited. Table II provides a summary of reported NO_x emissions along with the sources of the data (3, 6, 8, 19, 23, 24, 25). Emission levels (adjusted to a common basis of ppmv at 8% O_2 in flue gas) range from near zero to over 100 ppm.

By considering those data in Table II for which liquor solids concentrations are available, a trend is apparent. These data (plotted in Fig. 3), suggest that NO_x levels increased as solids increased. A similar trend has been reported by Netherton and Osborne (8). These authors reported NO_x emissions increasing monotonically from 35 ppm to 90 ppm as solids were increased from 65% to 80%. Although the data in Fig. 3 are few and are from a diversity of furnaces, a useful implication results from comparing the observed increase in NO_x emissions with increasing solids to that predicted for thermal NO formation. Theoretical flame temperature estimations for black liquor combustion (26) show a 230°C temperature increase for an increase in solids from 65% to 80%. Equation 7 (or Fig. 1) predicts an increase of thermal NO by a factor of several hundred for a 230°C temperature increase. Thus, the observed increase in NO_x with solids shown in Fig. 3 and reported by Netherton and Osborne (8) is two orders of magnitude less than predicted by thermal NO formation theory.

This difference between observation and theory implies that mecha-

nisms other than thermal NO formation play an important role in determining recovery furnace NO_x emissions. Two possibilities are: (a) a substantial portion of the total recovery furnace NO originates as fuel NO which is not as temperature-sensitive as thermal NO, and (b) NO destruction reactions are occurring and tending to mask or partially mask the temperature dependency.

The first of these possibilities has been discussed above. The second is discussed below.

NO_x destruction reactions

Levels of NO emissions depend not only on the rate of formation of NO, but also on the rate of destruction. Once NO is formed, it can be partially destroyed before leaving the furnace. Measurements of NO profiles as a function of distance from the flame have been made in several instances (22, 27) in laboratory and pilot-scale combustion. Results showed that NO is rapidly formed and then slowly destroyed. Concentrations pass through a maximum in or near the flame zone and undergo reduction in the post-flame gases. The effluent or flue gas concentration does not necessarily represent the maximum level of NO concentration formed in the furnace. The reduction can be up to 50% or more of the maximum level reached in the furnace, with fuel rich flames and particle laden flames giving the most destruction, and fuel lean and homogeneous flames giving less destruction (27, 28).

This NO reduction is due partially to gas-phase reaction of NO with nitrogen-containing intermediates to form N_2 (as shown in Fig. 2). The fact that the extent of NO reduction is greater in coal combustion than in gas or liquid combustion (26) showed that char and ash species are also responsible for NO reduction. Kinetic rates of reduction of NO to N_2 by chars have been measured (27-29). Rate expressions are generally reported in the form of Eq. 8:

$$-d(NO)/dt = A \exp[-E/(RT)]$$

$$A_i(NO) \qquad (8)$$

showing the dependence on char external surface area (A_E), NO concentration, temperature, and residence time.

Returning to the apparent trend in Fig. 3, it is possible that NO formation in recovery furnaces increased by much more than indicated by the flue gas measurements, but that NO destruction due to air staging served to counter or dampen the increase such that only some of the increase was seen in flue gases. As discussed by Galeano and Leopold (24), the conventional kraft recovery furnace, in order to promote formation of sulfide, uses the concept of air staging which is, coincidentally, a proven method for reducing NO emissions from utility boilers. Less than stoichiometric air in the lower furnace will decrease thermal NO formation by decreasing concentrations of atomic oxygen, and will decrease conversion of fuel nitrogen to NO while increasing conversion to N_2 (as shown in Fig. 2).

A destruction mechanism which may be important in recovery furnaces is the reaction of NO_x with fume species. Fume particulates represent a tremendously large surface area for reactions with gas-phase species. Sulfur gases including oxides of sulfur are known to react with fume species. It seems plausible that oxides of nitrogen may also undergo similar reducing reactions. Several possible reactions of nitrogen oxides with sodium species have been suggested (30) based on thermodynamic feasibility. If such reactions are occurring, burning black liquor at higher solids concentrations and higher combustion temperatures may serve to increase the fuming rate, and increases in fume-NO_x interactions would counter the increases in thermal NO formation.

Conclusions and research needs

Recovery furnace NO_x is presumed to be formed primarily by thermal and

fuel NO formation mechanisms. Little to no data are available to show the relative importance of each in black liquor combustion. This is an important question to answer and identifies a strong research need since the temperature dependence is very different for each mechanism.

Thermal NO is highly temperature-sensitive. Theory predicts that moderate increases in furnace temperature (100-140°F or 55-80°C) will yield order of magnitude increases in thermal NO concentrations. Based on theory, it appears unlikely that recovery furnace temperatures are high enough to produce significant thermal NO.

Fuel NO is much less temperature-sensitive, and thus fuel NO in recovery furnaces will not be affected by increasing solids concentrations to the same degree as will thermal NO. Black liquor solids contain 0.05-0.24 weight percent nitrogen. Conversion of 20% of this would produce NO in the range of 25-120 ppm, which is similar to the range of reported recovery furnace emissions. This suggests that fuel NO is an important source and that it may be the dominant source of recovery furnace NO emissions.

No information is available concerning the chemical form of nitrogen in black liquors, or concerning how much is released during devolatilization versus char combustion. This identifies a second research need, as this will affect when and where in the furnace the fuel nitrogen is released and will affect the relative distribution of NO and N_2 formed.

Published NO emissions data from operating recovery furnaces show values of near zero to over 100 ppm (at 8% O_2). Limited data show an increase in NO_x as solids increased from 62% to 80%. This observed increase is much less than predicted by the temperature dependence of thermal NO theory, suggesting the possibility that NO destruction reactions are occurring in recovery furnaces. This identifies a third area of research need—to evaluate the impact of potential NO_x destroying mechanisms. ⊞

Literature cited

1. Seinfield, J.H., Atmospheric Chemistry and Physics of Air Pollution, John Wiley & Sons, New York, 1986, p. 42.
2. Hood, K.T., A Study of Nitrogen Oxides Emissions From Kraft Recovery Furnaces, Technical Bulletin No. 105, National Council of the Paper Industry For Air and Stream Improvement (December 1979).
3. Hood, K.T. and Miner, R.A., TAPPI 1981 Environmental Conference Proceedings, TAPPI PRESS, Atlanta, p. 113.
4. State of Maine Department of Environmental Protection, Permit No. A-215-71-B-A/R, Georgia Pacific Corp.., Woodland, ME, issued April 12, 1989.
5. Barsin, J.A., Johnson, R.L., and Rissler, C.E., 1989 International Chemical Recovery Conference Proceedings, TSCPPA, Montreal, p. 29.
6. Bjorklund, H., Warnqvist, B., and Pettersson, B., 1989 International Chemical Recovery Conference Proceedings, TSCPPA, Montreal, p. 177.
7. Casale, F.S., and Fritz, P.A., TAPPI 1990 Engineering Conference Proceedings, TAPPI PRESS, Atlanta, p. 687.
8. Netherton, B., and Osborne, D.M., Tappi J. 74 (11): 71 (1991).
9. Hayhurst, A.N., and Vince, I.M., Progress in Energy and Combustion Sci. 6:35 (1980).
10. Zeldovich, J., Acta Physiochimica U.S.S.R. 21 (4): 577 (1946).
11. Bowman, C.T., Chemistry of Gaseous Pollutant Formation and Destruction, Chap. 4 of Fossil Fuel Combustion: A Source Book (Bartok, W. and Sarofim, A.F., Eds.), John Wiley & Sons, Inc., New York, 1991, p. 228.
12. Anderson, P.H. and Jackson, J.C., Tappi J. 74 (1): 115 (1991).
13. Nichols, K.M., Nitrogen Pollutant Formation in a High Pressure Entrained-Coal Gasifier, Ph.D. dissertation, Chemical Engineering Dept., Brigham Young University, Provo, UT (1987).
14. Boardman, R.D., Development and Evaluation of a Combined Thermal and Fuel Nitric Oxide Predictive Model, Ph.D. dissertation, Chemical Engineering Dept., Brigham Young University, Provo, UT (1990).
15. Fenimore, C.P., Combustion and Flame 26: 249 (1976).
16. de Soete, G.G., Overall Reaction Rates of NO and N_2 Formation From Fuel Nitrogen. Fifteenth Symposium (International) on Combustion, 1975, p. 1093. Sponsor is Combustion Institute, Pittsburgh, PA.
17. Hill, S.C., Smoot L.D., and Smith, P.J., Twentieth Symposium (International on Combustion, 1984, p. 1391. Sponsor is Combustion Institute, Pittsburgh, PA.
18. Pershing, D.W. and Wendt, J.O.L., Sixteenth Symposium (International on Combustion) 1977, p. 389. Sponsor is Combustion Institute, Pittsburgh, PA.
19. Braanland, R., Norden, S., and Lindstrom, L., Tappi J. 73 (5): 23 (1990).
20. Pershing, D.W., Martin, G.B. and Berkau, E.E. AIChE Symposium Series 71 (148): 19 (1975).
21. Pershing, D.W., Cichawanowizc, J.E., England, G.C., et al., Seventeenth Symposium (International) on Combustion. Sponsor is Combustion Institute, Pittsburgh, PA. 1979, p. 715.
22. Nichols, K.M., Hedman, P.O., and Smoot, L.D., Fuel 66 (9): 1257 (1987).
23. Galeano, S.F., Kahn, D.C., and Mack, R.A., Tappi 54 (5): 74 (1971).
24. Galeano, S.F. and Leopold, K.M., Tappi 56 (3): 74 (1973).
25. Oscarsson, B., Bentley, K.M., and Hood, S.H., TAPPI 1991 Environmental Conference Proceedings, Book 2, TAPPI PRESS, Atlanta, p. 1053.
26. Adams, T.N. and Frederick, W.J., Kraft Recovery Boiler Physical and Chemical Process, American Paper Institute, New York, 1988. p. 40.
27. Wendt, J.O.L., Pershing, D.W., Lee, J.W. et al., Seventeenth Symposium (International) on Combustion. 1979, p. 77. Sponsor is Combustion Institute, Pittsburgh, PA.
28. Levy, J.M., Chan, L.K., Sarofim, A.F., et al., Eighteenth Symposium (International) on Combustion. Sponsor is Combustion Institute, Pittsburgh, PA. 1981, p. 111.
29. Suuberg, E.M., Teng, H., and Calo, J.M., Twenty-third Symposium (International) on Combustion. 1990, p. 1199. Sponsor is Combustion Institute, Pittsburgh, PA.
30. Thompson, L.M., The Formation of Oxides of Nitrogen in Kraft Recovery Boilers. A39. Preparation for Research Problem, The Institute of Paper Science & Technology, Atlanta, GA (1990).

DISCUSSION

As a result of the survey of black liquor nitrogen content and NO_x emission levels, it was shown that conversion of only 20% of the black liquor nitrogen would correspond to NO_x emission levels typically reported for recovery furnaces. Subsequently, Clement and Barna have presented additional data for combustion of black liquor in commercial recovery furnaces.[35] The authors derived an empirical correlation for NO_x emission as a function of nitrogen content which follows:

$$[NO_x] = 138.6 \, N + 55.2 \qquad \text{(Eq. 18)}$$

where, $[NO_x]$ = concentration of NO_x in the flue gas (ppm at 8% O_2)

N = % nitrogen in as-fired liquor, dry solids basis.

Clement and Barna also investigated the conversion of nitrogen as a function of concentration by adding urea (NH_2CONH_2) to black liquor in amounts corresponding to 0.09 to 0.25% nitrogen. A correlation was derived which showed decreasing conversion with increased nitrogen content as follows:[35]

$$NC = -40.0 \, N + 21.7 \qquad \text{(Eq. 19)}$$

where, NC = % of nitrogen in liquor converted to NO_x

N = % nitrogen in as-fired liquor, dry solids basis.

The authors concluded that 10 to 20% of the fuel bound nitrogen was converted to NO_x with the percent conversion decreasing as nitrogen content increased.

In both the review and the combustion study, the results were discussed in terms of conversion of nitrogen corresponding to NO_x concentration levels. However, this type of correlation does not account for the occurrence of NO_x depletion reactions. It is possible that

more than 20% of the nitrogen is converted to NO and is then depleted by reaction with other species. In both cases, it would be more accurate to say that 20% of the black liquor nitrogen is emitted as NO_x in the flue gas.

Coal combustion studies have shown nonlinear correlations for conversion as a function of nitrogen content, especially at low nitrogen concentrations.[36] It has been suggested that the nonlinearity is related to the chemical structure of the different nitrogen species in coal. Thus, by using urea in the Clement and Barna study, the results may not reflect the behavior of structures found in black liquor. Furthermore, in the commercial combustion study, the lower range of black liquor nitrogen content was limited by the nitrogen content of the commercial liquor (0.09%). Because many commercial liquors have significantly lower levels of nitrogen and because the data may not be best represented by a linear fit, this empirical correlation should be used with caution and should certainly not be extrapolated for lower nitrogen levels.

Another important aspect from the review was that it was shown that, in general, temperatures in a recovery furnace are not hot enough to form significant amounts of thermal NO. While this conclusion was based on a simple estimate for conditions typically found in the lower part of the furnace, it was recognized that localized elevated temperatures and mixing patterns were not considered. Computational fluid dynamic (CFD) modeling has since been done to compare thermal NO_x formation for combustion of 67 and 80% solids cases.[37] Results of the CFD calculations gave less than 10 ppm NO in the flue gas. The authors of the CFD study also concluded that thermal NO is not a major source of NO_x in a recovery furnace.

As a result of the review, several research needs were identified to be able to better understand recovery furnace NO_x emissions, including the following:

1) Identification of the form of nitrogen in black liquor.
2) Experimental work to confirm the relative importance of fuel NO_x and thermal NO_x.
3) Determination of the amount of nitrogen released during the pyrolysis and char burning stages.
4) Identification and evaluation of potential NO_x depletion mechanisms.

Since the publication of the review, work has been conducted in each of these four areas.

The Form of Nitrogen in Black Liquor

The form of nitrogen in black liquor has been the subject of at least two publications.[38,39]

Martin *et al.* have reported the composition of nitrogen in commercial black liquor to be approximately one third inorganic and two thirds organic.[39] Of the inorganic portion, approximately two thirds of the nitrogen was reported to be in the form of nitrate. Organic species included protein species, amino acids, and heterocyclic ring compounds.

Experimental work was conducted at IPST to investigate the fate of nitrogen in wood as a result of pulping.[40] Results showed the majority of nitrogen in wood ended up in black liquor, while only a small portion (10 to 30%) stayed with the pulp stream. It was also shown that the amount of nitrogen in wood (~ 0.1%) can account for all of the nitrogen typically found in black liquor (i.e., additives and make-up chemicals do not contribute significantly to the nitrogen content in black liquor).

Fuel NO *vs.* Thermal NO

Concerning fuel *vs.* thermal NO formation, in addition to the CFD modeling that has been done,[37] laboratory work has been conducted in which black liquor was burned in both pilot scale

and bench top furnaces.[41] Results of the combustion experiments showed fuel NO to be the major source of NO in the flue gas. However, this work was conducted at maximum furnace temperatures of only 1000°C and should be conducted at higher temperatures to truly rule out thermal NO as a contributing factor.

The pilot scale study included measurements of NO_x concentration as a function of distance from the char bed.[41] Results indicated NO_x concentrations increased with increasing distance form the char bed which reached a maximum at 3.0 m from the bed. The concentration was shown to decrease from an average of 78 ppm to 50 ppm at a distance of 5 m from the bed. The authors assumed that the decrease in NO_x concentration was due to reactions of NO_x with other species.[41]

Nitrogen Release During Black Liquor Pyrolysis and Char Burning

Results from an experimental study of nitrogen release during pyrolysis showed 20 to 60% of fuel-bound nitrogen was released during pyrolysis.[42,43] The majority of the volatile nitrogen was found to be N_2 and NH_3 (in equal proportions) with a minor fraction (~ 1%) being released directly as NO. The authors concluded that oxidation of the ammonia released during pyrolysis could account for the concentrations of NO typically found in recovery furnace flue gases. However, the fate of the remaining 40 to 80% of the black liquor nitrogen was not accounted for in the pyrolysis study, and once again, the potential for NO depletion reactions was not considered.

Nitrogen analysis of smelt samples have shown that as much as 10 to 30% of the black liquor nitrogen could leave the furnace in the smelt.[44] This indicates that at least 70 to 90% of

the nitrogen is released during pyrolysis and char burning. Again, based on the observation that typically only 20% of the nitrogen is emitted as NO_x in the flue gas, it is clear that there is a need to further understand the impact of NO depletion reactions.

Depletion Mechanisms

In the preceding discussion, it has been illustrated that empirical correlations for NO_x emissions may not be able to predict flue gas concentrations for commercial furnaces over a wide range of operating conditions. There is clearly a need to understand the fundamental rates of formation and depletion reactions in order to adequately predict NO_x emissions. The importance of NO_x depletion reactions was chosen as the topic for this dissertation. The next section gives an overview of different depletion mechanisms as they relate to black liquor combustion.

A PROPOSED MECHANISM FOR THE DEPLETION OF NO$_x$ IN A KRAFT RECOVERY FURNACE[45]

SUMMARY

This paper presented an overview of both homogeneous and heterogeneous NO$_x$ depletion mechanisms and their potential importance in kraft recovery furnaces. It should be noted that throughout this dissertation the depletion of NO$_x$ refers to *in situ* reactions that should not be confused with controlling NO$_x$ formation or conversion of NO$_x$ after it has left the furnace.

Thermodynamic calculations of reactions involving NO$_x$ and several sodium species to form sodium nitrate (NaNO$_3$) were presented which demonstrate the feasibility of such reactions. In addition, three sorbent processes were discussed which have been developed using solid phase sodium species to scrub NO$_x$ and ultimately form NaNO$_3$.

A Proposed Mechanism for the Depletion of NO$_x$ in a Kraft Recovery Furnace

Laura M. Thompson
Graduate Student
Institute of Paper Science
and Technology
Atlanta, Georgia 30318

H. Jeff Empie
Professor of Engineering
Institute of Paper Science
and Technology
Atlanta, Georgia 30318

ABSTRACT

This study examines NO$_x$ destruction mechanisms and their impact on emissions from a kraft recovery furnace. The potential for NO$_x$ reactions with sodium species is presented and supported by thermodynamic calculations and analysis of industrial smelt samples.

INTRODUCTION

Higher emissions and more stringent regulations have recently brought more attention to the issue of NO$_x$ emissions from kraft recovery furnaces. In the late 1980's with the advent of high solids firing, increased NO$_x$ emissions were observed.[1,2,3] However, the impact of higher solids on NO$_x$ emissions is debatable. NO$_x$ emissions vary greatly depending on operating conditions and furnace configuration. Hyoty and Mantyniemi report emissions ranging from 40-135 ppm.[4] These numbers result from a survey of seven different furnaces operating at different loads and % dry solids. The authors suggest that NO$_x$ emissions can not be directly correlated with % solids and can indeed be controlled at high solids.

In order to predict emissions, one must understand both the rate of formation and the rate of depletion of the NO$_x$ species. Several recent publications have addressed the formation of NO$_x$ from black liquor combustion.[5,6,7] However, none of these publications fully address the depletion of NO$_x$. This study presents a brief review of NO$_x$ formation and depletion mechanisms known to occur in conjunction with the combustion of fossil fuels. In addition, a depletion mechanism which may be unique to black liquor combustion is presented and supported by thermodynamic calculations and experimental data.

It should be noted that by "depletion mechanisms" we are referring to *in situ* reaction chemistry which should not be confused with controlling NO$_x$ formation or conversion of NO$_x$ after it has left the furnace.

FORMATION of NO

NO is formed primarily by two mechanisms: thermal-NO$_x$ and fuel-NO$_x$. Each of these mechanisms is described briefly below including a discussion of their impact on recovery furnace emissions. For a more in-depth review of the formation of NO$_x$ in kraft recovery furnaces, the reader is referred to recent publications by Nichols *et al.* and NCASI.[5,6]

Thermal NO$_x$

Thermal NO$_x$ arises from the oxidation of the nitrogen in the combustion air at high temperatures. The reactions involved in thermal NO$_x$ formation are known as the extended Zeldovich mechanism. Because of the low temperatures resulting from black liquor combustion (as compared to fossil fuel combustion), thermal NO$_x$ is not an important formation mechanism. Two recent publications show that for conditions typically found in recovery furnaces, emissions due to thermal NO$_x$ are essentially negligible (less than 1 ppm).[5,6]

Fuel-NO$_x$

Fuel-NO$_x$ formation arises from the oxidation of fuel bound nitrogen. The fuel-NO$_x$ formation mechanism involves many intermediate steps and is not completely understood. In general, fuel-NO$_x$ formation has a weak temperature dependence, but is very dependent on stoichiometry and the rate of volatilization of nitrogen.

While it is believed that the majority of NO$_x$ in recovery furnace emissions arises from fuel-NO$_x$, it is not known how much of the nitrogen evolves during the volatilization of black liquor drops or what portion evolves from the char bed. Because the gas composition changes dramatically throughout the furnace, the point of nitrogen volatilization may have a large impact on the ultimate level of fuel NO$_x$ formed. The volatilization of nitrogen during black liquor pyrolysis is currently under investigation as part of a separate study at IPST.[8]

DEPLETION of NO$_x$

Once NO$_x$ is formed, it can be reduced by several different reaction pathways. In fossil fuel combustion, NO$_x$ is known to decay through homogeneous gas phase reactions and heterogeneous reactions with char and soot. The large amount of inorganic species present in black liquor combustion provide an additional depletion mechanism which may have an impact on recovery furnace emissions. The homogeneous gas phase reactions and reactions with char will be discussed in brief. The remainder of the paper will focus on potential depletion of NO$_x$ by reaction with sodium species.

Gas Phase Reactions

The Zeldovich mechanism describing thermal NO$_x$ formation includes reversible reactions which can contribute to the depletion of NO$_x$ under the right conditions. Depletion of NO$_x$ by this pathway involves reactions with N, O, and H radicals and is favored by high NO concentrations and high temperature. Just as the formation of thermal NO$_x$ requires high temperature, kinetic modeling has shown that thermal decomposition is only significant above 1800 K.[9] Acoustic temperature measurements in a recovery furnace show peak temperatures in the range of 1473-1588 K[10]; therefore, thermal decomposition should not have a significant impact on recovery furnace NO$_x$ emissions.

In addition to the reverse Zeldovich mechanism, NO can react with other gas phase species. Ammonia and other amines will selectively react with NO to form N_2 and H_2O.[11] These reactions are the basis of many injection type control strategies. Because these species are not believed to be present in large quantities in recovery furnaces, these reactions are probably not important. Other nitrogen species (such as CN and HCN) can also react with NO yielding N_2 as a final product.

Muzio and Arand investigated the effect of H_2, CH_4, C_2H_6, CO, and NH_4 over the temperature range of 700-1930 K.[12] Their data showed that CO, H_2, CH_4 and C_2H_6 react preferentially with excess oxygen in the combustion products and saw only minor reductions in NO at ratios of CO/NO or H_2/NO up to 14.

Heterogeneous Reactions with Char

Because the rate of reduction of NO_x species was found to be higher in burning coal than for gaseous or liquid fuel combustion, it was suggested that heterogeneous reactions with coal products may play an important role.[13] For this reason, several studies have been conducted investigating NO/char reactions. One such study proposed a mechanism for reduction of NO by char as follows:[13]

$$(1) \quad NO + 2C \longrightarrow C(N) + C(O)$$
$$(2) \quad C(N) + C(N) \longrightarrow N_2 + 2C$$
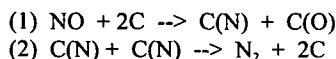
C(N) and C(O) represent chemisorbed species, and C represents a surface carbon. The authors proposed that the NO dissociates onto the carbon surface which is followed by diffusion of the dissociated atoms to form N_2. The adsorbed oxygen can either produce CO or react with CO to form CO_2, as shown in reactions 3 and 4.

$$(3) \quad C(O) \longrightarrow CO_{gas}$$
$$(4) \quad C(O) + CO \longrightarrow CO_2 + C$$
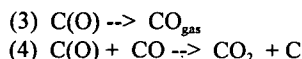
The effective rate of reaction for the temperature range of 1250-1750 K was found to be:

$$(5) \quad d[NO]/dt = 4.18 \times 10^4 \exp\left(^{-34,700\,cal}/_{RT}\right) A_{ext} P_{NO}$$
where, A_{ext} = external surface area, m^2/g;
$\qquad P_{NO}$ = partial pressure of NO, atm.

The rate of reaction was found to be inhibited by the presence of water and enhanced by the presence of CO which is consistent with the proposed mechanism. In general, depletion of NO by char has been shown to be dependent upon the surface area of char, the concentration of NO, and temperature.

The impact of heterogeneous reactions appears to be the subject of some debate. At least two studies have concluded that the primary reduction of NO occurs through gas phase reactions and not through a heterogeneous process.[14,15] Bose and Wendt indicate that the slow

devolatilization of nitrogenous species (from char) has an indirect influence on the destruction of NO.[15] The volatilized species form HCN which can react with NO to form N_2 under oxygen lean conditions.

In summary, for coal combustion, it is thought that the most significant pathway for depletion of NO is by homogeneous reactions with gas phase species such as NH_i, HCN, CO, and hydrocarbons. Also, at very high temperatures (T > 1800 K), the influence of the reverse Zeldovich mechanism may be important.

Due to the nature of fossil fuels, the impact of sodium species on NO emissions has been essentially ignored. However, regarding black liquor combustion, the presence of alkali species could play a significant role in the reduction of NO. While it is understood that sodium species react with SO_x, it seems likely that analogous reactions could occur for NO_x species. A brief review of alkali fume formation is presented with further discussion on potential reactions with NO_x species.

Formation of Alkali Fume

Alkali "fume" or "dust" collected in the electrostatic precipitators consists of 0.1-1 um particles, primarily composed of sodium sulfate (90%) and sodium carbonate (10%). The reactions leading to the formation of sodium sulfate act as a scrubbing mechanism for SO_2 and result in very low SO_2 emissions from recovery furnaces. Approximately 10% of the sodium entering the furnace ultimately forms fume.

Due to the extremely low vapor pressures of sodium carbonate and sodium sulfate, it is clear that the formation of fume is not a result of direct vaporization of these species from the char bed. In general, fume is believed to be the result of volatilization of sodium from the molten smelt which undergoes further reactions to form, primarily, sodium carbonate. The sodium carbonate reacts with SO_2 to form sodium sulfate and essentially scrubs the SO_2 from the flue gas.

A reaction enhanced vaporization mechanism has been proposed by Cameron,[16] who suggests that the reduction of Na_2CO_3 by Na_2S in the smelt bed enhances the volatilization of sodium from the molten smelt. As the sodium in the gas phase above the melt reacts, the volatilization is further enhanced by the reduction of the partial pressure of sodium in the gas phase.

The chemistry involved in fume formation is not completely understood. Blackwell and King provide a review of many proposed reactions which include the following:[17]

Formation of Na_2CO_3

$$(6) \quad Na_2O(s) + CO_2 \longrightarrow Na_2CO_3(l)$$
$$(7) \quad 2Na + CO_2 + O_2 \longrightarrow Na_2CO_3$$
$$(8) \quad 2NaOH(g) + CO_2 \longrightarrow Na_2CO_3(l) + H_2O(g)$$
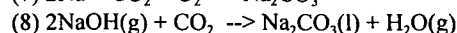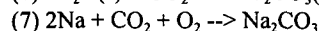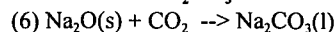
Formation of Na$_2$SO$_4$

(9) $Na_2O(s) + SO_2 + \frac{1}{2} O_2 \rightarrow Na_2SO_4(s,l)$

(10) $2Na(g) + 2CO_2 + SO_2 \rightarrow Na_2SO_4 + 2CO$

(11) $Na_2CO_3(s,l) + SO_2 + \frac{1}{2} O_2 \rightarrow Na_2SO_4(s,l) + CO_2$

(12) $Na_2CO_3(s,l) + SO_3 \rightarrow Na_2SO_4(s,l) + CO_2$

(13) $2NaOH(g) + SO_2 + \frac{1}{2} O_2 \rightarrow Na_2SO_4(s,l) + H_2O(g)$

Blackwell and King conclude that metallic sodium is the most important volatile intermediate and that reactions (11) and (12) above are the predominant reactions involved in the formation of sodium sulfate in the fume.[17]

NO$_x$ Reactions with Fume

As shown above, SO$_2$ and SO$_3$ react with sodium species in a recovery furnace to form sodium sulfate. It is possible to write analogous reactions for NO$_x$ species reacting with sodium carbonate and other sodium species to form sodium nitrate as the primary product. Some of these reactions are listed below.

(14) $Na(g) + NO + O_2 \rightarrow NaNO_3(s,l)$

(15) $Na(g) + NO_2 + \frac{1}{2} O_2 \rightarrow NaNO_3(s,l)$

(16) $Na_2O(s) + 2NO + \frac{3}{2} O_2 \rightarrow 2NaNO_3(s,l)$

(17) $Na_2O(s) + 2NO_2 + \frac{1}{2}O_2 \rightarrow 2NaNO_3(s,l)$

(18) $Na_2CO_3(s,l) + 2NO + \frac{3}{2}O_2 \rightarrow 2NaNO_3(s,l) + CO_2$

(19) $Na_2CO_3(s,l) + 2NO_2 + \frac{1}{2}O_2 \rightarrow 2NaNO_3(s,l) + CO_2$

The standard free energies of each of these reactions is shown below in Figure(1) over the temperature range, T = 300-1000 K.
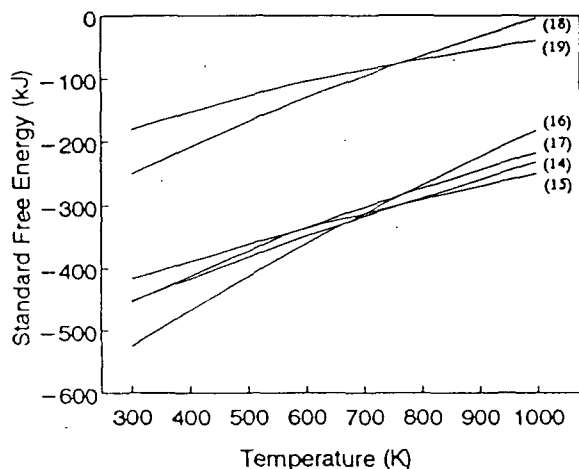
Figure 1: Standard Free Energy of Proposed Fume Reactions. (NaNO$_3$ begins to decompose at 700 K; thermodynamic data are extrapolated beyond 700 K).

Inspection of the data plotted above shows that reactions (14)-(19) are favorable in the forward direction at temperatures found in the upper furnace. One should be reminded that the thermodynamics indicates only that the reactions are feasible and does not imply that they will occur at a detectable rate.

Depletion by Reaction with Molten Salts

In addition to the potential for reactions with fume species, it is possible that reactions could occur between NO$_x$ and molten sodium species. Molten salts are present in the char bed as well as in black liquor drops that have reached the final stages of combustion (char burning and smelt coalescence) while in flight. The reaction chemistry would be similar to reactions higher in the furnace, but would occur at a much higher temperature. Also, the surrounding gases would be different which could have some effect on the reactions.

Supporting Evidence for NO$_x$ Reactions with Sodium Species

In addition to the thermodynamic data presented above, there are several other items which support the feasibility for NO$_x$/sodium reactions. One such body of supporting evidence is the work being conducted on NO$_x$ sorbent processes. Three of these processes are discussed below.

NO$_x$ Sorbent Processes

The NOXSO process is a flue gas treatment process which is currently being developed by the NOXSO Corporation to simultaneously remove both NO$_x$ and SO$_x$.[18,19,20] The process employs a sodium carbonate sorbent which is impregnated on a high surface area gamma alumina. In the proposed process, flue gas is exposed to the sorbent in a fluidized bed at approximately 120 C. Residence times are on the order of 40-80 minutes. For NO$_x$ flue gas concentrations at 470-720 ppm, NO$_x$ removal efficiency was reported at 80-92%. The SO$_2$ removal efficiency was reported as 90-99% for inlet concentrations ranging from 1465-5000 ppm.[20]

Analysis of reacted sorbent has shown the predominant sorption products contain nitrate (NO$_3^-$) and sulfate (SO$_4^-$) ions at weight percentages of 0.41-0.48 and 5.75-6.17, respectively.[18] The original sorbent had a sodium content of 3.6% by weight. Other ions present in small quantities included nitrite (NO$_2^-$), sulfite (SO$_3^-$), and sulfide (S$^-$).

Gorst and co-workers used thermogravimetric analysis to study the sorption of nitric oxide with a mixed oxide sorbent composed of Na$_2$O, Co$_3$O$_4$, and Fe$_2$O$_3$.[21] The authors proposed a sorption mechanism involving catalytic oxidation of NO to NO$_2$ with the subsequent reaction of NO$_2$ with Na$_2$O to form NaNO$_3$. Their experiments showed sorption to increase with temperature and NO concentration.

Another process to simultaneously reduce SO$_x$ and NO$_x$ involves in-duct injection of sodium bicarbonate (NaHCO$_3$). This type of process has been used commercially in both oil and coal-fired utility boilers. For several different utility applications, removal rates of SO$_2$ and NO$_x$ are reported as 20-90% and 0-40%, respectively.[22] The authors report that the majority of NO$_x$ removed forms sodium nitrate.

In each of the processes described above, solid phase sodium species are reacting with NO_x to form $NaNO_3$ as the primary product. Two of the examples report significant reduction of NO_x in the presence of SO_2.

Analysis of Industrial Samples

If NO_x does react with sodium species to form nitrate in a recovery furnace, the product should be present in fume and/or smelt. In order to verify this fact, samples were taken from several kraft mills in the Southeast and analyzed by ion chromatography (TAPPI Standard Method T-699) for nitrate. Unfortunately, due to the interference of sulfate in the analysis of fume samples, quantitative detection of nitrate was not possible. The results of the smelt analysis are reported below in Table 1.

Table 1: Ion Chromatographic Analysis of Industrial Smelt Samples

Mill	$[NO_3^-]$ (ppm)
A	6060
B	10,780
C	1590

Table 1 shows nitrate levels ranging from 1590 to 10,780 parts per million (by weight). It is difficult to explain the differences in the nitrate concentrations for the three mills without knowledge of the operating conditions of the furnaces. Less NO_x in the furnace would lead to lower levels of nitrate being formed, and there may be some influence due to smelt composition. It is possible that Mill C was running its boiler with lower levels of NO_x or that its smelt had a very different composition (such as low sulfidity or the presence of some species that interferes with the formation of nitrate).

CONCLUSIONS

A new mechanism for the depletion of NO in a kraft recovery furnace has been presented. The theory behind this mechanism has been supported by thermodynamic calculations and analysis of industrial smelt samples. Experimental work has been initiated to investigate the kinetics involved with the depletion of NO by different sodium species.

LITERATURE CITED

1. Barsin, J.A., Johnson, R.L., and Rissler, C.E., *Proceedings of the 1989 International Chemical Recovery Conference*, "The St. Francisville Recovery Low Odor Conversion and Capacity Upgrade," 29-37 (1989).

2. Bjorklund, H., Warnqvist, B., and Pettersson, B., *Proceedings of the 1989 International Chemical Recovery Conference*, "Inside a Kraft Recovery Boiler - Combustion of (High Sulphidity) Black Liquor at High Dry Solids," 177-181 (1989).

3. Casale, F.S., and Fritz, P.A., *Proceedings of the TAPPI 1990 Engineering Conference*, "Start up and Operation of a High-Solids Recovery Boiler at S.D. Warren Company, Westbrook, Maine," 687-688 (1990).

4. Hyoty, P., and Mantyniemi, J., *Proceedings of the 1992 International Chemical Recovery Conference*, "Emission of a Big Recovery Furnace; Results of a 2600 tds/24 h Boiler," 405-412 (1992).

5. Nichols, K.M., Thompson, L.M., and Empie, H.L., "A Review of NO_x Formation Mechanisms in Recovery Furnaces," To Be Published in *Tappi Journal*, Jan., 1993.

6. "An Analysis of Kraft Recovery Furnace NO_x Emissions and Related Parameters," *NCASI Technical Bulletin No. 636*, July, 1992.

7. Jones, A.K., and Stewart, R.I., *Proceedings of the 1992 International Chemical Recovery Conference*, "The High Solids Breakpoint - A Trade-Off Between SO_x and NO_x," 365-370 (1992).

8. Martin, D.M., *A490 Thesis Proposal*, "The Evolution of Fuel Nitrogen During Black Liquor Pyrolysis," The Institute of Paper Science and Technology, Atlanta, GA, June, 1992.

9. Klinger, J., Smyk, E.B., and Johnson, T.R., *Twenty-Second Symposium on Engineering Aspects of Magnetohydrodynamics*, "Validation of Kinetic Model for Nitric Oxide Decomposition in MHD Systems," 10:2:1-20 (1984).

10. Whitten, P.G., Barna, J.L., Ivie, L., and Abbot, S.R., *Proceedings of the 1989 International Chemical Recovery Conference*, "Application of Acoustic Temperature Measurement to Optimize Recovery Boiler Furnace Operation," 239-244 (1989).

11. Miller, J.A., Branch, M.C., and Kee, R.J., *Combustion and Flame*, "A Chemical Kinetic Model for the Selective Reduction of Nitric Oxide by Ammonia," 43:81-98 (1981).

12. Muzio, L.J., and Arand, J.K., *Sixteenth Symposium (International) on Combustion*, "Gas Phase Decomposition of Nitric Oxide in Combustion Products," 199-208 (1977).

13. Levy, J.M., Chan, L.K., Sarofim, A.F., and Beer, J.M., *Eighteenth Symposium (International) on Combustion*, "NO/Char Reactions at Pulverized Coal Flame Conditions," 111-120 (1981).

14. Glass, J.W., and Wendt, J.O.L., *Nineteenth Symposium (International) on Combustion*, "Mechanisms Governing the Destruction of Nitrogenous Species During the Fuel Rich Combustion of Pulverized Coal," 1243-51 (1982).

15. Bose, A.C., and Wendt, J.O.L., *Twenty-Second Symposium (International) on Combustion,* "Pulverized Coal Combustion: Fuel Nitrogen Mechanisms in the Rich Post-Flame," 1127-1134 (1988).

16. Cameron, J.H., *Chemical Engineering Communication,* "Reaction Enhanced Vaporization of Molten Salt," (59):243-257 (1987).

17. Blackwell, B., and King, T., *Chemical Reactions in Kraft Recovery Boilers,* Sandwell and Company Limited, Vancouver, B.C. (1985).

18. Haslbeck, J.L., Ma, W.T., Yeh, J.T., Pennline, H.W., and Solar, J.P., *Eighty-Second Annual AWMA Meeting and Exhibition,* "Life Cycle Test of the NOXSO Process: Simultaneous Removal of NO_x and SO_2 From Flue Gas," June (1989).

19. Haslbeck, J.L., Woods, M.C., Harkins, S.M., Ma, W.T., Gilbert, R.L., and Brundrett, C.P., *Proceedings of the Intersociety Energy Conversion Engineering Conference,* "The NOXSO Flue Gas Treatment Process: Simultaneous Removal of NO_x and SO_2 From Flue Gas," (4):161-170 (1990).

20. Haslbeck, J.L., Woods, M.C., and Bolli, R.E., *Integrating Environmental Controls and Energy Production,* "Pilot Plant Test Data on the NOXSO Flue Gas Treatment System," ASME, EC (2) (1991).

21. Gorst, J., Do, D.D., and Desai, N.J., *Fuel Processing Technology,* "Removal of Nitric Oxide From Flue Gas Using Mixed Oxide Sorbents," 22:5-24 (1989).

22. Bennet, R., and Darmstaedter, E., *Integrating Environmental Controls and Energy Production,* "Sodium Bicarbonate In-Duct Injection with Sodium Sulfate Recovery For SO_2/NO_x Control," ASME, EC (2):19-25 (1991).

ACKNOWLEDGMENTS

DISCUSSION

NO_x depletion reactions can be broadly classified as either homogeneous or heterogeneous. Homogeneous NO depletion mechanisms include the reverse Zeldovich mechanism, reactions with ammonia, and reactions with light hydrocarbons. Heterogeneous depletion mechanisms include reactions with char or sodium species. Each of these reaction mechanisms are discussed further below.

Homogeneous Depletion Reactions

The thermal NO_x formation, or Zeldovich, mechanism was discussed previously in the review of NO_x formation mechanisms. Each of the reactions leading to the formation of NO is reversible under proper conditions. The reactions include the following:

$$NO + N \leftrightarrow N_2 + O \qquad \text{(Eq. 20)}$$
$$NO + O \leftrightarrow N + O_2 \qquad \text{(Eq. 21)}$$
$$NO + H \leftrightarrow N + OH \qquad \text{(Eq. 22)}$$
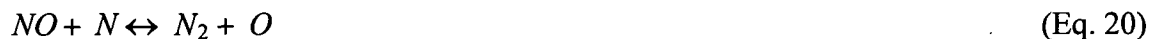
NO depletion by reactions 20 to 22 is favored by high concentrations of NO and high temperature. The reverse Zeldovich mechanism is also called thermal decomposition and has been shown to be only important at temperatures above 1500°C.[46]

The reaction between NO and ammonia is the basis for a well-established post-combustion control method for NO_x emissions: selective noncatalytic reduction (SNCR). The reaction involves the reduction of NO by ammonia to form water and N_2 according to the overall stoichiometry:[47]

$$4\,NO + 4\,NH_3 + O_2 \rightarrow 4\,N_2 + 6\,H_2O \quad \text{or} \qquad \text{(Eq. 23)}$$

$$6\,NO + 4\,NH_3 \rightarrow 5\,N_2 + 6\,H_2O \qquad \text{(Eq. 24)}$$

The mechanism involves many reactions that can be summarized in Figure 3 below.[48] A more detailed representation of this mechanism is included in Appendix 2 which begins on page 101.
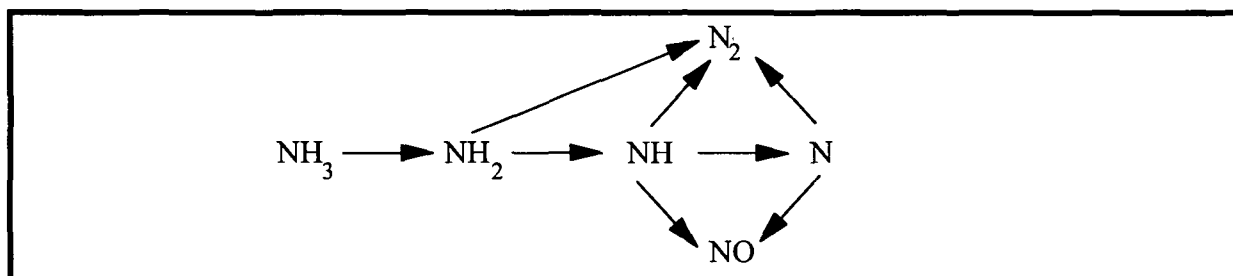
Figure 3. Mechanism for Reduction of NO by Reaction with Ammonia.

In general, SNCR has been shown to be most effective at temperatures between T = 1100 to 1400°K.[48] At high temperatures, ammonia may be oxidized to form more NO. At low temperatures, the reactions do not produce significant radicals to sustain the process, and ammonia may be emitted.[49]

In the article, reactions with ammonia were not considered to be an important depletion mechanism due to the fact that equilibrium calculations will predict extremely low concentrations of NH_3 (< 1 ppm at T = 1000°C).[30] As more data become available concerning nitrogen release during combustion and pyrolysis of black liquor, it will be possible to more accurately model the influence of ammonia/NO reactions based on reaction kinetics.

Muzio *et al.* studied the effect of light hydrocarbons as reducing agents for NO.[50] Specifically, it was shown that ethane, methane, carbon monoxide, and hydrogen will tend to react preferentially with excess oxygen in the flue gas.[50] Thus, NO depletion by reaction with these species will only occur under fuel rich (oxygen deficient) conditions.

In general, gas phase NO depletion reactions are believed to be insignificant in a recovery furnace. Because gas phase reaction kinetics have been studied extensively, there are ample rate data in the literature that could be used to more accurately model these types of reactions for a recovery furnace.

Heterogeneous Depletion Reactions

Heterogeneous depletion mechanisms include reactions with char or sodium species. An investigation of the depletion of NO by reaction with coal char showed the rate of depletion to be dependent upon the surface area of the char, the concentration of NO, and temperature.[51] The activation energy was found to be 34,700 cal/mol (145.2 kJ/mol). Wu and Iisa investigated the depletion of NO by reaction with black liquor char and found the rate of depletion was approximately three times faster than for the equivalent surface area of activated carbon.[52] The activation energy was reported to be 70 kcal/mol (292.9 kJ/mol).

The impact of sodium species on NO emissions has been essentially ignored. However, regarding black liquor combustion, the presence of sodium species could play a significant role in the depletion of NO. While it is understood that sodium species react with SO_x, it has been hypothesized that analogous reactions could occur with NO_x species.

Thermodynamic calculations of potential NO_x/sodium reactions were presented which demonstrate the feasibility of such reactions. In addition, three sorbent processes were discussed which have been developed using solid phase sodium species to scrub NO_x and ultimately form

$NaNO_3$. Because sodium nitrate begins to decompose at approximately 700°K, extrapolation of thermodynamic data beyond this point must be considered with reservations.

As mentioned in the discussion of fume formation, SO_x depletion reactions are believed to be primarily due to reactions with molten sodium carbonate.[27] The lack of any kinetic data for reactions of NO with molten sodium species led to the experimental investigation of the rate of depletion of NO with molten sodium salts.

KINETICS OF NO DEPLETION BY REACTION WITH MOLTEN SODIUM CARBONATE[53]

SUMMARY

This paper presented the results of nitric oxide depletion by reaction with sodium carbonate. In addition to a description of the experimental apparatus, the paper gave a brief overview of theory of gas absorption with chemical reaction.

Gas flow rate, NO concentration, temperature, and the mass of salts in the system were selected as the independent variables in this study. By feeding a known concentration of NO to the system and measuring the NO in the exit gas, it was possible to determine the amount of NO depleted over a wide range of conditions.

Experimental results showed a 10 to 75% conversion of NO over the temperature range of 860 to 973°C. The rate of depletion of NO was shown to follow a pseudo first-order rate expression. For all of the experimental conditions, the Hatta number was greater than three. Values of the rate constant, k_1, ranged from 5.0 x 10^4 to 7.0 x 10^6 sec^{-1} with an activation energy of 372 kJ/mol (89.0 kcal/mol).

EXPERIMENTAL APPARATUS

To determine the rate of depletion of NO by reaction with molten sodium species, an apparatus had to be designed which would provide intimate gas-liquid contact and at the same time be resistant to corrosion at high temperatures. A system was constructed in which gases were bubbled through molten salts contained in an alumina crucible. A more detailed description

of the apparatus is included in the article. Additional information regarding calibration methods and materials of construction is included in Appendix 3 which begins on page 102.

Preliminary experiments were conducted in which no salt was present in the system to check whether or not the materials of the apparatus would cause any decay of NO. For these experiments, the system was sealed and heated to a desired temperature while purging the system with argon. Upon reaching a desired temperature, NO was fed to the system at a known concentration and flow rate. The exit concentration was monitored for five minutes at which point the NO was shut off and a new temperature set point was established. This was repeated over a wide range of temperatures and flow rates.

Results indicated minimal drift in calibration of the NO_x analyzer and that there was no depletion of NO in the system over the temperature range of T = 300 to 930°C. Using an inlet concentration of 1857 ppm NO, the average measured exit concentration was found to be 1835 ppm with a standard deviation of 6 ppm. The average measured value was less than 1.2% different than the actual feed concentration.

Kinetics of NO Depletion by Reaction With Molten Sodium Carbonate

L. M. Thompson and H.J. Empie

Institute of Paper Science and Technology, Atlanta GA

This study presents results of an investigation of nitric oxide (NO) depletion by reaction with molten sodium carbonate ($Na_2 CO_3$). Experiments have been conducted in which NO in Helium is bubbled through molten sodium carbonate. Preliminary results show a 10 to 75% reduction of NO over the temperature range of 860 to 973°C. The rate of depletion of NO is shown to follow a postulated pseudo first order rate law. Values of the rate constant range from 5.0 x 10^4 to 7.0 x 10^6 sec^{-1} with an activation energy of 372 kJ/mol (89.0 kcal /mol).

In order to predict NO_x emissions from a kraft recovery furnace, one must understand both the *in situ* rate of formation and rate of depletion of the NO_x species. In a previous paper, it has been suggested that the reaction of NO with sodium species could provide a depletion mechanism which is unique to kraft recovery furnaces[1].

Many reactive sodium species are present in a kraft recovery furnace. These species exist in different phases depending on location (as temperature varies with location in the furnace). In the lower furnace, molten smelt is a source for volatilization of sodium species which form fume [2]. At this point, the potential for reactions between NO_x species and the molten smelt exists. Above the smelt bed and traveling up the furnace, vapor phase alkali species (e.g. Na and Na_2O) could potentially react with NO_x before precipitating as fume. In the upper furnace, it is understood that fume particles react with SO_2 forming sodium sulfate (Na_2SO_4) as the final product[3]. It is suggested that these fume particles could also react with NO_x.

The kinetics of sulfation reactions has been the subject of many studies [3,4,5,6]. One review article concludes that the reaction of SO_2 with sodium carbonate below the melting point (850 °C) does not occur fast enough to account for the amount of SO_2 depletion that occurs in a recovery furncace[6]. The authors suggest that the reaction is most likely occurring with molten sodium carbonate.

The smelt in a recovery furnace is composed primarily of sodium carbonate (~ 78 wt %), sodium sulfide (~18 wt %), and sodium sulfate (~4 wt %). The fraction of each species depends on the composition of the black liquor burned in the furnace and the operation of the furnace. The objective of this study is to investigate the rate of depletion of NO in contact with these smelt species. Initial work is presented here for sodium carbonate reactions. Results of NO depletion with mixtures of the different species will be presented in the future.

THEORY OF GAS ABSORPTION WITH CHEMICAL REACTION

This study investigates the heterogeneous reaction of a gas (NO) with a nonvolatile liquid (molten Na_2CO_3). In general terms the reaction can be written as: A(g) + B(l) → products, or specifically, $NO(g) + Na_2CO_3(l)$ → products. The rate of depletion of NO has been assumed to follow the kinetic expression,

$$-r_{NO} = kC_{NO}C_{Na_2CO_3}. \tag{1}$$

Assuming that the concentration of sodium carbonate, $C_{Na_2CO_3}$, is high and remains essentially constant, equation (1) can be written as a pseudo first order rate expression:

$$-r_{NO} = k_1 C_{NO}. \tag{2}$$

Levenspiel derives a rate expression for pseudo first order reactions for gas-liquid systems which are considered to react totally within the liquid film[7]. The rate expression accounts for diffusion in both the gas and liquid films and can be written as:

$$-r_{NO} = -\frac{1}{V_L}\frac{\delta N_{NO}}{\delta t} = \frac{a p_{NO}}{\frac{1}{k_g} + \frac{H_{NO}}{\sqrt{D_{NO/Na}k_1}}}. \tag{3}$$

By substituting $\frac{P_{NO}}{H_{NO}} = \frac{N_{NO}}{V_l}$, separating variables and integrating over time, equation (3) can be reduced to:

$$-\ln\left(\frac{P_{NO_f}}{P_{NO_i}}\right) = \frac{a}{\frac{1}{H_{NO}k_g} \cdot \frac{1}{\sqrt{D_{NO/Na}k_l}}} . \tag{4}$$

Rearranging terms, equation (4) can be written as:

$$k_1 = \frac{1}{\left(-\ln\left(\frac{P_{NO_f}}{P_{NO_i}}\right)\frac{1}{H_{NO}k_g}\right)^2}(D_{NO/Na})^{-1} \qquad (\sec^{-1}). \tag{5}$$

For this expression, time is calculated as the expanded volume of the liquid divided by the volumetric flow rate of the gas, $t = m/(V\rho(1-\varepsilon))$. Other constants in equation (5) are calculated from correlations found in the literature. In short, a and t are functions of the gas flow rate. H_{NO}, k_g, and $D_{NO/Na}$ are dependent on temperature. Thus, the pseudo first order rate constant can be found as a function of concentration, flow rate, and temperature. A complete list of equations and notation is included at the end of the paper.

It is possible to classify the reaction as fast or slow depending on the value of the Hatta number[8]. The Hatta number, $\sqrt{M_A}$, is a measure of the ratio of A reacting in the film to that going unreacted in the bulk B phase.

$$\sqrt{M_A} = \sqrt{\frac{2}{m+1}D_A k[A^*]^{m-1}[B_o]^n}/k_L \tag{6}$$

In general, fast reactions are those where $\sqrt{M_A} \geq 1$; the reaction of A occurs while it is diffusing in the film. For $\sqrt{M_A} \ll 1$, no A reacts in the film and the reaction is considered slow. It will be shown that for the experimental conditions considered in this study, the reaction of NO in molten Na_2CO_3 is fast and it is appropriate to use equation (3) described above.

EXPERIMENTAL APPARATUS

Experiments have been conducted in which NO is bubbled through molten sodium carbonate. The experimental apparatus is depicted in Figures 1 and 2.

Helium and a mixed gas of nitric oxide in helium are fed from pressurized gas cylinders. Flow is measured by Hastings-Teledyne™ digital mass flowmeters and is controlled manually by needle valves. The gas is fed to the reaction chamber which is described in detail below. Exit gas from the system is analyzed by a chemiluminescent NO_x analyzer.

Molten salt is contained in a 4 cm x 10 cm alumina crucible which is cemented to a stainless steel flange. A graphite gasket is placed between the flange and the lid which is held in place by eight bolts to form a gas-tight seal. The reaction vessel is heated by a tube furnace. Gases are bubbled through the salt using a 0.4 cm ID alumina tube. A type-K thermocouple, protected by an alumina well, is used to measure the temperature of the molten salt. The mass flowmeters, thermocouple, and NO_x analyzer are connected to

a personal computer for data acquisition. Data is acquired at a sampling rate of 0.5 Hz.

EXPERIMENTAL CONDITIONS

Gas flow rate, NO concentration, temperature, and mass of salt in the system have been selected as independent variables in this study. The mass of salt is either 17.5, 25.0, or 35.0 g, gas flow rate is targeted between 0.65 to 1.00 L/min (as air at STP), and temperature is varied between 860 to 975 °C. The NO inlet concentration is either 1857 ppm or 8400 ppm. The experimental conditions for each run are listed in Table 1.

Each experimental condition is run for six to nine minutes. Data for the flow rate, temperature and NO exit concentration are averaged over the last two minutes of this time interval. This allows the system to reach a pseudo steady state before averaging data. A sample of the time averaged data is shown below in Table 2 for experiment 1A.

Inspection of Table 2 indicates that the variables remain essentially constant over the time averaging period. Temperature fluctuations are on the order of 1 °C while the NO exit concentrations vary by approximately 10 to 30 ppm (1 to 2.5 %).

RESULTS

Figure 3 is a plot of the conversion of NO as a function of temperature. The percent conversion is calculated as: $X = 100\left(1 - \frac{P_{NO_f}}{P_{NO_i}}\right)$. Calculation of the conversion does not account for residence time or temperature but is presented as a means of normalizing the raw data.

Inspection of Figure 3 reveals conversion increasing as a function of temperature. The conversion varies from approximately 10 to 75 % over the temperature range 860 to 973 °C.

Equations (5) and (6) are used to calculate the rate constant, k_1, and the Hatta number for each of the data points represented in Figure 3. The results of these calculations for experiment 2A are listed in Table 3. Inspection of the data reveals the Hatta number is much greater than one over the range of experimental conditions which supports the validity of the pseudo first order rate expression.

The interfacial area, a, is on the order of 0.25 cm^{-1}. This value is considerably lower than measured values for interfacial area in melts contained in agitated and sparged contactors. Ghorpade, et al. report values in the range of 2.3 to 4.5 cm^{-1} for a mechanically agitated contactor and 1.7 to 2.7 cm^{-1} for a bubble column [9]. However, it is not surprising that the calculated value is low as the reaction

vessel has only one sparging tube with a large diameter which creates large gas bubbles.

To determine the activation energy, the experimental data is plotted in Figure 4 as $\ln(k_1)$ vs $1/T$. The solid line in Figure 4 is based on linear regression of the data. Based on this analysis, the slope of the line, $-Ea/R$, is $-44,780$ K and the intercept, $\ln(k_o)$, is 51.78. Thus, the pseudo first order rate constant for the depletion of NO may be written as:

$$k = k_o e^{-Ea/RT} = 3.09 \times 10^{22} e^{-44,780/T}. \qquad (7)$$

Substituting these values into equation (1) gives the rate expression:

$$-r_{NO} = 3.09 \times 10^{22} e^{-44,780/T} C_{NO}. \qquad (8)$$

Table 4 lists activation energies for several different heterogeneous reaction systems. The activatioon energy for the depletion of NO by molten sodium carbonate is considerabley higher than the other systems.

Data from experiment 1 has not been included in the regression analysis of the data. The data from experiment 1 gives a much lower activation energy than the rest of the experiments. It is suggested that the low mass of salt (17.5 g) provides mixing conditions that are significantly different than for the larger quantities of salt. The smaller mass is subject to splashing and may not behave according to the bubble flow that is assumed in the calculations of k_1.

DISCUSSION

The experimental data has been fitted to a pseudo first order rate expression. Errors in the analysis may arise from some of the assumptions that have been made. One possible source of error is the calculation of the gas hold up. The correlation used is derived for bubble columns which typically have more than one sparger. Thus the calculated values for gas hold up and the surface to volume ratio may not be representative of the experimental conditions. Another source of error is the assumption that the rate is first order with respect to each of the reactants. This assumption will be addressed experimentally in future work.

Preliminary results show that NO does indeed react in the presence of molten sodium carbonate. A conversion of 10 to 75 % is observed over the temperature range of 860 to 973 °C. The reaction follows a postulated pseudo first order rate law for the depletion of NO.

Sodium carbonate has been chosen as the starting material for the first phase of this study. Future work will include adding sodium sulfide (Na_2S) to more closely simulate recovery furnace smelt. Work is also planned to identify the gas phase reaction products by on line gas chromatographic analysis.

EQUATIONS

$$a = \frac{s}{v} \quad [10, \text{ p.}144]$$

$$d_b = \left[\left(\frac{\pi D_t}{A \epsilon \delta}\right)^2 + 9.5\left(\frac{v_s^2 D_t}{\epsilon}\right)^{0.867} \right]^{\frac{1}{6}} \quad [11, \text{ p.}228]$$

$$D_{NOHe} = \frac{10^{-4}\left(1.084 - 0.249\sqrt{1/M_{NO} + 1/M_{He}}\right)T^{1.5}\sqrt{1/M_{NO} + 1/M_{He}}}{P_t \left(r_{NOHe}\right)^2 f\left(\frac{kT}{\epsilon_{AB}}\right)} \quad [10, \text{ p.}31]$$

$$D_{NONa} = \frac{\left(117.3 \times 10^{-18}\right)\left(\phi M_{Na}\right)^{0.5}T}{\mu v^{0.6}} \quad [10, \text{ p.}35]$$

$$\epsilon = 0.5\left(\frac{U_{br}}{\sqrt{gR_c}}\right)^{0.4}\left(\frac{U_{sp}}{U_{br}}\right)^{0.8} \quad [11, \text{ p.}1199]$$

$$H_{NO} = 1/K_H$$

$$k_s = \frac{D_{NOHe} P_t}{RT P H_{Km}} \quad [10, \text{ p. }49]$$

$$k_L = 0.42\left(\frac{D_{NONa}}{\epsilon}\right)\left(\frac{d_b^3 g \rho^2}{\mu^2}\right)^{\frac{1}{3}}\left(\frac{\mu}{\rho D_{NONa}}\right)^{0.5} \quad [12, \text{ p. }230]$$

$$K_H = \frac{\exp\left(\frac{-4TN_2}{8.314T}\right)}{82.06T} \quad [13]$$

Physical properties of molten sodium carbonate can be calculated as a function of temperature according to the following:

$$\rho = 2.4797 - 0.4487 * 10^{-3} \, T \; (g/cm^3) \quad [14]$$

$$\mu = 3.832 * 10^{-5} \exp(13215/T) \; (cp) \quad [14]$$

$$\gamma = (254.8 - 0.0502 \, t)/1000 \; (N/m), \; t = \text{temperature (°C)} \quad [15]$$

NOTATION

a = interfacial area per unit volume (cm^2/cm^3)

A = solute gas

$[A^*]$ = interfacial concentration of A (mol/cm^3)

B = non-volatile reactant

$[B_o]$ = concentration of B in the bulk (mol/cm^3)

C_{Na2CO3} = concentration of molten Na_2CO_3 (mol/cm^3)

C_{NO} = concentration of NO in liquid film (mol/cm^3)

d_b = bubble diameter (cm)

D_{NOHe} = diffusivity of NO in Helium (m^2/s)

D_{NONa} = diffusivity of NO in Na_2CO_3 (m^2/s)

D_t = outside diameter of purge tube (m)

Ea = activation energy (J/mol)

$f(kT/\epsilon_{AB})$ = collision function (= 0.31) (Treybal[10], p. 32)

g = gravitational constant = (9.81 m/s)

H_{NO} = phase distribution coefficient (atm cm^3/mol)

k = second order rate constant (mol/cm^3 s)

k_o = pre-exponential factor (1/s)

k_1 = pseudo first order rate constant (1/s)

K_H = Henry's Law constant (mol/cm^3 atm)

m = order of reaction with respect to A

m_{Na} = mass of Na_2CO_3 (g)

$\sqrt{M_A}$ = Hatta number

M_i = molecular weight of species, i

n = order of reaction with respect to B

N = Avogadro's number = (6.022×10^{23})

N_{NO} = moles of NO (mol)

$[NO]_f$ = exit concentration of NO (ppm)

$[NO]_i$ = inlet concentration of NO (ppm)

$P_{He,m}$ = log mean pressure of helium (atm)

P_{NO} = partial pressure of NO (atm)

P_t = total pressure (atm)

r = molecular radius (m)

$-r_{NO}$ = rate of depletion of NO based on volume of liquid $(mol/cm^3 \, s)$

$r_{NO/He}$ = molecular separation at collision (nm)

R = universal gas constant = $(8.314 \, m^3 \, J/mol \, K)$

R_c = radius of column = (0.02 m)

t = time (s)

T = absolute temperature (K)

U_{br} = bubble rise velocity (m/s)

U_{gs} = superficial gas velocity (m/s)

V = flow rate of gas (cm^3/s)

V_g = flow rate of gas (m^3/s)

V_l = volume of molten salt (cm^3)

X = percent conversion of NO

z = film thickness = $(10^{-4} \, m)$ (estimated)

α = correlation factor (assumed 30)

ε = gas hold up

ϕ = association factor for solvent = 1

v_{NO} = solute molal volume at boiling point (= 0.0236 $m^3/kmol$)

LITERATURE CITED

1. Thompson, L.M., and Empie, H.J., A Proposed Mechanism for the Depletion of NO_x in a Kraft Recovery Furnace, Proceedings of the 1993 TAPPI Environmental Conference, Boston, MA, 643-647(1993).

2. Cameron, J.H., Chemical Engineering Communications, 59:243-257(1987).

3. Backman, R., Hupa, M., and Uusikartano, Kinetics of Sulphation of Sodium Carbonate in Flue Gases, Proceedings of the 1985 International Chemical Recovery Conference, New Orleans, LA, 445-450(1985).

4. Maule, G., and Cameron, J., Reaction of Na_2CO_3 Fume Particles with SO_2 and O_2, IPC Technical Paper Series, No. 317, January, 1989.

5. Keener, T., and Davis, W., Journal of the Air Pollution Control Association, 34:651-654(1984).

6. Kauppinen, E.I., Mikkanen, P., Jokiniemi, J.K., Iisa, K., Boonsongsup, L., Sinquefield, S.A., and Frederick, W.J., Fume Particle Characteristics and Their Reactions with SO_2 at Kraft Recovery Boiler Conditions, Proceedings of the 1993 TAPPI Engineering Conference, Boston, MA, 369-376(1993).

7. Levenspiel, O., Chemical Reaction Engineering, 2nd Edition, Chapter 13: Fluid-Fluid Reactions, John Wiley & Sons, New York, 1972.

8. Chhabria, M.C.,and Sharma, M.M., Chemical Engineering Science, 29:993-1002(1974).

9. Ghorpade, A.K., Chipalkatti, S.V., and Sharma, M.M., Chemical Engineering Science, 36:1227-1232(1981).

10. Treybal, R.E., Mass-Transfer Operations, 3rd Edition, McGraw-Hill Book Company, New York, 1980.

11. Cheremisinoff, N.P., Encyclopedia of Fluid Mechanics, Volume 3: Gas-Liquid Flows, Gulf Publishing Company, Houston, 1986.

12. Cussler, E.L., Diffusion: Mass Transfer in Fluid Systems, Cambridge University Press, New York, 1984.

13. Andresen, R.E., J. Electrochemical Society, 328-334(1979).

14. Janz, G.J., Dampier, F.W., Lakshminarayanan, G.R., Lorenz, P.K., and Tomkins, R.P.T., Molten Salts: Volume 1, Electrical Conductance, Density, and Viscosity Data, National Standard Reference Data Series-National Bureau of Standards 15, October, 1968.

15. Janz, G.J., Lakshminarayanan, G.R., Tomkins, R.P.T., and Wong, J., Molten Salts: Volume 2, Section 2: Surface Tension Data, National Standard Reference Data Series-National Bureau of Standards 28, August, 1969.

16. Suberg, E.M., Teng, H., and Calo, J.M., Twenty-Third Symposium (International) on Combustion, The Combustion Institute, 1199-1205(1990).

17. Thorman, R.P., and Macur, T.S., Kinetics of Sodium Sulfate Reduction by Carbon in Molten Sodium Carbonate, Proceedings of the 1985 International Chemical Recovery Conference, New Orleans, LA, 451-458(1985).

18. Hedden, K., Rao, B.R., and Reitz, F., Desulfurization of Manufactured Gases with Liquid Metals, Proceedings of the 1986 International Gas Research Conference, 1124-1133(1986).

Table 1: Experimental Conditions for the Depletion of NO in Molten Sodium Carbonate.

Exp.	1A	1B	2A	2B	2C	3A	3B	3C	4A	4B	5A	5B	6A	6B
Mass (g)	17.5	17.5	25.0	25.0	25.0	25.0	25.0	25.0	35.0	35.0	35.0	35.0	35.0	35.0
V (L/min)	0.75	1.00	0.65	0.80	0.95	0.65	0.80	0.95	0.75	1.00	0.75	1.00	0.75	1.00
[NO]i (ppm)	1,857	1,857	8,400	8,400	8,400	8,400	8,400	8,400	1,857	1,857	1,857	1,857	1,857	1,857

Table 2: Time averaged data for Experiment 1A.

V avg (L/min)	V std (L/min)	T avg (°C)	T std (°C)	[NO]f avg (ppm)	[NO]f std (ppm)	[NO]f % rsd
0.76	0	871	0.9	1,559	22.9	1.5
0.76	0	889	0.9	1,346	15.4	1.1
0.76	0.01	908	1	1,260	14.9	1.2
0.75	0	919	0.9	1,179	13	1.1
0.76	0	931	1.2	1,113	8.4	0.8
0.76	0	943	0.9	967	13.1	1.4
0.77	0	955	0.9	889	20.9	2.3
0.76	0	959	1.1	861	11.7	1.4

(V = volumetric flow rate, T = temperature, [NO]f = NO exit concentration)
(avg = average, std = standard deviation, rsd = relative standard deviation)

Table 3: Calculated values for the Hatta number and the pseudo first order rate constant, k_1, for Experiment 2A.

Temp. (K)	a (1/cm)	t (s)	-ln(P_f/P_i)	H_{NO} (cm³atm/mol)	k_g (mol/cm² atm s)	$D_{NO/Na}$ (cm²/s)	k_L (cm/s)	Hatta #	k_1 (1/s)
1138	0.251	0.247	0.161	1.37E+06	.7.28E-03	3.05E-05	4.37E-02	59	2.21E+05
1162	0.253	0.245	0.299	1.30E+06	7.36E-03	3.98E-05	5.19E-02	93	5.89E+05
1180	0.255	0.241	0.504	1.26E+06	7.41E-03	4.82E-05	5.88E-09	139	13.95E+05
1199	0.257	0.238	0.788	1.21E+06	7.47E-03	5.83E-05	6.65E-02	194	28.55E+05
1199	0.257	0.237	0.854	1.21E+06	7.47E-03	5.84E-05	6.66E-02	210	33.62E+05
1217	0.259	0.235	1.047	1.17E+06	7.53E-03	6.97E-05	7.47E-02	231	42.78E+05
1218	0.258	0.236	1.142	1.17E+06	7.53E-03	7.00E-05	7.49E-02	250	50.27E+05
1218	0.258	0.236	1.125	1.17E+06	7.53E-03	7.06E-05	7.53E-02	245	48.39E+05
1241	0.260	0.233	1.321	1.12E+06	8.66E-03	8.75E-05	8.66E-02	252	54.35E+05
1242	0.260	0.233	1.333	1.12E+06	8.72E-03	8.85E-05	8.72E-02	252	54.76E+05

Table 4: Activation Energies for Heterogeneous Reaction Systems.

Reaction System	Temperature (K)	Activation Energy (kJ/mol)	Reference
Na_2CO_3 (s) + SO_2 (g)	623-973	65	[3]
NO (g) + C (s)	923-1073	180	[16]
Na_2S (l) +C (s) in Na_2CO_3 (l)	1190-1340	204	[17]
SnO_2 (l) + CO (g)	873-1073	147	[18]
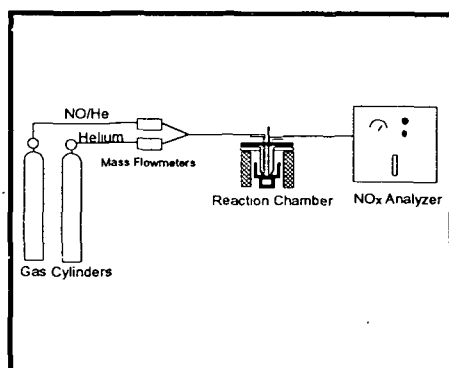
Figure 1: Experimental Apparatus
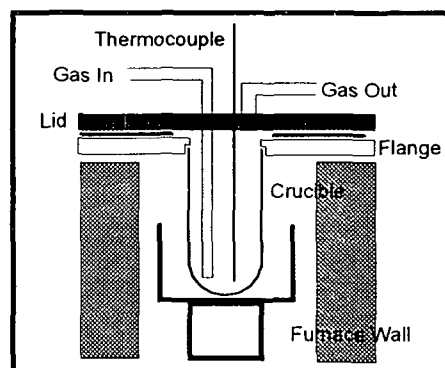
Figure 2: Reaction Chamber
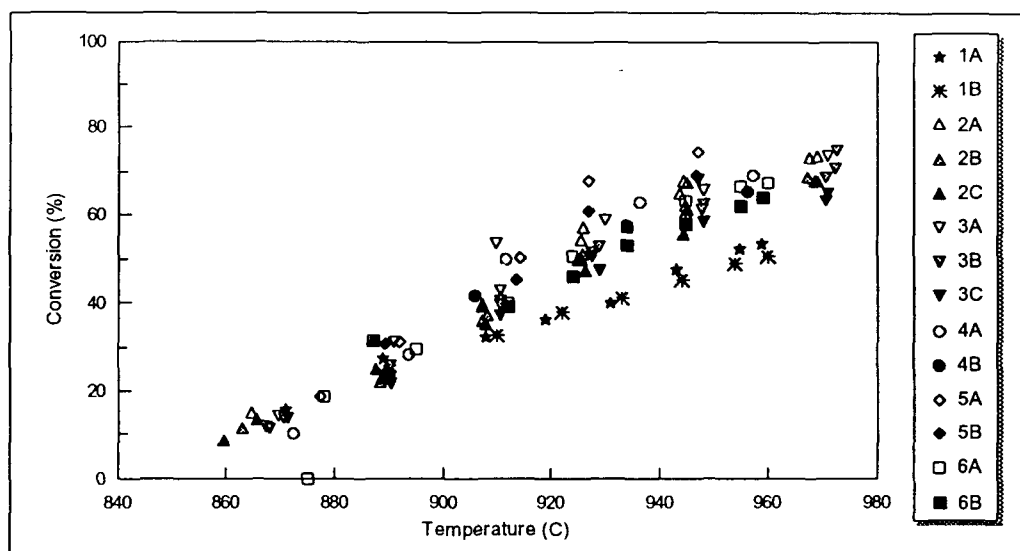
Figure 3: Conversion of Nitric Oxide by Reaction with Molten Sodium Carbonate
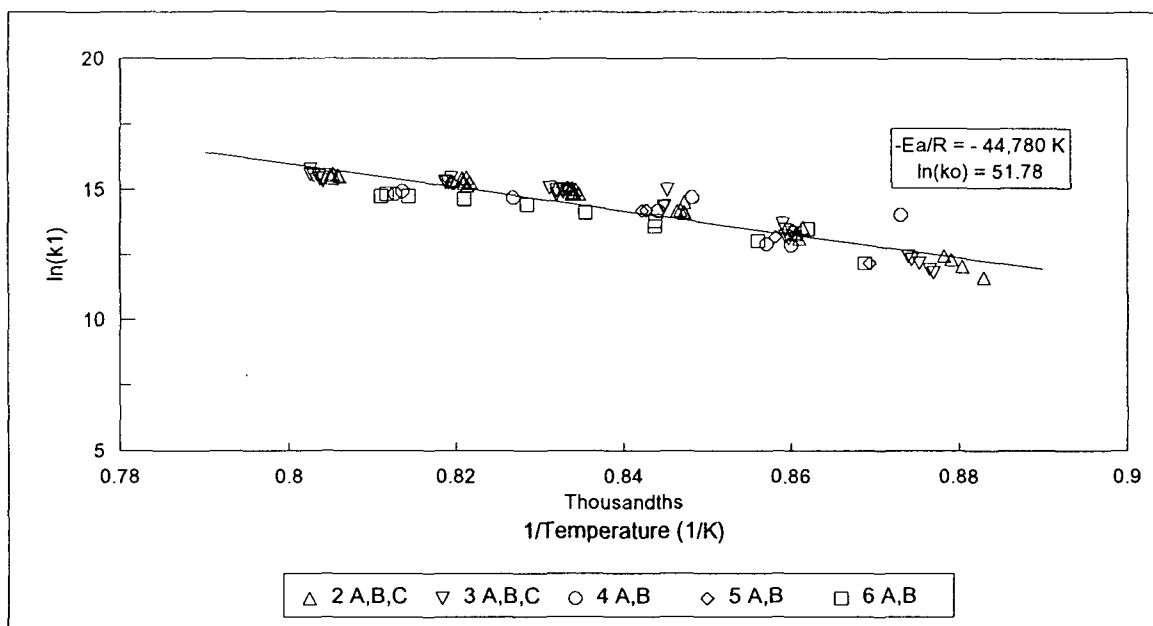
Figure 4: Determination of the Activation Energy; ln(ko) vs 1/T for Experiments 2-6.

DISCUSSION

The depletion of NO by reaction with molten sodium carbonate has been shown to follow a fast, pseudo first-order rate expression. The data were also fitted to several other expressions which were rejected for a variety of reasons. Each of the other expressions that was tested is described briefly in addition to the criteria for which it was rejected. Background material on the two-film theory and the rigorous derivation of the pseudo first-order rate expression is also presented below.

Two-film Theory

Treybal provides an overview of several models which have been developed to describe mass transfer at a fluid-fluid interface:[54]

Film theory	Combination film-surface renewal theory
Penetration theory	Surface-stretch theory
Surface-renewal theory	

In his discussion, Treybal concludes that the film theory is best suited for situations involving high mass transfer flux, predicting the effect of mass transfer on heat transfer, and for predicting the effect of chemical reaction rate on mass transfer.

The two-film theory model assumes that there is a stagnant film close to any interface through which transport processes take place.[55] Furthermore, the model assumes that the conditions in the bulk phase are constant so that the driving forces exist only across the stagnant film. The film model is represented in Figure 4.
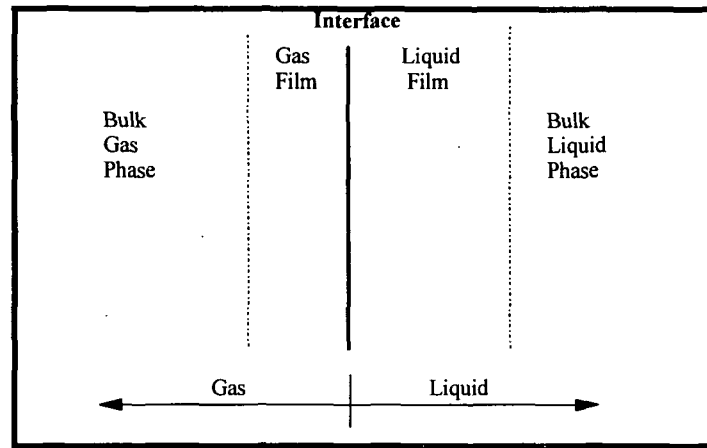
Figure 4. Two-film or Two-resistance Model for a Gas-liquid Interface.

When dealing with heterogeneous systems, the rate of mass transfer (through gas and liquid films) and the rate of chemical reaction need to be considered in the overall rate expression. Depending on the reaction system and conditions, the rate can be controlled by mass transfer, reaction rate, or a combination of the two.

Heterogeneous Rate Expressions

Levenspiel has derived several rate expressions based on different assumptions of the controlling mechanism including the following:[56]

Infinitely slow reaction (reaction occurs totally in the bulk phase)

$$-r'' = kC_{NO}C_{Na}$$ (Eq. 25)

Instantaneous chemical reaction (limited by gas film resistance)

$$-r'' = k_g P_{NO}$$ (Eq. 26)

Slow reaction (diffusion in two films and reaction in bulk phase act as resistances in series)

$$-r'' = \frac{P_{NO}}{\frac{1}{k_g} + \frac{H_{NO}}{k_L} + \frac{H_{NO}^a}{kC_{Na}}}$$ (Eq. 27)

Fast reaction (reaction occurs totally within the liquid film)

$$-r'' = \frac{P_{NO}}{\frac{1}{k_g} + \frac{H_{NO}}{k_L E}} \quad \text{where, } E = \text{Enhancement Factor} \quad \text{(Eq. 28)}$$

$$E = \frac{\sqrt{D_{NO} k C_{Na}}}{k_L} \text{ for pseudo first-order reactions.}$$

Each of the rate expressions above was tested for the depletion of NO by reaction with

sodium carbonate. It was concluded that the experimental data were best represented by the

pseudo first-order reaction rate expression (Eq. 28). The other rate expressions were ruled out

for a variety of reasons as discussed below.

Infinitely Slow Reaction

Calculated activation energies varied by as much as 100% depending on experimental

conditions. There appeared to be a correlation between the mass of salt in the system and the

calculated activation energy. This indicates mass transfer is affecting the activation energy. The

calculated activation energies for each experiment are included in Appendix 4 which begins on

page 106.

Instantaneous Chemical Reaction

Experimentally calculated values for gas film mass transfer coefficient, k_g, were two

orders of magnitude lower than calculated values based on the definition of the mass transfer

coefficient. This indicates that the experimentally calculated mass transfer coefficient is not

representative of the gas film coefficient, but is more likely an overall coefficient, K, (i.e., the

sum of two or more resistances) as in the following: $K = \frac{1}{\frac{1}{k_g} + \frac{1}{k_2}}$, where k_2 represents either the

liquid film mass transfer coefficient or some function of an Arrhenius reaction rate constant. A

comparison of the experimentally determined and calculated values are included in Appendix 5 which begins on page 108.

Slow Reaction

Experimentally calculated values for reaction rate constant, k_1, were negative, indicating that the reaction is not slow. This can be seen more clearly by integrating equation 27 and rewriting to solve for k_1:

$$k_1 = \frac{a}{\frac{at}{-\ln(P_{NO,f}/P_{NO,i})} - \frac{1}{H_A k_g} - \frac{1}{k_L}}. \text{ Thus, values for } k_1 \text{ will be negative if } \frac{at}{-\ln(P_{NO,f}/P_{NO,i})} < \frac{1}{H_A k_g} + \frac{1}{k_L}.$$

Based on the experimental data, the left-hand side (l.h.s.) of the inequality ranges from approximately 0.1 to 10 s/cm, while values for $1/k_g$ are on the order of 100 s/cm. To increase the value for the l.h.s. (in order to get positive values for the rate constant), the contact area or residence time would have to be increased by at least a factor of 10. In other words, if the reaction were slower (requiring longer times for equivalent conversion), then this rate expression could be appropriate. Thus, because the calculated values for k_1 are negative, it is implied that the reaction may be considered fast.

Clues for Identifying Kinetic Regime

In addition to ruling out the first three rate expressions based on experimental results, there is more evidence to suggest that the depletion of NO would behave as a pseudo first-order reaction. It is possible to gain insight to the controlling mechanism by inspection of solubility data, mass transfer coefficients, and diffusion coefficients. Levenspiel describes clues to the kinetic regime based on solubility data, and shows that, in general, gas film resistance controls for highly soluble gases and liquid film resistance controls for slightly soluble gases.[56]

Table 2 lists the solubilities for several gas-liquid systems. Inspection of Table 2 reveals that solubility can vary greatly depending on the components involved and temperature. In general, solubilities are found through experimental measurements; however, correlations exist in the literature for predicting solubility based on the physical properties of the system and temperature. The Uhlig-Blander equation has been used extensively for calculating the solubility of gases in molten salts.[57,58]

Table 2. Gas Solubilities at Various Temperatures and 1.0 atm Pressure of Gas.

Gas-Liquid System	Temperature (°C)	Solubility (mol gas/mol liq)	Reference
$N_2 - H_2O$	25	0.119×10^{-4}	59
$N_2 - (CH_3)_2C_6H_{12}$	25	15.39×10^{-4}	59
$CO_2 - (CH_3)_2C_6H_{12}$	25	138.7×10^{-4}	59
$CH_4 - H_2O$	5	0.386×10^{-4}	60
$CH_4 - H_2O$	100	0.143×10^{-4}	60
$CO_2 - Na_2CO_3$	880	1.97×10^{-4}	58
$NO - Na_2CO_3$	900	0.16×10^{-4}	calculated
$NO - Na_2CO_3$	1000	0.19×10^{-4}	calculated

Inspection of Table 2 shows the estimated solubility of nitric oxide in molten sodium carbonate to be three orders of magnitude lower than the CO_2/isooctane system. The low solubility of NO indicates that diffusion in the liquid film will play an important role in the overall reaction rate.

In addition to solubility data, clues to the governing rate controlling mechanism can be gained by inspection of the Hatta number. The Hatta number is defined as a measure of the ratio

of (the gas) A reacting in the (liquid) film to that going unreacted in the bulk (liquid) phase.[61] The Hatta number, $\sqrt{M_A}$, is calculated as:

$$\sqrt{M_A} = \sqrt{\tfrac{2}{m+1} D_A k [A^*]^{m-1} [B_o]^n} / k_L \qquad \text{(Eq. 29)}$$

where, m,n = order of reaction with respect to A (gas phase) and B (liquid phase)
D_A = diffusivity of gas in liquid B, (cm^2/s)
k = (m + n)th order rate constant, ((cm^3/mol)$^{m+n-1}$/s)
$[A^*]$ = interfacial concentration of A, (mol/cm^3)
$[B_o]$ = concentration of B in the bulk, (mol/cm^3)
k_L = mass transfer coefficient, (cm/s)

Reactions can be classified as slow or fast, depending on the value of the Hatta number. A slow reaction, $\sqrt{M_A} \ll 1$, is one in which no reaction occurs while it is diffusing in the film. A reaction is considered to be fast if reaction occurs while diffusing in the film, $\sqrt{M_A} \geq 1$. If the concentration of the reactant in the liquid phase, B, remains high and constant, the reaction may behave as first-order with respect to the gas phase reactant, A. For a pseudo first-order reaction, $3.0 < \sqrt{M_A} \ll \frac{[B_o]}{b[A^*]}$.[61] Without *a priori* knowledge of the rate constant, it is not possible to calculate the Hatta number; however, inspection shows fast reactions will be favored by high concentration and low values for the liquid film mass transfer coefficient, k_L.

Derivation of the Pseudo First-order Rate Expression

The rigorous derivation of the enhancement factor in equation 28 was first presented by van Krevelen and Hoftijzer.[62] The derivation is repeated here substituting notation specifically for the depletion of NO by Na_2CO_3. For this derivation, the reaction of NO by Na_2CO_3 is assumed to follow the general stoichiometry: NO + z Na_2CO_3 = products, where z is the number of moles of Na_2CO_3 that reacts with one mole of NO. The two-film model is depicted below for a fast pseudo first-order reaction.
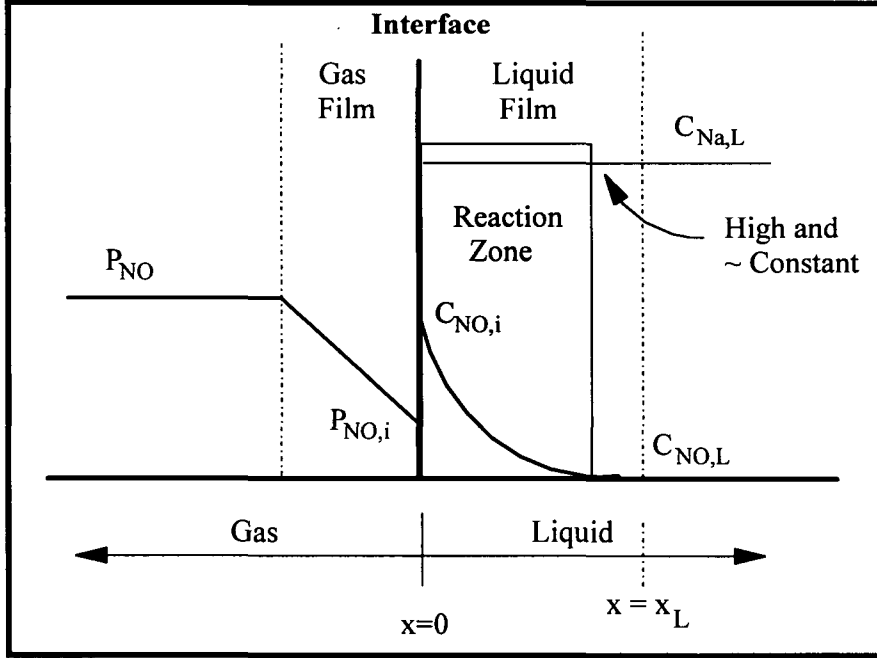
Figure 5: Two-film Model for Pseudo First-order Reaction; The Concentration of the Sodium Salt Is Assumed to be High and Approximately Constant.

When we consider a point x of the liquid film (thickness x_L), the rate of diffusion of NO in an element of unit area can be expressed as :

$$w_{NO} = -D_{NO}\frac{dC_{NO}}{dx}.$$

The rate of diffusion out of the element at the point x + dx will be:

$$w'_{NO} = -D_{NO}\left(\frac{dC_{NO}}{dx} + \frac{d^2C_{NO}}{dx^2}dx\right).$$

The rate of consumption of NO within the element is therefore:

$$w_{NO} - w'_{NO} = D_{NO}\frac{d^2C_{NO}}{dx^2}dx.$$

For the sodium salt, the analogous expression will be:

$$-(w'_{Na} - w_{Na}) = D_{Na}\frac{d^2C_{Na}}{dx^2}dx.$$

If the reaction is first-order with respect to each reactant, the consumption of each species per unit time is also expressed by the rate of reaction:

$$-\frac{dC_{NO}}{dt} = -\frac{1}{z}\frac{dC_{Na}}{dt} = kC_{NO}C_{Na}$$

so the number of molecules of NO and salt disappearing within the volume element will be:

$$-\frac{dC_{NO}}{dt}dx = -\frac{1}{z}\frac{dC_{Na}}{dt}dx = kC_{NO}C_{Na}\,dx.$$
(Eq. 35)

By assuming $D_{NO} \sim D_{Na}$, we obtain:

$$D_{NO}\frac{d^2C_{NO}}{dx^2} = \frac{1}{z}D_{NO}\frac{d^2C_{Na}}{dx^2} = kC_{NO}C_{Na}.$$
(Eq. 36)

For the special case when the concentration of the sodium salt is constant throughout the liquid

film, this equation can be transformed into a dimensionless form and integrated as follows:

Let, $R_o = \sqrt{kC_{Na}D_{NO}}\,C_{NO,i}$ $\qquad M_1 = \frac{D_{NO}}{x_L}C_{NO,i} = k_LC_{NO,i}$ $\qquad X = R_o/M_1$

$$\frac{d^2C_{NO}}{d\left(\frac{x}{x_L}\right)^2} = \frac{x_L^2 kC_{Na}D_{NO}}{D_{NO}^2}C_{NO} \approx \frac{kC_{Na}D_{NO}C_{NO,i}^2}{\left(\frac{D_{NO}}{x_L}\right)^2 C_{NO,i}^2}C_{NO} = \left(\frac{R_o}{M_1}\right)^2 C_{NO} = X^2 C_{NO}.$$
(Eq. 37)

Integration of Eq. 37 for the limits $C_{NO} = C_{NO,i}$ at $x/x_L = 0$ and $C_{NO} = C_{NO,L}$ at $x/x_L = 1$ gives:

$$C_{NO} = C_{NO,i}\frac{\sinh\left[\left(1-\frac{x}{x_L}\right)X\right]}{\sinh X} + C_{NO,L}\frac{\sinh\left[\frac{x}{x_L}X\right]}{\sinh X}.$$
(Eq. 38)

At the interface, $x = 0$, the rate of absorption into the liquid film becomes:

$$J_{NO} = \frac{D_{NO}}{x_L}\left[C_{NO,i}\frac{X}{\tanh X} - C_{NO,L}\frac{X}{\sinh X}\right] = k_LC_{NO,i}\frac{X}{\tanh X}\left[1 - \frac{C_{NO,L}}{C_{NO,i}}\frac{1}{\cosh X}\right].$$
(Eq. 39)

J_{NO} has units of mol/s cm^2 and is often referred to as the specific rate of absoption ($J_{NO} = -r_{NO}''$).

Similarly, at $x = x_L$, the specific rate of diffusion into the main body is:

$$W_{NO} = \frac{D_{NO}}{x_L}\left[C_{NO}\frac{X}{\sinh X} - C_{NO,L}\frac{X}{\tanh X}\right] = k_LC_{NO,i}\frac{X}{\sinh X}\left[1 - \frac{C_{NO,L}}{C_{NO,i}}\cosh X\right].$$
(Eq. 40)

The number of molecules reacting in the main body of the liquid will be:

$$r' = kC_{NO,L}C_{Na,L}\varphi \qquad \text{where, } \varphi = \text{liquid holdup.}$$
(Eq. 41)

Similarly,

$$r' = W_{NO}a \qquad \text{where, } a = \text{interfacial area per unit volume.}$$
(Eq. 42)

Combining the three equations above gives:

$$k_LC_{NO,i}\frac{X}{\sinh X}\left[1 - \frac{C_{NO,L}}{C_{NO,i}}\cosh X\right] = kC_{NO,L}C_{Na,L}\frac{\varphi}{a} = R_2\frac{C_{NO,L}}{C_{NO,i}}$$
(Eq. 43)

$$\text{where, } R_2 = kC_{NO,i}C_{Na,L}\frac{\varphi}{a}.$$

Rearranging terms to solve for $C_{NO,L}/C_{NO,i}$ gives:

$$\frac{C_{NO,L}}{C_{NO,i}} = \frac{M_1\frac{X}{\sinh X}}{R_2 + M_1\frac{X}{\tanh X}}.$$
(Eq. 44)

Finally, the equation for the overall rate of absorption per unit interfacial area is obtained as:

$$\frac{J_{NO}}{M_1} = \frac{X}{\tanh X}\left[1 - \frac{M_1 \frac{X}{\sinh X \cosh X}}{R_2 + M_1 \frac{X}{\tanh X}}\right].$$ (Eq. 45)

From equation 45 it is possible to determine the rate of absorption depending on different rate determining factors. If it is assumed that the reaction is fast, i.e., k is large, then $\tanh X \sim 1$ and sinhX and coshX tend toward infinity, so that the equation above becomes simply:

$$\frac{J_{NO}}{M_1} = \frac{R_o}{M_1} \text{ or } J_{NO} = R_o = \sqrt{kC_{Na}D_{NO}}\, C_{NO,i}.$$ (Eq. 46)

For the gas film, we can write:

$$J_{NO} = k_g(P_{NO} - P_{NO,i}).$$ (Eq. 47)

At the interface, the relationship between P_{NO} and C_{NO} is given by the distribution coefficient:

$$P_{NO,i} = H_{NO}C_{NO,i}$$ (Eq. 48)

Combining terms from equations 46, 47, and 48 allows us to solve for $P_{NO,i}$ and eliminate $C_{NO,i}$:

$$P_{NO,i} = \frac{k_g P_{NO}}{k_g + \frac{\sqrt{kC_{Na}D_{NO}}}{H}}$$ (Eq. 49)

Upon substituting the above expression into Eq. 47, we arrive at Levenspiel's rate expression for fast pseudo first-order reactions:

$$-r_{NO} = aJ_{NO} = \frac{-1}{V_L}\frac{\delta N_{NO}}{\delta t} = \frac{aP_{NO}}{\frac{1}{k_g} + \frac{H_{NO}}{\sqrt{kC_{Na}D_{NO}}}}.$$ (Eq. 28)

By substituting $\frac{P_{NO}}{H_{NO}} = \frac{N_{NO}}{V_L}$, separating variables, and integrating over time, equation (28) can be written as:

$$-\ln\left(\frac{P_{NO,f}}{P_{NO,i}}\right) = \frac{at}{\frac{1}{H_{NO}k_g} + \frac{1}{\sqrt{D_{NO}kC_{Na}}}}.$$ (Eq. 50)

Rearranging terms, equation 50 can be written as:

$$k_1 = kC_{Na} = \left(\frac{1}{\frac{at}{-\ln\Psi} - \frac{1}{H_{NO}k_g}}\right)^2 \frac{1}{D_{NO/Na}} \quad \text{where, } \Psi = \left(\frac{P_{NO,f}}{P_{NO,i}}\right).$$ (Eq. 51)

Constants in equation 51 can be calculated from correlations found in the literature. In short, a and t are functions of the gas flow rate. H_{NO}, k_g, and D_{NO} depend on temperature. Thus,

the pseudo first-order rate constant, k_1, can be found as a function of concentration, flow rate, and temperature. A sample calculation of k_1 is included in Appendix 6 which begins on page 112.

Results

Values of the rate constant, k_1, ranged from 5.0×10^4 to 7.0×10^6 sec^{-1} over the temperature range, T = 860 to 973°C. At a 90% confidence level, the values for $\ln(k_o)$ and the activation energy are 51.78 ± 0.65 and 372 ± 25 kJ, respectively. The experimental data used to calculate the activation energy are included in Appendix 7 which begins on page 116. Possible sources of error are discussed below.

Sensitivity Analysis

The condition $\frac{1}{H_{NO}k_g} << \frac{at}{-\ln\Psi}$ is true for all of the experimental conditions in this study. Therefore, the value k_1 can be reasonably estimated by:

$$k_1 = \left(\frac{-\ln\Psi}{at}\right)^2 \frac{1}{D_{NO/Na}}. \qquad\qquad (Eq.\ 52)$$

Equation 52 clearly illustrates the relationship between the calculated values for k_1 and the variables Ψ, a, t, and $D_{NO/Na}$. Table 3 includes results from a simple sensitivity analysis which shows the calculated value for k_1 based on a 10% change or doubling of each variable as compared to the conditions used in the sample calculation in Appendix 6. This analysis is provided to show the effect of error in measurement or calculation of the different variables on the rate constant.

In the table, $k_{1,bc}$ = the base case value.

$k_{1,\Delta}$ = the calulated value corresponding to a change in one of the variables.

Table 3. Sensitivity Analysis for Calculation of the Pseudo First-order Rate Constant.

	a (m^{-1})	t (s)	Ψ	$D_{NO/Na}$ (m^2/s)	k_1 (s^{-1})	$k_{1,\Delta}/k_{1,bc}$
Base Case	31.7	0.23	0.42	6.33E-9	2.24E+6	---
a + 10%	**34.9**	0.23	0.42	6.33E-9	1.85E+6	0.83
a x 2	**63.4**	0.23	0.42	6.33E-9	5.59E+5	0.25
t + 10%	31.7	**0.25**	0.42	6.33E-9	1.89E+6	0.85
t x 2	31.7	**0.46**	0.42	6.33E-9	5.59E+6	0.25
Ψ + 10%	31.7	0.23	**0.46**	6.33E-9	1.79E+6	0.80
Ψ x 2	31.7	0.23	**0.84**	6.33E-9	9.03E+4	0.04
$D_{NO/Na}$ + 10%	31.7	0.23	0.42	**6.93E-9**	2.04E+6	0.92
$D_{NO/Na}$ x 2	31.7	0.23	0.42	**1.27E-8**	1.11E+6	0.50

The results shown in Table 3 illustrate the dramatic effect of the NO concentration variable, Ψ. However, it is believed that very little error in the results is actually due to the measurement of the NO concentration because of the excellent sensitivity of the analyzer. The manufacturers report the accuracy of the instrument to be ±1%.

The calculated values of k_1 are linearly proportional to the diffusivity of NO in sodium carbonate, $D_{NO/Na}$, which is primarily a function of temperature and viscosity. It is believed that the error introduced by this variable is negligible, as the temperature measurement and calculation of viscosity are believed to be accurate. Temperature measurement is discussed further in Appendix 3.

Both the interfacial area and residence time have a significant impact on the determination of the rate constant, as $k_1 \alpha$ $(at)^2$. Both of these variables are calculated based on empirical correlations found in the literature which were derived for bubble columns. The large estimated bubble diameter in conjunction with the low volume of salt give rise to very low

values for gas holdup and interfacial area (approximately 0.2 and 30 m^{-1}, respectively). This indicates that the gas phase is not as highly dispersed as typically found in bubble columns.

Ghorpade *et al.* reported values of the interfacial area in the range of 170 to 270 m^{-1} for a 2.54 cm i.d. bubble column operated with superficial velocities in the range of 4.8 to 9.1 cm/s.[63] Ghorpade's conditions were very similar to the conditions in this study with the exception of the height of the column. In Ghorpade's study the height of the column was 90 cm whereas in our work the depth was less than 5 cm. It is feasible that the dispersion of bubbles is simply not well established in the shallow depth of the melt. Thus, it is believed that the majority of error in determining k_l may be due to the calculation of a and t which are primarily dependent on the gas holdup and bubble diameter.

THE RATE OF DEPLETION OF NO BY REACTION WITH MOLTEN SODIUM SALTS[64]

SUMMARY

This article summarized results for the depletion of NO by reaction with molten Na_2CO_3 and mixtures of Na_2CO_3/Na_2S. The data from both reaction systems were fitted to the postulated first-order rate expression which has been discussed in great detail in the previous section.

Previous results showed 10 to 70% conversion of NO by Na_2CO_3 over the temperature range of 860 to 970°C. When Na_2S was added, conversion was found to be 90 to 99.9% over the same temperature range. Calculated activation energies were 89.0 and 41.2 kcal/mol for reaction with Na_2CO_3 and Na_2CO_3/Na_2S mixtures, respectively.

Gas chromatography was used to measure oxygen (O_2) and nitrogen (N_2) concentration in the exit gas stream. Results showed that for reaction with sodium carbonate all of the NO that was depleted could be accounted for as N_2 and O_2 in the exit gas. When sodium sulfide was added to the salt mixture, it was not possible to detect any oxygen in the exit gas; however, all of the nitrogen was still recovered as N_2. It was assumed that the oxygen reacted with Na_2S to form sodium sulfate (Na_2SO_4). Analysis of the sodium mixture by ion chromatography verified this assumption.

Based on the results of the GC analysis, a global mechanism for the depletion of NO by reaction with Na_2CO_3 can be written as $NO \rightarrow \frac{1}{2}N_2 + \frac{1}{2}O_2$. In the presence of Na_2S, the oxygen is consumed to form Na_2SO_4 which can be represented by the stoichiometry: $4NO + Na_2S \rightarrow Na_2SO_4 + 2N_2$. Each of these reactions is thermodynamically feasible over the temperature range, T = 850 to 1150°C.

The Rate of Depletion of NO by Reaction with Molten Sodium Salts

Laura M. Thompson and H. Jeff Empie

Institute of Paper Science and Technology

Atlanta, Georgia

Abstract

Reactions of NO with molten sodium species have been identified as a possible depletion mechanism in a kraft recovery furnace. Experiments have been conducted in which nitric oxide in helium was bubbled through molten sodium carbonate (Na_2CO_3) and mixtures of Na_2CO_3 and sodium sulfide (Na_2S). Results show that the depletion of NO follows a pseudo first order rate expression. The rate of reaction is enhanced by the presence of sodium sulfide. Calculated activation energies are 89.0 and 41.2 kcal/mol for reaction with Na_2CO_3 and Na_2CO_3/Na_2S mixtures, respectively. Analysis of gaseous products indicate that NO is being reduced to nitrogen and oxygen according to the overall stoichiometry:
$NO \rightarrow \frac{1}{2}N_2 + \frac{1}{2}O_2$.

Introduction

The formation of NO_x in a kraft recovery furnace is believed to occur by way of the fuel NO_x formation mechanism. However, it has been estimated that only ~ 25 % of the nitrogen in black liquor is emitted as NO_x from a typical recovery furnace.[1] Thus, the question remains as to the fate of the remaining nitrogen. It is feasible that a portion of the nitrogen does not get oxidized and either remains in the char or is released as a reduced nitrogen species in the flue gas. It is also possible that once NO_x is formed it reacts with other species present in the furnace and is reduced.

In previous papers we presented the concept that the concentration of nitric oxide could potentially be reduced in a recovery furnace by reacting with molten sodium species.[2,3] Experiments were conducted in which nitric oxide in helium was bubbled through molten sodium carbonate (Na_2CO_3). Results showed that NO was reduced by 10 to 75% over the temperature range of 860 to 973°C.[3] The rate of depletion was shown to follow a pseudo first order rate expression as follows:

$$-r_{NO} = -\frac{1}{V_L}\frac{\delta N_{NO}}{\delta t} = \frac{aP_{NO}}{\frac{1}{k_g} + \frac{H_{NO}}{\sqrt{D_{NO/Na}k_1}}}.$$

(Eq. 1)

Upon integration and rearranging terms, equation (1) can be written as:

$$k_1 = \left(\frac{1}{\frac{at}{-\ln\Psi} - \frac{1}{H_{NO}k_g}}\right)^2 \frac{1}{(D_{NO/Na})} \quad (\text{sec}^{-1}) \text{ where, } \Psi = P_{NO,f}/P_{NO,i}.$$

(Eq. 2)

Constants in equation (2) are calculated from correlations found in the literature. In short, a and t are functions of the gas flow rate. H_{NO}, k_g, and $D_{NO/Na}$ are dependent on temperature. Thus, the pseudo first order rate constant can be found as a function of concentration, flow rate, and temperature. A complete list of equations and notation is included at the end of the paper.

The derivation of equation (1) assumes the reaction to be first order with respect to NO.[4] Data verifying this assumption will be presented here. This paper also presents results of experiments investigating the reaction of NO with mixtures of Na_2CO_3 and sodium sulfide (Na_2S). In addition to the rate data, analysis of the gaseous products has been conducted by on-line gas chromatography to determine the products of the reaction.

Experimental Apparatus

A schematic of the experimental apparatus is shown below in Figure 1. Helium and a mixed gas of nitric oxide in helium are fed from pressurized gas cylinders. Flow is measured by Hastings-Teledyne™ digital mass flowmeters and is controlled manually by needle valves. The gas is fed to the reaction chamber (Figure 2) which is described in detail below. Exit gas from the system is analyzed by a chemiluminescent NO_x analyzer (Thermo Environmental™ Model 10AR). A Carle™ Model 8000 Basic Gas Chromatograph equipped with a six port sampling valve was used for detection of oxygen (O_2) and nitrogen (N_2) in the exit gas. The GC was fitted with a 15 foot x 1/8 inch stainless steel column packed with Carboxen™ 1000. The column and inlet temperatures were held constant at approximately 40°C. Chromatographic grade helium was used as the carrier gas at a flow rate of 28 ml/min. The sample loop on the sampling valve had a volume of 1.0 ml.
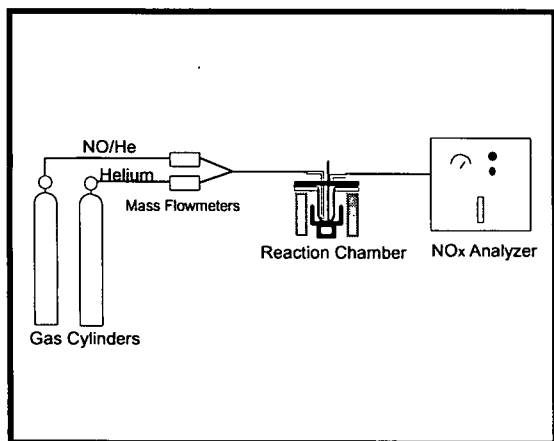
Figure 1: Experimental Apparatus
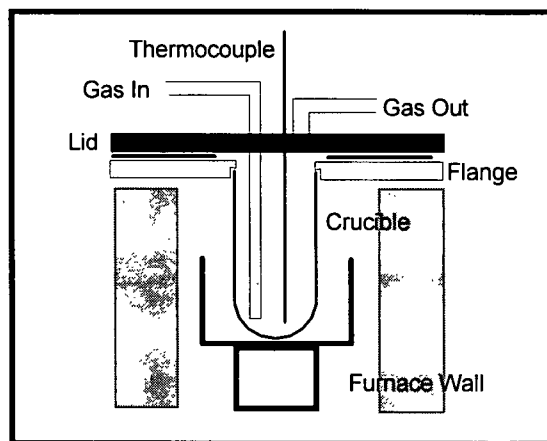
Figure 2: Reaction Chamber

Molten salt is contained in a 4 cm x 10 cm alumina crucible which is cemented to a stainless steel flange. A graphite gasket is placed between the flange and the lid which is held in place by eight bolts to form a gas-tight seal. The reaction vessel is heated by a tube furnace. Gases are bubbled through the salt using a 0.4 cm ID alumina tube. A type-K thermocouple, protected by an alumina well, is used to measure the temperature of the molten salt. The mass flowmeters, thermocouple, and NO_x analyzer are connected to a personal computer for data acquisition. Data are acquired at a rate of 0.5 Hz.

Experimental Conditions

The independent variables for each experiment include: gas flow rate, NO concentration, temperature, and the mass of each salt. The experimental conditions for each run are listed below in Tables 1, 2, and 3. The first set of experiments was conducted to verify the assumption of the first order behavior with respect to the concentration of NO. For the second set of experiments, the exit gases were analyzed by on-line GC. The third set of experiments was conducted to compare the rate of reaction for mixtures of Na_2CO_3/Na_3S with the results for Na_2CO_3 only. On-line GC analysis was conducted for all of the experiments with the mixed salts. For experiments where samples were analyzed by GC, three to five replicate samples were analyzed at each set of conditions.

Table 1: Experimental Conditions For Determining Order of Reaction With Respect to [NO].

Experiment	Total Flow Rate (L/min)	$[NO]_{in}$ (ppm in helium)	Temperature (°C)	Mass of Na_2CO_3 (g)	Mass of Na_2S (g)
1	1.3	2700-8400	864-946	35.0	---
2	1.3	2700-8400	868-954	35.0	---
3	1.3	2000-9400	883-890	38.0	2.0
4	1.3	2000-9400	895-912	38.0	2.0

Table 2: Experimental Conditions For Depletion of NO by Na_2CO_3 With Gas Analysis by GC.

Experiment	Total Flow Rate (L/min)	$[NO]_{in}$ (ppm in helium)	Temperature (°C)	Mass of Na_2CO_3 (g)	Mass of Na_2S (g)
5	1.1	8400	887-961	30.0	---
6	1.1	8400	897-962	30.0	---
7	1.0	8400	894-966	40.0	---
8	1.0	8400	905-962	40.0	---
9	1.2	8400	910-946	25.0	---
10	1.3	9600	889-951	40.0	---

Table 3: Experimental Conditions For Depletion of NO by Mixtures of Na_2CO_3 and Na_2S With Gas Analysis by GC.

Experiment	Total Flow Rate (L/min)	[NO]$_{in}$ (ppm in helium)	Temperature (°C)	Mass of Na_2CO_3 (g)	Mass of Na_2S (g)
11	1.3	9600	887-934	40.0	1.5
12	1.3	9600	860-914	40.0	1.5
13	1.3	9600	878-920	40.0	1.5
14	1.0	9600	878-917	35.0	1.3
15	1.0	9600	879-914	35.0	1.3
16	1.1	9600	882-915	30.0	2.0
17	1.1	9600	864-928	30.0	2.0
18	0.92-1.3	9600	870-916	37.0	3.0

Results

To verify that the depletion of NO is first order with respect to [NO], experiments were conducted in which the inlet concentration was varied between 2000 to 9400 ppm at a constant temperature. This was repeated at several temperatures between 860 to 955°C for reactions with Na_2CO_3 and a mixture of Na_2CO_3 and Na_2S. The results of these experiments were plotted as conversion vs. inlet concentration. The data are shown below in Figures 3 and 4. The percent conversion is defined as:

$$X = 100\left(1 - \frac{[NO]_f}{[NO]_i}\right).$$
(Eq. 3)

Tav = 870, Xav = 14.4 ▼ Tav = 917, Xav = 39.5 ● Tav = 954, Xav = 63.9
□ Tav = 868, Xav = 10.5 ▽ Tav = 907, Xav = 35.6 ○ Tav = 945, Xav = 56.1

■ Tav= 889.6, Xav=96.8 ▽ Tav = 896.2, Xav=98.8 ● Tav = 910.8, Xav=99.2
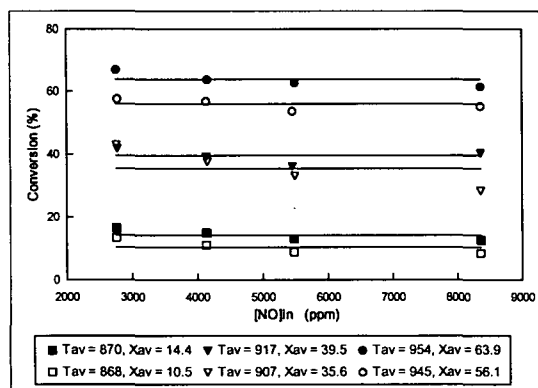
Figure 3: Conversion of NO is Independent of Inlet Concentration. Data From Experiments 1 and 2. Reactant: Na_2CO_3.
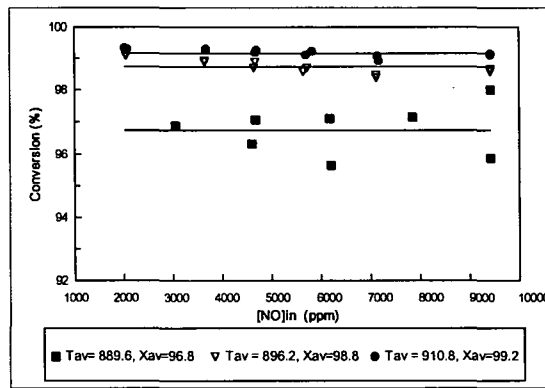
Figure 4: Conversion of NO is Independent of Inlet Concentration. Data From Experiments 3 and 4. Reactant: Na_2CO_3/Na_2S Mixture.

Inspection of Figures 3 and 4 shows constant conversion over the range of inlet concentrations at each temperature. This behavior is indicative of a first order reaction. It should also be noted that much higher conversions are observed for the reactions with the mixed salt.

The gas chromatograph was calibrated using a certified gas mix standard of 5100 ppm O_2 and 5040 ppm N_2 in UHP helium. By mixing the standard with NO in helium, the GC was calibrated at five concentrations between 0 to 5100 ppm O_2, 0 to 5040 ppm N_2, and 0 to 4600 ppm NO. The peak areas for nitrogen were linear with respect to concentration. It was found that the presence of nitric oxide reduces the peak area for oxygen. Therefore, a multiple linear regression for peak area as a function of NO and O_2 concentration was used. Typical results from the regression analyses are as follows:

For Nitrogen: Peak Area = 9.40 x $[N_2]$ (R-squared = 0.975)   (Eq. 4)

For Oxygen: Peak Area = 7.05 x $[O_2]$ - 2.13 x [NO]   (R -squared = 0.953)   (Eq. 5)

It should be noted that at low peak areas for O_2 and/or high concentrations of NO, the multiple regression model will over predict the O_2 concentration.
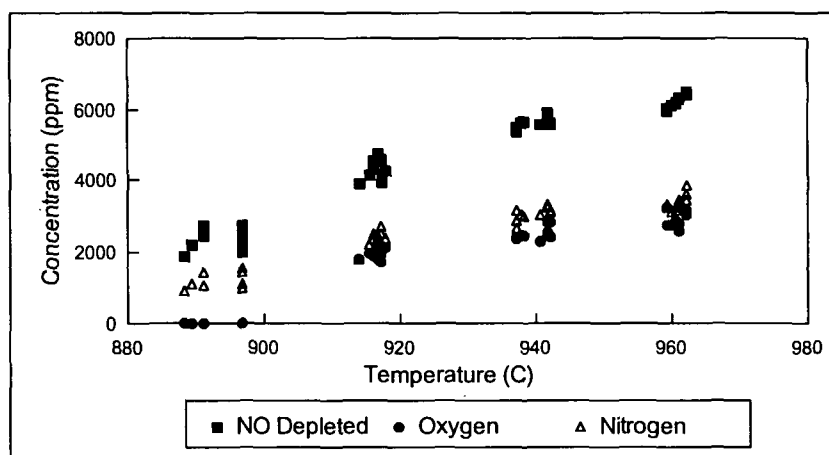
Figure 5: GC Analysis of Exit Gas For Experiments 5 and 6.

Figure 5 shows the amount of NO depleted (NO_{in} - NO_{out}) and the exit gas concentrations for oxygen and nitrogen for experiments 5 and 6. These data show that over the temperature range 890 to 965°C, the O_2 and N_2 concentrations are approximately equal to each other and approximately half of the NO concentration that was depleted. This indicates that the NO is being reduced completely to N_2 and O_2 which can be represented by the stoichiometric equation : NO = ½ N_2 + ½ O_2. By assuming this stoichiometry, the percent recovery for each species can be calculated as follows:

$$\% \text{ Recovery} = 100 * 2 * [O_2 \text{ or } N_2] / [NO]_{depleted}. \qquad \text{(Eq. 6)}$$

Figures 6 and 7 show the percent recovery of each species for experiments 5 through 10. The data shown in Figures 6 and 7 are summarized in Table 4. The percent recovery is reported as the average for each experiment plus or minus one standard deviation.
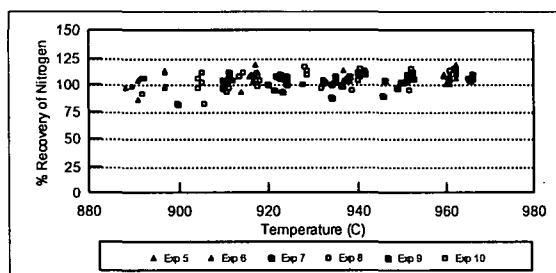
Figure 6: Recovery of NO as Nitrogen (N_2).
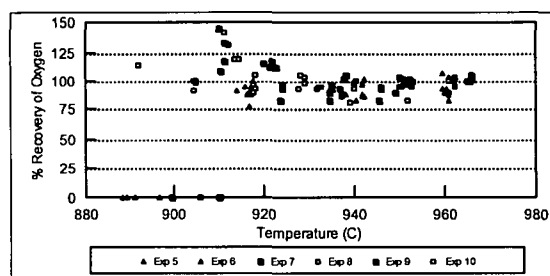
Figure 7: Recovery of NO as Oxygen (O_2).

Table 4: Recovery of NO as Nitrogen and Oxygen For Experiments 5 - 10.

Experiment	5	6	7	8	9	10
% Recovery as N_2	103.5 ± 6.3	109.8 ± 5.3	103.9 ± 6.4	107.2 ± 8.5	102.2 ± 6.3	102.7 ± 4.4
% Recovery as O_2	89.8 ± 5.8	92.6 ± 6.4	103.8 ± 7.1	102.0 ± 13.7	99.2 ± 17.0	97.2 ± 5.8

The third set of experiments (11-18) was conducted to determine the rate of depletion of NO by reaction with mixtures of Na_2CO_3 and Na_2S. During these experiments the exit gas was also analyzed by on-line GC. In the presence of sodium sulfide it was not possible to detect any oxygen in the exit gas. It was therefore assumed that the oxygen was reacting with sulfide to form sodium sulfate. Results of analysis of the salts from experiments 16 and 17 is shown below in Table 5. These results verify the assumption of complete conversion of all sulfide to sulfate with minor amounts of thiosulfate indicated.

Table 5: Analysis of Na_2CO_3/Na_2S Mixtures After Exposure To Nitric Oxide. All Concentrations are Reported as Percent by Weight. Results Indicate Complete Conversion of Sodium Sulfide to Sodium Sulfate. ND Indicates Not Detectable.

Ion	Experiment 16	Experiment 17
Sulfite, SO_3^-	-ND-	-ND-
Thiosulfate, $S_2O_3^-$	0.04 %	0.02 %
Sulfate, SO_4^-	6.38 %	6.26 %
Carbonate, CO_3^-	54.25 %	51.34 %
Sodium, Na^+	40.4 %	44.6 %
Total	101.07 %	102.22 %

By assuming the overall reaction: $4NO + Na_2S \rightarrow Na_2SO_4 + 2N_2$, it is possible to calculate the rate of depletion of Na_2S as a function of the amount of NO depleted. Figure 8 shows the measured values of the NO concentration along with the calculated values for total NO consumed and total Na_2S remaining as a function of time for experiment 15.
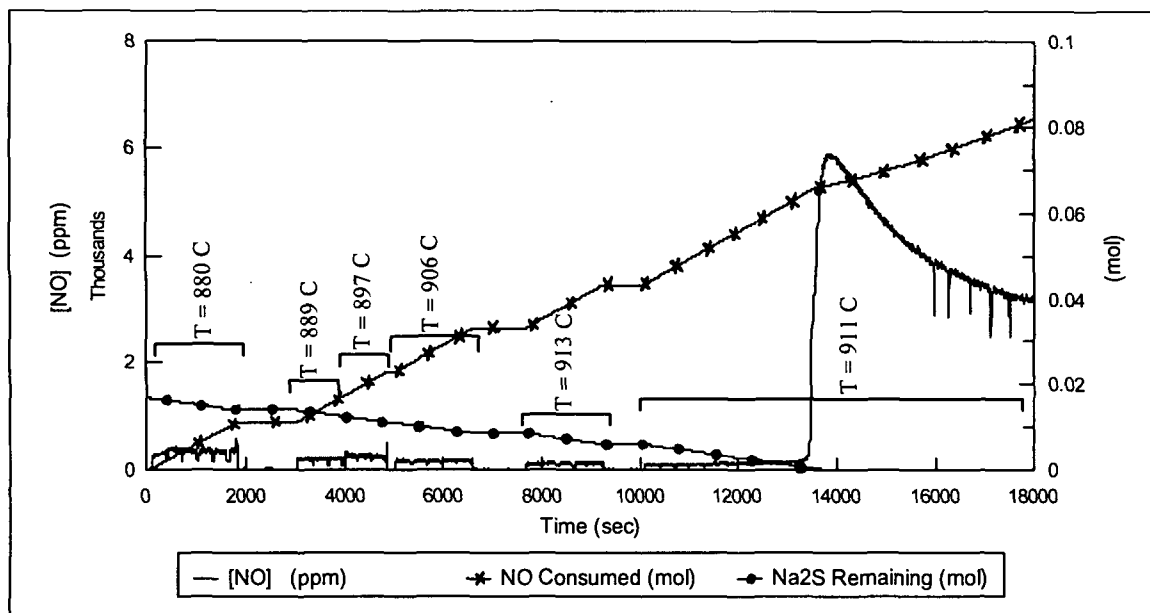
Figure 8: Depletion of NO by Reaction with Molten Na_2CO_3/Na_2S; Experiment 15.

Inspection of Figure 8 reveals several interesting points:

- When all of the sodium sulfide has reacted (Na_2S remaining = 0) there is a sudden rise in the concentration of NO. This indicates a shift in the reaction mechanism upon total consumption of Na_2S.

- GC analysis of gas samples analyzed after this point show the presence of oxygen (O_2) in equal proportion to N_2. This also supports the concept that the sulfide has been completely oxidized.

- As long as Na_2S is present, the concentration of NO is constant at any given temperature independent of the concentration of Na_2S. Just before the sulfide is completely consumed, the NO concentration starts to change. This supports the concept that the reaction is pseudo first order as long as there is at least approximately 0.002 mol of Na_2S in the melt.

Equation 2 was used to calculate values for k_1 over the temperature range, T= 860 to 934°C, for experiments 11 through 17. These results were then used to calculate the activation energy (E_a) and the pre-exponential factor (k_o) by plotting $\ln(k_1)$ vs. 1/T as shown in Figure 9.
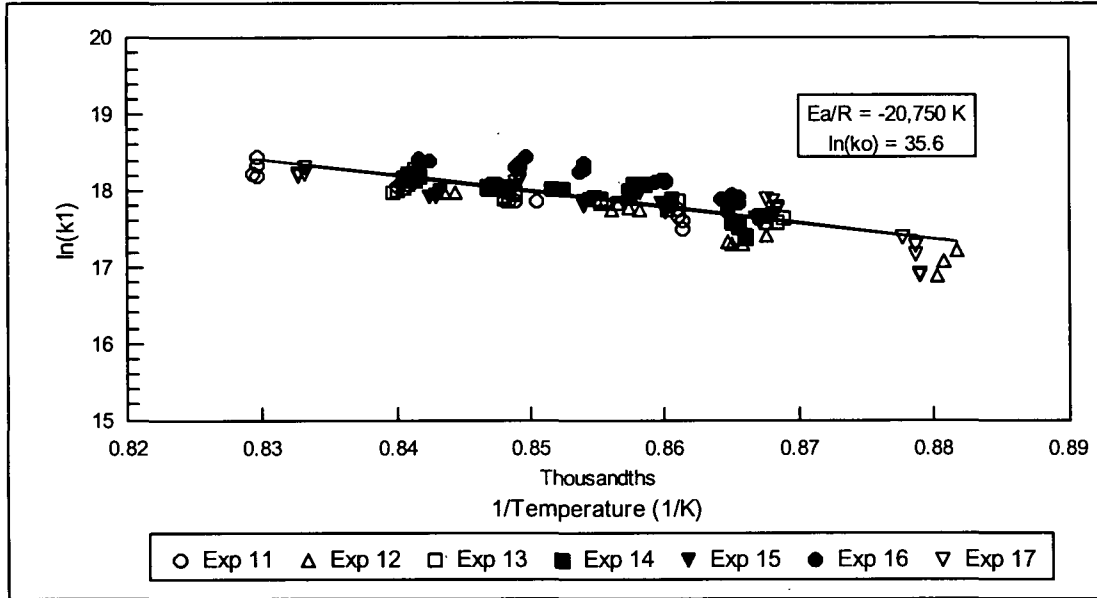
Figure 9: Determination of Activation Energy for Depletion of NO by Na_2CO_3/Na_2S Mixtures. Experiments 11-17.

Based on the results in Figure 9, the slope, $-E_a/R$, and intercept, $\ln(k_o)$, were found to be -20,750 ± 2457 K and 35.63 ± 0.37, respectively. These results are reported at a confidence level of 95%. Thus, the pseudo first order rate constant, k_1, may be written as: $k_1 = 2.98 \times 10^{15} \, e^{-20,750/T} \, (s^{-1})$.

With values for the rate constant it becomes possible to predict the exit gas concentration as:

$$[NO]_f = [NO]_i \times \exp\left(-\frac{at}{\frac{1}{H_{NO}k_g}+\frac{1}{\sqrt{D_{NO/Na}k_1}}}\right).$$ (Eq. 7)

This expression was used to compare predicted values for NO concentration with the measured values. Results of this comparison are shown in Figures 10A-D for experiments 13, 14, 17, and 18. Inspection of Figures 10A-D shows excellent agreement between the experimental and predicted values for the concentration of NO in the exit gas over a wide range of experimental conditions.

(A)

(B)

(C)

(D)
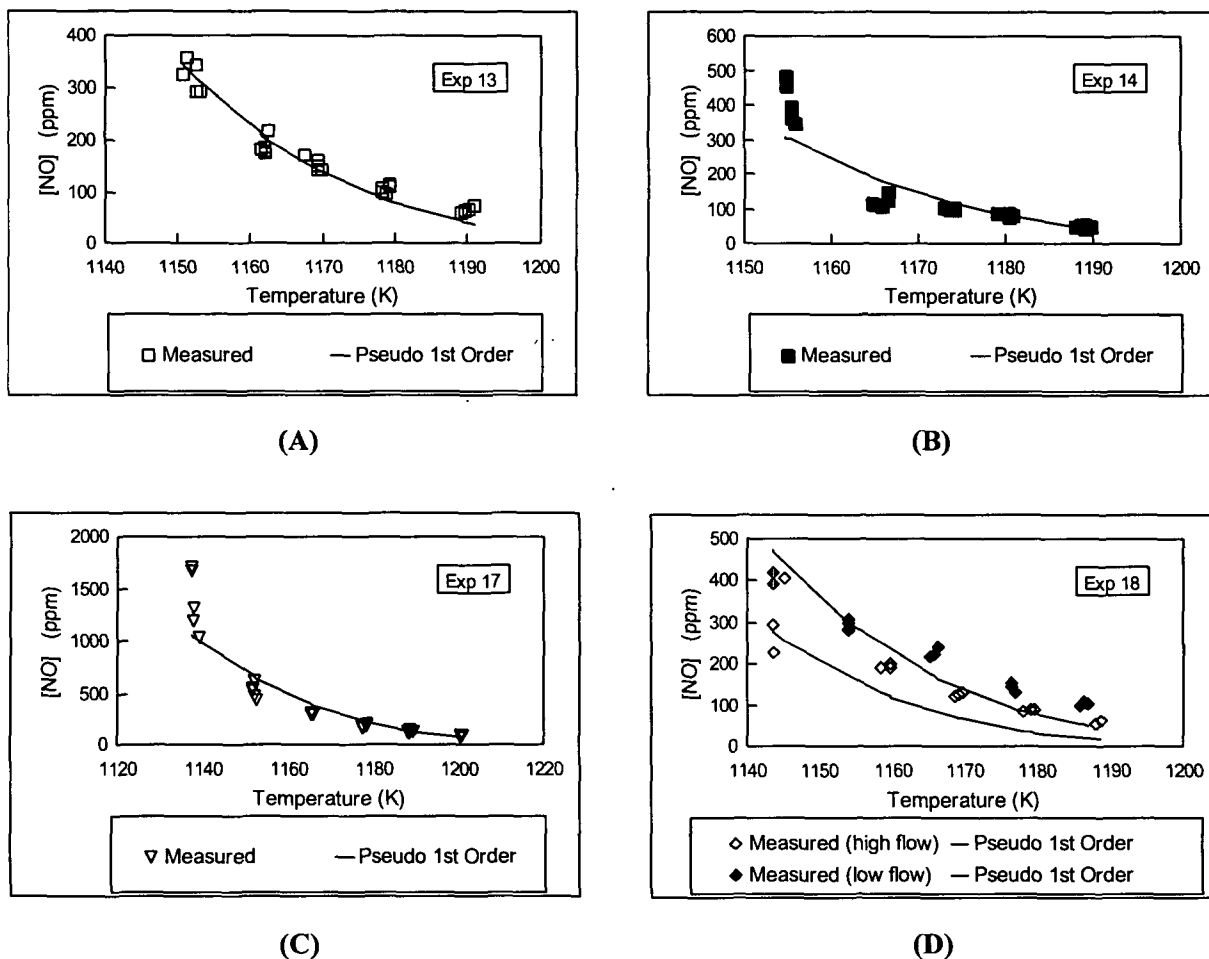
Figure 10: Comparison of Predicted and Measured Values for Concentration of Nitric Oxide in Exit Gas; Experiments 13,14,17 and 18. $[NO]_{in}$ = 9600 ppm for Each Experiment.

Discussion/Conclusions

The rate of depletion of nitric oxide by reaction with molten Na_2CO_3 and Na_2CO_3/Na_2S has been shown to follow a pseudo-first order rate expression. A comparison of the two systems is summarized in Table 6 below. The results show the depletion of NO to be greatly enhanced by the presence of Na_2S.

Table 6: A Comparison of Kinetic Parameters for the Depletion of NO by Reaction with Na_2CO_3 and Na_2CO_3/Na_2S Mixtures.

Reactant	Temperature Range (°C)	% Conversion of NO	E_a/R (°K)	k_1 at T = 900 °C (s⁻¹)
Na_2CO_3	860-973	10-75	44,780	8.14×10^5
Na_2CO_3/Na_2S	860-934	90-99.9	20,750	6.19×10^7

It is not clear at this point what the mechanism for the reaction is; however, analysis of the exit gas shows that all of the NO that is depleted can be detected as O_2 and N_2. It is feasible that a nitrite or nitrate intermediate is formed which then thermally decomposes to nitrogen and oxygen. In the presence of sulfide, the oxygen is consumed forming sodium sulfate. Because the rate is independent of the concentration of Na_2S, the consumption of Na_2S does not affect the rate of reaction until nearly all of the sulfide has been oxidized.

These reaction data coupled with an aerosol (fume) formation model should be able to predict the amount of depletion that occurs in the upper region of a recovery furnace. However, it should be noted that it is not known what affect other gases (e.g. H_2O, O_2, CO, CO_2, SO_x) may have on the rate of depletion of NO.

Acknowledgments

Equations

(Eq. 8)[5] $a = \frac{6\varepsilon}{d_b}$

(Eq. 9)[6] $\varepsilon = 0.5\left(\frac{U_{br}}{\sqrt{gR_c}}\right)^{0.4}\left(\frac{U_{gs}}{U_{br}}\right)^{0.8}$

(Eq. 10)[7] $d_b = \left[\left(\frac{\alpha\gamma D_t}{\Delta\rho g}\right)^2 + 9.5\left(\frac{V_g^2 D_t}{g}\right)^{0.867}\right]^{\frac{1}{6}}$

(Eq. 11)[8] $D_{NO/He} = \frac{10^{-4}\left(1.084 - 0.249\sqrt{1/M_{NO}+1/M_{He}}\right)T^{1.5}\sqrt{1/M_{NO}+1/M_{He}}}{P_t(r_{NO/He})^2 f\left(\frac{kT}{\varepsilon_{AB}}\right)}$

(Eq. 12)[9] $D_{NO/Na} = \frac{\left(117.3\times10^{-18}\right)(\varphi M_{Na})^{0.5}T}{\mu\upsilon^{0.6}}$

(Eq. 13)[10] $k_g = \frac{D_{NO/He}P_t}{RTzP_{He,m}}$

(Eq. 14)[11] $k_L = 0.42\left(\frac{D_{NO/Na}}{d_b}\right)\left(\frac{d_b^3\, g\rho^2}{\mu^2}\right)^{\frac{1}{3}}\left(\frac{\mu}{\rho D_{NO/Na}}\right)^{0.5}$

(Eq. 15)[12] $K_H = \frac{\exp\left(\frac{-4\Pi Nr^2\gamma}{8.314T}\right)}{82.06T}$

Physical properties of molten sodium carbonate can be calculated as a function of temperature according to the following:

(Eq. 16)[13] $\rho = 2.4797 - 0.4487 * 10^{-3}\, T$ (g/cm³)

(Eq. 17)[13] $\mu = 3.832 * 10^{-5} \exp(13215/T)$ (cp)

(Eq. 18)[14] $\gamma = (254.8 - 0.0502\, t)/1000$ (N/m), t = temperature (°C)

Notation

a = interfacial area per unit volume (cm²/cm³)

A = solute gas

$[A^*]$ = interfacial concentration of A (mol/cm³)

B = non-volatile reactant

$[B_o]$ = concentration of B in the bulk (mol/cm³)

C_{Na2CO3} = concentration of molten Na_2CO_3 (mol/cm³)

C_{NO} = concentration of NO in liquid film (mol/cm³)

d_b = bubble diameter (cm)

$D_{NO/He}$ = diffusivity of NO in Helium (m²/s)

$D_{NO/Na}$ = diffusivity of NO in Na_2CO_3 (m²/s)

D_t = outside diameter of purge tube (m)

Ea = activation energy (J/mol)

$f(kT/\varepsilon_{AB})$ = collision function (= 0.31) (Treybal[10], p. 32)

g = gravitational constant = (9.81 m/s)

H_{NO} = phase distribution coefficient (atm cm³/mol)

k = second order rate constant (mol/cm^3 s)
k_0 = pre-exponential factor (1/s)
k_1 = pseudo first order rate constant (1/s)
K_H = Henry's Law constant (mol/cm^3 atm)
m = order of reaction with respect to A
m_{Na} = mass of Na_2CO_3 (g)
M_i = molecular weight of species, i
n = order of reaction with respect to B
N = Avogadro's number = (6.022×10^{23})
N_{NO} = moles of NO (mol)
$[NO]_f$ = exit concentration of NO (ppm)
$[NO]_i$ = inlet concentration of NO (ppm)
$P_{He,m}$ = log mean pressure of helium (atm)
P_{NO} = partial pressure of NO (atm)
P_t = total pressure (atm)
r = molecular radius (m)
$-r_{NO}$ = rate of depletion of NO based on volume of liquid (mol/cm^3 s)
$r_{NO/He}$ = molecular separation at collision (nm)
R = universal gas constant = $(8.314$ m^3 J/mol K)
R_c = radius of column = $(0.02$ m)
t = time (s)
T = absolute temperature (K)
U_{br} = bubble rise velocity (m/s)
U_{gs} = superficial gas velocity (m/s)
V = flow rate of gas (cm^3/s)
V_g = flow rate of gas (m^3/s)
V_l = volume of molten salt (cm^3)
X = percent conversion of NO
z = film thickness = $(10^{-4}$ m) (estimated)
α = correlation factor (assumed 30)
ε = gas hold up
ϕ = association factor for solvent = 1
v_{NO} = solute molal volume at boiling point (= 0.0236 m^3/kmol)

References

1. Nichols, K.M., and Lien, S.J. Formation of Fuel NO$_x$ During Black Liquor Combustion, Tappi Journal, 76(3):185(1993).

2. Thompson, L.M., and Empie, H.J. A Proposed Mechanism for the Depletion of NO$_x$ in a Kraft Recovery Furnace, Proceedings of the 1993 TAPPI Environmental Conference, Boston, MA, 643-647(1993).

3. Thompson, L.M., and Empie, H.J. Kinetics of NO Depletion by Reaction with Molten Sodium Carbonate, AIChE Symposium Series, Volume 90:33-38(1994).

4. Levenspiel, O. Chemical Reaction Engineering, 2nd Edition, Chapter 13: Fluid-Fluid Reactions, John Wiley & Sons, New York, 1972.

5. Treybal, R.E. Mass-Transfer Operations, 3rd Edition, McGraw-Hill Book Company, New York, 1980, p.144.

6. Cheremisinoff, N.P. Encyclopedia of Fluid Mechanics, Volume 3: Gas-Liquid Flows, Gulf Publishing Company, Houston, 1986, p.1199.

7. Cheremisinoff, N.P. Encyclopedia of Fluid Mechanics, Volume 3: Gas-Liquid Flows, Gulf Publishing Company, Houston, 1986, p.228.

8. Treybal, R.E. Mass-Transfer Operations, 3rd Edition, McGraw-Hill Book Company, New York, 1980, p.31.

9. Treybal, R.E. Mass-Transfer Operations, 3rd Edition, McGraw-Hill Book Company, New York, 1980, p.35.

10. Treybal, R.E. Mass-Transfer Operations, 3rd Edition, McGraw-Hill Book Company, New York, 1980, p. 45.

11. Cussler, E.L. Diffusion: Mass Transfer in Fluid Systems, Cambridge University Press, New York, 1984, p.230.

12. Andresen, R.E. Journal of the Electrochemical Society, 328-334(1979).

13. Janz, G.J., Dampier, F.W., Lakshminarayanan, G.R., Lorenz, P.K., and Tomkins, R.P.T. Molten Salts: Volume 1, Electrical Conductance, Density, and Viscosity Data, National Standard Reference Data Series-National Bureau of Standards 15, October, 1968.

14. Janz, G.J., Lakshminarayanan, G.R., Tomkins, R.P.T., and Wong, J. Molten Salts: Volume 2, Section 2: Surface Tension Data, National Standard Reference Data Series-National Bureau of Standards 28, August, 1969.

DISCUSSION

In the article, it was concluded that the conversion of NO is independent of the inlet

concentration of NO, and therefore, the reaction is considered first-order with respect to [NO].

Visual inspection of the data presented in Figures 3 and 4 in the article show a slight negative

slope. Linear regression of the data gives values of the slope ranging from -2.0×10^{-4} to

-8.6×10^{-4} $[NO]^{-1}$. However, considering the values of the standard error, the confidence

intervals for the slope always include zero. Therefore, at a 90% confidence level, it is

statistically sound to conclude that the data can be represented by a zero slope. The raw data for

these experiments are included in Appendix 8 which begins on page 125.

Gas chromatography was used to measure the concentration of oxygen (O_2) and nitrogen

(N_2) in the exit gas stream. Results showed that for reaction with sodium carbonate all of the NO

that was depleted could be accounted for as N_2 and O_2 in the exit gas. Based on the results of the

GC analysis, a global mechanism for the depletion of NO by reaction with Na_2CO_3 can be written

as:

$$NO \rightarrow \tfrac{1}{2}N_2 + \tfrac{1}{2}O_2 . \qquad \text{(Eq. 53)}$$

It is not possible to determine intermediate reaction steps based on these experiments. It

is feasible that a nitrite or nitrate intermediate is formed which then thermally decomposes to

nitrogen and oxygen. It is also conceivable that the sodium carbonate is not a reactant, but acts

as a catalyst.

When sodium sulfide was added to the salt mixture, it was not possible to detect any

oxygen in the exit gas; however, all of the nitrogen was still recovered as N_2. It is believed that

the NO reacts to form N_2 and O_2 followed by reaction of oxygen with Na_2S to form sodium

sulfate (Na_2SO_4). Thus, the depletion of NO by Na_2S/Na_2CO_3 mixtures could be represented as:

$$NO \rightarrow \tfrac{1}{2}N_2 + \tfrac{1}{2}O_2, \text{ followed by}$$ (Eq. 53)

$$Na_2S + 2O_2 \rightarrow Na_2SO_4.$$ (Eq. 54)

These two steps can be represented by the overall stoichiometry:

$$4NO + Na_2S \rightarrow Na_2SO_4 + 2N_2.$$ (Eq. 55)

Analysis of the sodium mixture by ion chromatography verified the formation of sodium sulfate.

All of the experimental data for experiments conducted with gas analysis by GC are included in

Appendix 9 which begins on page 131. The GC calibration data are in Appendix 10 which

begins on page 154.

Comparison of Reaction Rate Data

The article presented a comparison of the kinetic rate data for the two systems which is

repeated below in Table 4. The data used for the determination of the pseudo first-order rate

constant for the depletion of NO by Na_2CO_3 and Na_2CO_3/Na_2S mixtures are included in

Appendices 7 and 9, respectively. For depletion of NO by Na_2CO_3/Na_2S mixtures, results

showed $\ln(k_o)$ and Ea to be 35.63 ± 0.30 and 172 ± 17 kJ/mol, respectively. These values are

reported at a confidence level of 90%.

Table 4. A Comparison of Kinetic Parameters for the Depletion of Nitric Oxide.

Reactant	Temperature Range (°C)	Activation Energy, E_a (kJ/mol)	(kcal/mol)	Pre-exponential Constant, k_o (sec^{-1})	k_1 at T = 900°C (sec^{-1})
Na_2CO_3	860-973	372	89.0	3.09×10^{22}	8.14×10^5
Na_2CO_3/Na_2S	860-934	172	41.2	2.98×10^{15}	6.19×10^7

Inspection of Table 4 shows the pre-exponential constant for the reaction with Na_2CO_3 to be approximately seven orders of magnitude higher than for the Na_2CO_3/Na_2S system. Based on collision theory, the pre-exponential constant, also known as the frequency factor, is proportional to the size of the reactants as follows:[57]

$$k_o \propto \frac{(\sigma_A + \sigma_B)^2}{2}, \text{ where } \sigma = \text{diameter of molecule, (cm).} \qquad \text{(Eq. 56)}$$

Because Na_2S and Na_2CO_3 are both ionic compounds with the same cations (Na^+), it is possible that the difference in reactivity is due to the different anions, S^{2-} and CO_3^{2-}. The S^{2-} ion is spherical and has an ionic radius of 170 pm.[65] Because CO_3^{2-} is a nonspherical ion, it is not possible to determine the ionic radius. However, Huheey discusses a technique in which an apparent ionic radius can be calculated based on measurements of the lattice energy of compounds containing the nonspherical ion.[65] The apparent, or thermochemical, radius for CO_3^{2-} is reported as 185 pm.[65] Reaction of NO with the larger CO_3^{2-} ion would tend to give higher a frequency factor than the S^{2-} ion. However, the relatively small difference in size does not account for the vast difference in the experimentally determined values for k_o.

It is not clear from these experiments what is responsible for the enhanced rate of reaction when Na_2S is added to the system. If both salts act as catalysts, it is feasible that the Na_2S is simply a better catalyst for promoting the NO depletion reaction (Eq. 53). Another possibility is that the reaction rate is enhanced by the removal of O_2 from the system by reaction with Na_2S.

Additional graphs showing predicted and measured values for the concentration of NO in the exit gas are in Appendix 11 which begins on page 163. Calculated values of the free energy of reaction, ΔG_{rxn}, for the overall depletion reactions are included in Appendix 12 which begins on page 168.

Error Analysis

The methods used in determing the rate constants were essentially the same for Na_2CO_3 and Na_2CO_3/Na_2S mixtures. As discussed previously, it is believed that the majority of error is introduced in calculating the gas holdup and interfacial area. For the Na_2CO_3/Na_2S system, additional error may be introduced by the values used for the physical properties of the salt, which were based on sodium carbonate only. While the mass fractions of Na_2S were typically on the order of 5%, it is not believed that the physical properties of the mixtures are much different than for pure Na_2CO_3.

THE FATE OF NITROGEN IN A KRAFT RECOVERY FURNACE[44]

SUMMARY

The paper presented results of nitrogen analysis of samples taken from two commercial kraft recovery furnaces. Samples that were analyzed included black liquor, economizer deposits, ESP saltcake, smelt, weak wash, green liquor, dregs, and slaker grits. The results were used to perform a nitrogen mass balance around the recovery furnace.

Results of the mass balance indicate that ~ 9 to 31% of the nitrogen in the black liquor leaves the furnace in the smelt. Less than 0.1% of the black liquor nitrogen can be accounted for in some form of deposit (tube deposits or fume captured in the ESP). It was assumed that 25% of the nitrogen was emitted as NO_x in the flue gas, which corresponds to a flue gas concentration of 50 ppm based on dry volume. The remaining 44 to 66% of the black liquor nitrogen was assumed to leave the furnace in the form of molecular nitrogen (N_2).

Green liquor dregs were shown to have a nitrogen content ranging from 37 to 100 ppm. However, due to the low mass flow rate of dregs, the disposal of dregs would not be considered a significant purge point for nitrogen.

All of the nitrogen analysis was conducted using an Antek Instruments™, Inc. Model 7000N/S analyzer. The analyzer employs an oxygen rich combustion environment at 1100°C to convert all forms of nitrogen in the sample to nitrogen oxides which are detected by chemiluminescence. The paper presents a comparison of this method to the more common Kjeldahl method for nitrogen analysis.

The Fate of Nitrogen in a Kraft Recovery Furnace

L.M. Thompson
Graduate Student

D.M. Martin
Graduate Student

H.J. Empie
Professor of Engineering

E.W. Malcolm
Professor of Engineering

Institute of Paper Science and Technology
Atlanta, Georgia

M. Wood
Process Engineer
Georgia-Pacific Corporation
Ashdown, Arkansas

ABSTRACT

Samples taken from the kraft recovery furnaces at the Georgia-Pacific Corporation's Ashdown, Arkansas mill have been analyzed for total nitrogen content. Results have been used to perform a nitrogen mass balance around the recovery furnace. Approximately 9% of the nitrogen found in the black liquor leaves the furnace in the smelt. Less than 0.1% of the black liquor nitrogen can be accounted for in some form of deposit. If 25% is emitted as NO_x in the flue gas, the remaining 66% is presumed to leave in the flue gas as molecular nitrogen (N_2).

Keywords: Black Liquor, Combustion, Deposit, Emission, Fume, Nitrogen, Nitrogen Oxides, NO_x, Recovery Furnace, Smelt.

INTRODUCTION

As mills become more concerned with NO_x emissions, it becomes increasingly important to understand as much as possible about nitrogen chemistry in a kraft recovery furnace. Ongoing student research at the Institute of Paper Science and Technology has been focused on understanding factors affecting the release of black liquor nitrogen during pyrolysis and potential *in situ* NO_x depletion mechanisms.

Nitrogen oxides (NO_x) can be formed during combustion in the presence of nitrogen. The thermal NO_x mechanism accounts for oxidation of atmospheric nitrogen (N_2). This mechanism requires extremely high temperatures which are typically not obtained during the combustion of black liquor. Several papers addressing recovery furnace NO_x emissions have concluded that the majority of NO_x is fuel NO_x, formed from the oxidation of nitrogen in the black liquor.[1-3] The concentration of nitrogen in black liquor solids is typically on the order of 0.1%.[1]

Considering a mass balance around a recovery furnace, the exit streams consist of the flue gas, particulates, and the smelt. It has been shown that conversion of only 25% of the nitrogen in the black liquor can account for the level of NO_x measured in the flue gas from furnaces.[3] Thus, the question arises as to the fate of the remaining nitrogen.

It is understood that sodium species react with SO_2 in the upper region of the furnace forming sodium sulfate (Na_2SO_4) which is captured in the electrostatic precipitators.[4] These reactions act as a scrubbing mechanism and essentially control SO_2 emissions from recovery furnaces. It has been suggested that similar reactions could occur between sodium compounds and nitric oxide (NO) forming sodium nitrate.[5] If such reactions do occur, one would expect to find nitrogen in furnace deposits and in particulates. It is also conceivable that similar reactions could occur between NO and the molten smelt. In order to quantify the presence of nitrogen in these different streams, samples were taken from the two recovery furnaces at Georgia-Pacific Corporation's Ashdown, Arkansas operations.

SAMPLE SOURCE

There are currently two recovery furnaces in operation at the G-P Ashdown mill. The No. 2 Recovery Boiler is a conventional two-drum Combustion Engineering (CE) unit. Installed in 1979, the unit was equipped with a screen superheater, economizer, and cascade direct

contact evaporator (DCE). The original design burning rate was 3.5 million lbs of dry solids per day (MMlb ds/day). In 1990, the unit was upgraded by Babcock & Wilcox to a low order configuration. The DCE was replaced by a second economizer, and a third level of air delivery was added. The unit has three FD fans, two ID fans, and four oscillating liquor guns. The upgrade design conditions for the No. 2 Recovery Boiler specify a design burning rate of 4.2 MMlb ds/day with a liquor heating value of 5700 BTU/lb, as fired solids of 68%, and a steam production rate of 543,400 lb/hr at 850°F and 900 psig. The unit is currently operating around 4.0 MMlb ds/day.

The No. 3 Recovery Boiler is a 1989 single drum Götaverken boiler equipped with a large superheater and economizer. The designed burning rate is 4.5 MM lb ds/day. The unit is designed to deliver 730,000 lb steam/hr at an outlet temperature and pressure of 850 °F and 900 psig, respectively. These conditions are based on firing black liquor solids at 68% with a heating value of 6300 BTU/lb (prior to addition of saltcake and ash recycle). The No. 3 Recovery Boiler has eight gun ports and is normally fired with six stationary liquor guns. Secondary air port rodders and a larger tertiary air fan were added to the furnace in 1994. Presently, this unit operates around 4.5 MMlb ds/day.

Two sets of samples were taken from these furnaces. The first set of samples was taken from both furnaces on February 21, 1994, and consisted of: black liquor feed, "as fired" black liquor, economizer deposits, ESP saltcake, and green liquor from the dissolving tank. The second set of samples was taken on April 15, 1994, only from the No. 3 recovery furnace and consisted of: "as fired" liquor, smelt, weak wash, green liquor, dregs, and slaker grits. Each of these samples was analyzed for total nitrogen content. In addition, the "as fired" liquor samples were sent to an outside source (Huffman Laboratories) for elemental analysis.

NITROGEN ANALYSIS

All samples were analyzed for nitrogen using an Antek Instruments, Inc. 7000N/S analyzer. The analyzer employs an oxygen rich combustion environment at 1100°C to convert all forms of nitrogen in the sample to nitrogen oxides which are detected by chemiluminescence. The analyzer is equipped with a multi-matrix sample inlet and is capable of measuring gas, liquid, and solid samples in the range of low ppb - 17% with a relative standard deviation of $\pm$ 2%. Analysis was conducted using the following gas flow rates for the analyzer: inlet oxygen ~20 cc/min, inlet helium as a carrier gas ~145 cc/min, oxygen to the combustion chamber ~365 cc/min, and oxygen to the ozone generator (for chemiluminescence detection) ~ 30 cc/min. The detector gain was set on high at a factor of 1. The instrument was calibrated using standards composed of silver nitrate in water between the concentration range 0 to 1000 ppm as N. Excellent linearity (R-Squared = 0.99993) was achieved over this range.

Solid samples were oven dried and crushed before being placed in a sample boat and weighed. The sample boat was driven into the combustion chamber by a sample drive. Solid sample sizes were approximately 10 to 20 mg. Liquid samples were injected by syringe into a sample boat containing glass wool to increase surface area for improved heat transfer and more complete combustion of the samples. All liquid samples were 5.0 μL. Due to its viscous nature, black liquor samples were weighed in sample boats at a sample size of 30 to 45 mg. A minimum of three replicates was done for each sample with the average nitrogen concentration being reported.

While this combustion method for total nitrogen measurement is relatively new, the technique provides many advantages over the wet chemical Kjeldahl method. The combustion technique offers greater safety and time savings in both sample preparation and analysis compared to the Kjeldahl method. Solids, gases, and

liquids can be analyzed to very low nitrogen levels with high accuracy and precision. With the Kjeldahl technique, only liquids and solids can be analyzed, and the accuracy for solids becomes questionable at concentrations below 0.5% N.[6] This is considerably higher than the 0.1% N concentration typical of black liquor samples. This lack of accuracy becomes even more critical when attempting to analyze samples such as fume and smelt which have an even lower nitrogen concentration.

While the total nitrogen combustion method is more accurate and precise, additional results from using this method have shown a dependence on the sample matrix. While this may affect the accuracy, the numbers are still considered more reliable than those obtained by the Kjeldahl method. The effect of the matrix is such that the nitrogen content measured may be considerably lower than the actual nitrogen content, i.e., there may be more than 0.1% N in black liquor. Evaluation of the effect of the liquor composition on the release of nitrogen is the subject of a future publication.[7]

RESULTS

The results of the nitrogen analysis are shown below in Tables 1 and 2. All concentrations are reported as parts per million on a weight basis. The black liquor samples are reported as ppm by weight of black liquor solids.

Table 2: Analysis of Samples Taken on April 15, 1994.

SAMPLE SET 2 No .3 Recovery Furnace	[N] (ppm)
As Fired Liquor	631
Smelt	155
Weak Wash	18
Green Liquor	88
Green Liquor Dregs	37
Slaker Grits	10

For both furnaces, the "as fired" liquor has essentially the same concentration as the black liquor feed. This indicates that any makeup chemicals or saltcake added in the mix tank do not have a significant amount of nitrogen in the liquor. This makes sense based on the analysis of saltcake and precipitator catch.

The second "as fired" liquor sample taken from the No. 3 Recovery Furnace had a significantly higher nitrogen concentration than the first (36% higher). This indicates that the wood supply or other cooking process variables can have an effect on the nitrogen content. This may ultimately affect the NO_x emissions as they are dependent on the nitrogen content of the liquor.[8,9] The elemental analysis of the "as fired" liquor samples is shown in Table 3.

Table 1: Analysis of Samples Taken on Feb. 21, 1994.

No. 2 RB	[N] ppm	No. 3 RB	[N] (ppm)
Black Liquor Feed	487	Black Liquor Feed	487
As Fired Liquor	486	As Fired Liquor	486
Economizer 1	5	Generating Bank	72
Economizer 2	7	Economizer 1	40
ESP Saltcake	27	Economizer 2	13
N. Dissolving Tank	103	ESP Saltcake	7
S. Dissolving Tank	90	Dissolving Tank	78
Green Liquor Dregs	75 - 100	Green Liquor Dregs	60

Table 3: Elemental Analysis of Black Liquor Solids.

Component	Sample Set 1 No. 2 RB	Sample Set 1 No. 3 RB	Sample Set 2 No. 3 RB
Carbon (C)	39.38%	38.53%	37.54%
Carbonate Carbon (CO_3^-)	0.60%	0.54%	0.63%
Hydrogen (H)	3.68%	4.18%	3.88%
Oxygen (O)	35.95%	35.89%	36.19%
Sulfur (S)	4.31%	4.42%	4.3%
Sulfate Sulfur (SO_4^-)	1.08%	1.26%	1.22%
Sodium (Na)	14.9%	15.1%	16.2%
Nitrogen (N)	0.049%	0.046%	0.063%

A simple mass balance has been performed around the No 3. Recovery Furnace based on the following assumptions and operating conditions:

* Basis   100 kg dry solids
* Solids Concentration   67%
* Excess Air   15%
* Reduction Efficiency   92%
* 25% of the N in black liquor is emitted as NO in the flue gas.
* 10% of Na in black liquor forms fume, 80% of which is captured in the ESP. The remaining 20% of the fume is deposited on the generating bank (8%), and the two economizer sections (6% each).

The results of the mass balance are depicted below in Figure 1.
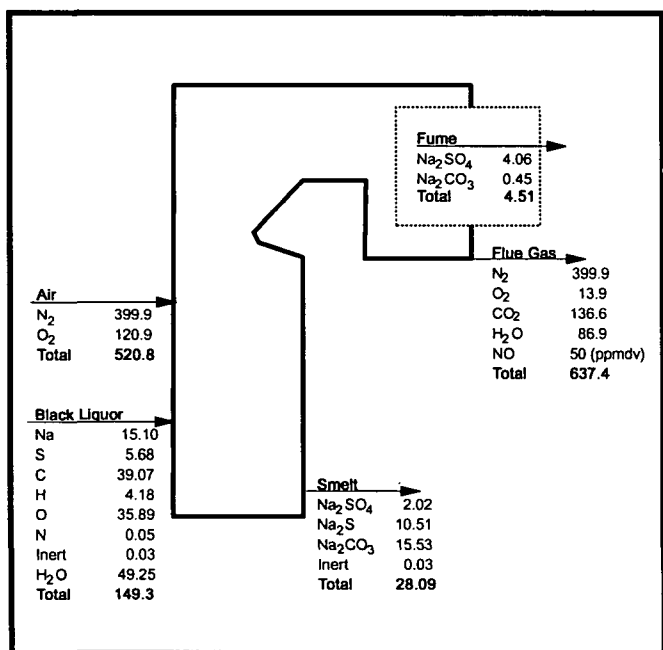
Figure 1: Mass Balance on a Recovery Furnace Based on 100 kg Dry Solids.

Based on the mass balance above and the analysis of samples taken from the furnaces, it is possible to calculate the percentage of the black liquor nitrogen that ends up in each of the exit streams. These results are shown below in Table 4.

Table 4: Nitrogen Content in Various Recovery Furnace Exit Streams.

"Exit Stream"	[N] in Stream (g N/ 10^6 g)	Mass of Stream (kg)	Mass of Nitrogen (kg)	% of Input N
Generating Bank	72	0.36	25.9 x 10-6	0.052
Economizer 1	40	0.27	10.8 x 10-6	0.022
Economizer 2	13	0.27	3.51 x 10-6	0.007
ESP Catch	7	3.61	25.3 x 10-6	0.050
Smelt	155	28.1	43.6 x 10-4	8.71

Inspection of Table 4 shows less than 0.1% of the black liquor nitrogen can be accounted for in the electrostatic precipitator. Thus, fume scrubbing reactions (capturing N as $NaNO_3$) are not thought to be a significant source for the reduction of NO. It is, however, feasible that reduction reactions are occurring with fume species that give rise to gaseous products. The work of Thompson and Empie has shown that NO can be reduced to N_2 and O_2 in the presence of molten sodium carbonate (Na_2CO_3).[10] In addition, a study at Oregon State University has shown nitric oxide can be reduced in the presence of black liquor char.[11]

Results of the furnace mass balance indicate that approximately 9% of the nitrogen entering with the liquor leaves with the smelt. It is not clear at this point what form the nitrogen is in smelt. It could be nitrogen from the black liquor that did not get released during combustion or it could be a reaction product that forms between NO and the inorganic salts.

Assuming that the mass flow rate of weak wash is 6.6 times the mass flow rate of the smelt,[12] it was not possible to close the nitrogen mass balance around the dissolving tank. Results indicated that the measured concentration of nitrogen in the smelt may be low by as much as 350%. Because the smelt was analyzed as a solid, there may be an effect due to the sample matrix. If the smelt concentration is actually higher by a factor of 3.5, then the amount of nitrogen leaving in the smelt

84

corresponds to approximately 31% of the black liquor nitrogen.

Clarified green liquor was shown to have an average concentration of 90 ppm, while the dregs had concentrations ranging from 37 to 100 ppm. Due to the low mass flow rate of dregs (on the order of 2% of the unclarified green liquor flow),[12] landfilling dregs would not be considered a significant purge point for nitrogen.

The assumed 25% of the nitrogen emitted in the flue gas as NO_x corresponds to a flue gas concentration of 50 ppm based on dry volume. This is equivalent to approximately 30 ppm when adjusting to the common basis of ppmv at 8% O_2. Nichols *et al*, report a brief survey of NO_x emissions in the range of near zero to 120 ppmv at 8% O_2.[1]

The remaining 44 to 66% is presumed to leave the furnace in the flue gas as molecular nitrogen (N_2). It should be noted that the nitrogen content of black liquor is only one of the parameters that influences NO_x emissions. Feck has reported great variability in NO_x emissions depending on the operation of the furnace.[13]

ACKNOWLEDGMENTS

REFERENCES
1. Nichols, K.M., Thompson, L.M., and Empie, H.J., *Tappi Journal*, 76(1):119(1993).

2. Someshwar, A.V., An Analysis of Kraft Recovery Furnace NO_x Emissions and Related Parameters, Technical Bulletin No. 636, National Council of the Paper Industry for Air and Stream Improvement, New York, July 1992.

3. Nichols, K.M., and Lien, S.J., *Tappi Journal*, 76(3):185(1993).

4. Kauppinen, E.I., Mikkanen, P., Jokiniemi, J.K., Iisa, K., Boonsongsup, L., Sinquefield, S.A., and Frederick, W.J., 1993 TAPPI Engineering Conference Proceedings, TAPPI PRESS, Atlanta, p. 369.

5. Thompson, L.M., and Empie, H.J., 1993 TAPPI Engineering Conference Proceedings, TAPPI PRESS, Atlanta, p. 643.

6. ASTM Standard D3590-90.

7. Martin, D.M., Malcolm, E.W., and Hupa, M., The Effect of Liquor Composition on the Release of Nitrogen During Black Liquor Combustion and its Implications on Recovery Boiler Operations, Proceedings of the Technical Meeting of the Eastern States Section, Combustion Institute, Clearwater Beach, FL, p. 294 (1994).

8. Chen, S.L., Heap, M.P., Pershing, D.W., and Martin, G.B., 19th Symposium (International) on Combustion, The Combustion Institute, 1982, p. 1271.

9. Clement, J.L., and Barna, J.L., 1993 TAPPI Environmental Conference Proceedings, TAPPI PRESS, Atlanta, p. 653.

10. Thompson, L.M., and Empie, H.J., Depletion of Nitric Oxide in the Presence of Molten Smelt Species, Submitted for Publication to JPPS, January 1995.

11. Wu, S.L., and Iisa, K., Kinetics of NO Reduction by Black Liquor Char, Paper 251e, AIChE 1994 National Meeting, San Francisco, November 13-18, 1994.

12. Hough, G., *Chemical Recovery in the Alkaline Pulping Process*, TAPPI PRESS, Atlanta, p. 243, (1985).

13. Feck, R., 1992 International Chemical Recovery Conference Proceedings, TAPPI PRESS, Atlanta, p. 391.

DISCUSSION

The most significant aspect of this paper relating to the overall thesis objectives is the fact that approximately half of the nitrogen entering the furnace could not be accounted for. It was therefore assumed that nitrogen leaves the furnace as a gas phase species, e.g., N_2 or NH_3. As illustrated by the experimental work in this thesis, reactions of NO with Na_2CO_3 or Na_2S can reduce NO to N_2. Thus, nitrogen in black liquor could be reduced to N_2 by the following pathway:

$$\text{Fuel N} \xrightarrow[\text{Oxidation}]{} \text{NO} \xrightarrow[\substack{\text{Reduction by}\\ \text{Na Species}}]{} \tfrac{1}{2}\, N_2 + \tfrac{1}{2}\, O_2.$$
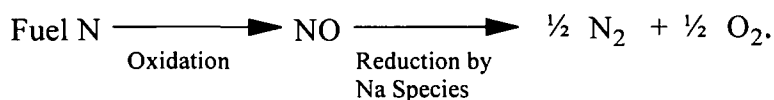
The presence of nitrogen in smelt is also a significant observation. Because it is not known what the form of nitrogen is, it is not possible to predict what will happen upon contact with weak wash in the dissolving tank and subsequent processing of the green liquor. The odor of ammonia around green liquor clarifiers and emission of NO from dissolving tank vent stacks have been observed in a number of mills.[66,67] The presence of these nitrogen species is most likely due to reactions of the nitrogen originally found in the smelt.

It is difficult to make generalizations on the behavior of nitrogen in a recovery furnace based on the analysis of the limited number of samples in this study. It is, however, clear that NO depletion reactions may play an important role in controlling NO_x emissions.

CONCLUSIONS

As a result of this study, a rate expression for the depletion of NO by reaction with molten Na_2CO_3 and mixtures of Na_2CO_3/Na_2S has been developed. In addition to the kinetic rate data that were gathered, many other important aspects regarding NO_x emissions from a kraft recovery furnace were discovered. A list of conclusions from this work is presented below.

1. Theoretical calculations showed that the majority of NO_x formed in a kraft recovery furnace is a result of the fuel NO_x mechanism. Thermal NO_x does not contribute significantly to the amount of NO_x that is formed.

2. The nitrogen concentration of black liquor is typically on the order of 0.1% of the black liquor solids. Oxidation of only 20% of the nitrogen in black liquor can account for the level of NO_x typically emitted from a recovery furnace. It is likely that more than 20 % of the nitrogen is oxidized and that NO depletion mechanisms reduce the concentration of NO before it is emitted in the flue gas.

3. Reactions between NO_x and sodium species provide a potential mechanism for the depletion of NO in a kraft recovery furnace. Reactions between NO and several sodium species to form sodium nitrate have been shown to be thermodynamically feasible.

4. Nitric oxide is consumed in the presence of molten Na_2CO_3 and mixtures of Na_2CO_3/Na_2S. In regards to the two-film model for heterogeneous systems, it has been hypothesized that the reaction takes place entirely within the liquid film.

5. The rate of depletion of NO has been shown to follow a pseudo first-order rate expression as

follows:
$$-r_{NO} = -\frac{1}{V_L}\frac{\delta N_{NO}}{\delta t} = \frac{aP_{NO}}{\frac{1}{k_g}+\frac{H_{NO}}{\sqrt{D_{NO}k_1}}} \quad \left(\frac{mol}{cm^3\,\text{sec}}\right)$$

where, $-r_{NO}$ = rate of reaction based on volume of molten salt   (mol/cm³ sec)

V_L = volume of molten salt (cm³)

N_{NO} = moles of nitric oxide (mol)

a   = interfacial area per volume of molten salt (cm²/cm³)

P_{NO} = partial pressure of nitric oxide (atm)

k_g = gas film mass transfer coefficient (mol/cm² sec atm)

H_{NO} = P_{NO}/C_{NO} = phase distribution coefficient (atm cm³/mol)

C_{NO} = concentration of NO in molten salt (mol/cm³)

D_{NO} = diffusivity of NO in molten salt (cm²/sec)

k_1 = pseudo first-order rate constant (1/sec)

k_1 = $k_o \exp(-E_a/RT)$

k_o = pre-exponential constant (1/sec)

E_a = activation energy (J/mol)

R   = gas constant = (8.314 J/mol °K)

T   = absolute temperature (°K)

6. Values for the pseudo first-order rate constant have been determined experimentally over the

temperature range, T = 860 to 973°C. For NO depletion by Na_2CO_3, $k_1 = 3.09 \times 10^{22}\,e^{(-44,780/T)}$.

For NO depletion by mixtures of Na_2CO_3/Na_2S, $k_1 = 2.98 \times 10^{15}\,e^{(-20,750/T)}$.

7. Analysis of the gaseous products indicate that all of the NO that is depleted by reaction with

Na_2CO_3 is being converted to oxygen (O_2) and nitrogen (N_2). This can be represented as simply

$NO \rightarrow \frac{1}{2}N_2 + \frac{1}{2}O_2$.

8. For Na_2CO_3/Na_2S mixtures, no oxygen can be detected in the gas stream. It was assumed that

the oxygen formed by depletion of NO is consumed by the sodium sulfide to form sodium

sulfate. The overall stoichiometry can be written as follows: $4NO + Na_2S \rightarrow Na_2SO_4 + 2N_2$.

The presence of sodium sulfate was confirmed by analysis of salt mixtures.

9. A nitrogen mass balance performed by sampling industrial furnaces has shown that approximately half of the nitrogen entering the furnace in black liquor cannot be accounted for. These results indicate that nitrogen is leaving the furnace in the flue gas, presumably in the form of N_2. The reduction of black liquor nitrogen to N_2 could follow the pathway:

$$\text{Fuel N} \xrightarrow{\text{Oxidation}} \text{NO} \xrightarrow[\text{Na Species}]{\text{Reduction by}} \tfrac{1}{2} N_2 + \tfrac{1}{2} O_2.$$
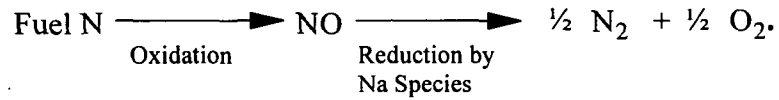
RECOMMENDATIONS FOR FUTURE WORK

The experimental apparatus used in this study created limitations in the ranges of the independent variables. Due to the small size of the crucible, the mass of salt and gas flow rate could not be changed by more than a factor of two. The rate data obtained in this study could be used to design a more versatile experimental apparatus. The following features should be considered in redesigning the apparatus:

A larger (longer) crucible would allow for higher masses of salt and gas flow rates without excessive splashing and liquid entrainment.

The method for introducing the gas to the liquid could be improved. The purge tube could be replaced by a smaller diameter tube or multiple tubes to create smaller bubbles and improve the interfacial surface area.

A higher temperature furnace should be considered. The maximum temperature of 973°C was limited by the furnace in this study. Rate data collected at higher temperatures would prevent extrapolating kinetic data beyond the conditions where they were collected which can often lead to inaccurate results.

The mechanism for depletion of NO is not well understood. It is possible that the sodium species act as catalysts for the depletion of NO. It is also feasible that intermediate species such as sodium nitrite or sodium nitrate could be formed which then decompose to form N_2 and O_2. Experimental work could be conducted to determine whether or not these intermediate species exist (e.g., sampling and quenching the salt mixture during reaction).

In addition to Na_2CO_3 and Na_2S, there are many other molten species that are present in a recovery furnace. Sodium hydroxide (NaOH) has been identified as a potential reactant leading to the formation of Na_2SO_4. Experimental work could be done to look at the depletion of NO by reaction with NaOH and/or Na_2SO_4.

ACKNOWLEDGMENTS

I would like to thank the Institute of Paper Science and Technology and its member companies for the opportunity and financial support to complete my graduate studies. My experiences at the Institute both educationally and recreationally have provided me with a lifetime of memories and a foundation of knowledge and opportunity for what promises to be an exciting career in the pulp and paper industry.

Many of the faculty, staff, students, and alumni have contributed to my education. I would like to thank both Tom Spielbauer and Pat Medvecz who have been strong influences since my first visit to the Institute in Appleton in the Spring of 1988. Thanks to my office mates, Stacy Lee and Denise Martin, who as well as being excellent friends have been an invaluable resource for sharing ideas and solving problems. And, thanks to Todd Schwantes who taught me that graduate school is a lot like running a marathon and that the finish will come eventually if you just keep going.

I would like to thank the members of my advisory committee, all of whom have been with me throughout the duration of my doctoral studies: Dr. Jeff Colwell, Dr. Lucy Sonnenberg, and especially my primary advisor, Dr. Jeff Empie, who has taught me objectivity and the importance of the fundamentals. Each member of my committee has had a major influence on the success of my project.

Finally, I would like to thank each member of my family for their love and support throughout a lifetime of academia: Elaine Jackson, who has given me emotional support, friendship, and balance throughout my doctoral studies; my mother, who gave me creativity and

the ability to sometimes look at things in a different perspective; my father, who instilled in me

that hard work for a short while will pay lifelong dividends; and my brother, who has served as a

constant reminder that there is much more to life than school or work.

LITERATURE CITED

1. Leaf, D.A. Acid rain and the clean air act. Chemical Engineering Progress. 25-29(May 1990).

2. Lyons, C.E. Environmental problem solving: The 1987-1988 metro Denver brown cloud study. Chemical Engineering Progress. 61-71(May 1990).

3. Anderson, P.H., and Jackson, J.C. An analysis of best available control technology options for kraft recovery furnace NO_x emissions. Tappi Journal. 74(1):115-118(1991).

4. Dyer, H. ed. 1994 Lockwood-Post's Directory of the Pulp, Paper and Allied Trades. New York, Miller Freeman, Inc., 1993.

5. Hough, G. Chemical Recovery in the Alkaline Pulping Processes. TAPPI Press, Atlanta, GA, 1985.

6. Vakkilainen, E. Personal communication. October 1991.

7. Sherman, R. Personal communication. January 1991.

8. Thorn, P. Personal communication. July 1991.

9. Adams, T.N., and Frederick, W.J. Kraft Recovery Boiler Physical and Chemical Processes. New York, American Paper Institute, 1985.

10. Spielbauer, T.M., Adams, T.N., Monacelli, J.E., and Bailey, R.T. Droplet size distribution of black liquor sprays. Proceedings of the 1989 International Chemical Recovery Conference. Ottawa, Ontario, 119-125(1989).

11. Empie, H.J., Lien, S.J., Yang, W.R., and Adams, T.N. Spraying characteristics of commercial black liquor nozzles. Proceedings of the 1992 TAPPI/CPPA International Chemical Recovery Conference, Seattle, WA, 429-440(1992).

12. Hupa, M., Solin, P., Hyoty, P. Combustion of black liquor droplets. Proceedings of the 1985 TAPPI International Chemical Recovery Conference, New Orleans, LA, 335-344(1985).

13. Frederick, W.J., Noopila, T., and Hupa, M. Swelling of spent pulping liquor droplets during combustion. Journal of Pulp and Paper Science. 7(15):J164-J170(1991).

14. Grace, T.M., Cameron, J.H., and Clay, D.T. Role of the sulfate/sulfide cycle in char burning - experimental results and implications. Proceedings of the 1985 TAPPI International Chemical Recovery Conference, New Orleans, LA, 371-379(1985).

15. Lee, S.R. The Role of Carbon Dioxide in the Combustion of Kraft Black Liquor Char. Doctoral Dissertation, Atlanta, GA, Institute of Paper Science and Technology, 1994.

16. Li, J., and van Heiningen, A.R.P. Reaction kinetics of gasification of black liquor char. The Canadian Journal of Chemical Engineering. 67(8):693-697(1989).

17. Kulas, K.A. An Overall Model of the Combustion of a Single Droplet of Kraft Black Liquor. Doctoral Dissertation, Atlanta, GA, Institute of Paper Science and Technology, 1990.

18. Feck, R. Emission control for recovery boilers. Proceedings of the TAPPI/CPPA 1992 International Chemical Recovery Conference, Seattle, WA, 391-404(1992).

19. Prouty, A.L., Stuart, R.C., and Caron, A.L. Nitrogen oxide emissions from a kraft recovery furnace. Tappi Journal. 76(1):115-118(1993).

20. Kauppinen, E.I., Jokiniemi, J.K., Mikkanen, P., Lazaridis, M., Backman, R., and Frederick, W.J. Aerosols in black liquor combustion, LIEKKI Combustion Research Program Technical Review 1988-1992. Project 2-28, 619-645(1992).

21. Borg, A. Teder, A., and Warnqvist, B. Inside a kraft recovery furnace - studies on the origins of sulfur and sodium emission. Tappi Journal. 57(1):126-120(1974).

22. Cameron, J.H. Reaction enhanced vaporization of molten salt. Chemical Engineering Communications. 59:243-257(1987).

23. Blackwell, B., and King, T. Chemical Reaction in Kraft Recovery Boilers. Sandwell and Company Limited, Vancouver, BC, 1985.

24. Keener, T., and Davis, W. Study of the reaction of SO_2 with $NaHCO_3$ and Na_2CO_3. Journal of the Air Pollution Control Association, 34:651-654(1984).

25. Backman, R., Hupa, M., and Uusikartano, T. Kinetics of sulphation of sodium carbonate in flue gases. Proceedings of the 1985 TAPPI International Chemical Recovery Conference, New Orleans, LA, 445-450(1985).

26. Maule, G.P., and Cameron, J.H. Reaction of Na_2CO_3 fume particles with SO_2 and O_2. IPC Technical Paper Series. No. 317, January 1989.

27. Kauppinen, E.I., Mikkanen, P., Jokiniemi, J.K., Iisa, K., Boonsongsup, L., Sinquefield, S.A., and Frederick, W.J. Fume particle characteristics and their reactions with SO_2 at kraft recovery boiler conditions. Proceedings of the 1993 TAPPI Engineering Conference, Orlando, FL, 369-376(1993).

28. Rishinshivili, G.V., and Kaplun, L.V. Means to reduce furnace emissions of soda recovery boilers. Bumazhnaya Promyshlennost'. (1):26-28(1983).

29. Skrivars, B.J., Hupa, M., and Hyoty, P. Composition of recovery boiler dust and its effect on sintering. Tappi Journal. 74(6):185-189(1991).

30. Pejryd, L. and Hupa, M. Bed and furnace gas compositions in recovery boilers - advanced equilibrium calculations. Proceedings of the 1984 TAPPI Pulping Conference, San Francisco, CA, 579-589(1984).

31. Hupa, M., Backman, R., Skrivars, B.J., and Hyoty, P. The influence of chlorides on the fireside behavior in the recovery boiler. Tappi Journal. 73(6):153-158(1990).

32. Hoshino, Y., Utsunomiya, T., and Abe, O. The thermal decomposition of sodium nitrate and the effects of several oxides on the decomposition, Bulletin of the Chemical Society of Japan. 54:1385-1391(1981).

33. Cases-Casanova, J. Thermal decomposition of sodium nitrate. I. Thermogravimetric study and evidence of the reaction between nitric oxide and sodium oxide. Bull. Soc. Chim. France. 429-440(1959).

34. Nichols, K.M., Thompson, L.M., and Empie, H.J. A review of NO_x formation mechanisms in recovery furnaces. Tappi Journal 76(1):119-124(1993).

35. Clement, J.L., and Barna, J.L. The effect of black liquor fuel-bound nitrogen on NO_x emissions. Proceedings of the 1993 TAPPI Environmental Conference, Boston, MA, 653-660(1993).

36. Seinfield, J.H. Atmospheric Chemistry and Physics of Air Pollution, Chapter 3: Sources of Pollutants in Combustion Processes, Wiley-Interscience, New York, 1986.

37. Adams, T.N., Stewart, R.I., and Jones, A.K. Using CFD calculations to estimate thermal-NO_x from recovery boilers at 67% and 80% dry solids. Proceedings of the 1993 Engineering Conference. Orlando, FL, 625-634(1993).

38. Veverka, P.J., and Nichols, K.M. On the source and chemical form of nitrogen in kraft black liquors. IPST Technical Paper Series. No. 449. July 1992. 10 p.

39. Martin, D.M., Malcolm, E.W., and Hupa, M. The effect of fuel composition on nitrogen release during black liquor pyrolysis. Proceedings of the Technical Meeting of the Eastern States Section, Combustion Institute. Clearwater Beach, FL 294-297(1994).

40. Veverka, P.J., Nichols, K.M., Horton, R.R., and Adams, T.N. On the form of nitrogen in wood and its fate during kraft pulping. Poster presentation at the 1993 TAPPI Environmental Conference. Boston, MA, 1993.

41. Nichols, K.M., and Lien, S.J. Formation of fuel-NO_x during black liquor combustion. Tappi Journal. 76(3):185-191(1993).

42. Aho, K., Hupa, M., and Vakkilainen, E. Fuel nitrogen release during black liquor pyrolysis. Part 1: Laboratory measurements at different conditions. Tappi Journal. 77(5):121-127(1994).

43. Aho, K., Hupa, M., and Nikkanen, S. Fuel nitrogen release during black liquor pyrolysis. Part 2: Comparison between different liquors. Tappi Journal. 77(8):182-188(1994).

44. Thompson, L.M., Martin, D.M., Empie, H.J., Malcolm, E.W., and Wood, M. The fate of nitrogen in a kraft recovery furnace. Accepted for presentation at the 1995 International Chemical Recovery Conference, Toronto, April 1995.

45. Thompson, L.M., and Empie, H.J. A proposed mechanism for the depletion of NO_x in a kraft recovery furnace. Proceedings of the 1993 TAPPI Environmental Conference, Boston, MA, 643-647(1993).

46. Klinger, J., Smyk, E.B., and Johnson, T.R. Validation of a kinetic model for nitric oxide decomposition in MHD systems. Twenty Second Symposium on Engineering Aspects of Magnetohydrodynamics. 10(2):1-20(1984).

47. Cho, S.M. Properly apply selective catalytic reduction for NO_x removal. Chemical Engineering Progress, January 1994(39-45).

48. Roslyakov, P.V., Dvoinishnikov, V.A., Burkova, A.V., and Stepanova, E.N. Controlling emissions of nitrogen oxides by introducing ammonia to combustion products. Thermal Engineering. 36(9):506-510(1989).

49. Bowman, C.T. Control of combustion generated nitrogen oxide emissions: Technology driven by regulations. Twenty-Fourth Symposium (International) on Combustion. The Combustion Institute. 859-878(1992).

50. Muzio, L.J., Arand, J.K., and Teixeira, D.P. Gas phase decomposition of nitric oxide in combustion products. Sixteenth Symposium (International) on Combustion. The Combustion Institute. 199-208(1976).

51. Levy, J.M., Chan, L.K., Sarofim, A.F., and Beer, J.M. NO/char reactions at pulverized coal flame conditions. Eighteenth Symposium (International) on Combustion. 111-120(1981).

52. Wu, S. L., and Iisa, K. Kinetics of NO Reduction by Black Liquor Char. Paper 251e. AIChE 1994 National Meeting. San Francisco, CA, November 13-18, 1994.

53. Thompson, L.M., and Empie, H.J. Kinetics of NO depletion by reaction with molten sodium carbonate. Advances in Forest Products Environmental and Process Engineering: The 1993 Forest Products Symposium. AIChE Symposium Series No. 302(90)33-38(1994).

54. Treybal, R.E. Mass Transfer Operations, 3rd ed. McGraw-Hill Book Company, New York, 1980.

55. Astarita, G. Mass Transfer With Chemical Reaction, Elsevier Publishing Company, New York, 1967.

56. Levenspiel, O. Chemical Reaction Engineering, 2nd ed. John Wiley and Sons, New York, 1972.

57. Blander, M., Grimes, W.R., Smith, N.V., and Watson, G.M. Solubility of noble gases in molten fluorides. II. In the LiF-NaF-KF eutectic mixture. Journal of Physical Chemistry. 63:1164-1167(1959).

58. Andresen, R.E. Solubility of oxygen and sulfur dioxide in molten sodium sulfate and oxygen and carbon dioxide in molten sodium carbonate. Journal of the Electrochemical Society. 126(2):328-334.

59. Dack, M.R.J. Techniques of Chemistry Volume 8: Solutions and Solubilities Part 1. John Wiley and Sons, New York, 1975.

60. Perry, R.H., and Green, D.W. Perry's Chemical Engineer's Handbook, Sixth Edition, McGraw Hill Book Company, New York, 1984.

61. Chhabria, M.C., and Sharma, M.M. Kinetics of absorption of oxygen in aqueous solutions: (1) acidic chromous chloride. (2) acidic titanous chloride and (3) ammoniacal cuprous chloride. Chemical Engineering Science. 29:993-1002(1974).

62. van Krevelen, D.W., and Hoftijzer, P.J. Kinetics of gas-liquid reactions part 1. General Theory. Recueil. 67:563-586(1948).

63. Ghorpade, A.K., Chipalkatti, and Sharma, M.M. Kinetics of oxidation of cuprous benzoate/ toluate and cobaltous benzoate in benzoic/toluic acid melts; measurement of interfacial area in melts in agitated and sparged contactors. Chemical Engineering Science. 36:1227-1232(1981).

64. Thompson, L.M., and Empie, H.J. The Rate of Depletion of NO by Reaction with Molten Sodium Salts, Submitted for Publication to the Journal of Pulp and Paper Science, January 1995.

65. Huheey, J.E. Inorganic Chemistry: Principles of Structure and Reactivity, Second Edition, Harper and Row, New York, 1978.

66. Jones, A.K. Personal communication. June 1992.

67. Someshwar, A. Personal communication. July 1992.

APPENDIX 1: NOMENCLATURE

a = interfacial area per unit volume (cm^2/cm^3)

A = solute gas

[A*] = interfacial concentration of A (mol/cm^3)

B = nonvolatile reactant

[B_o] = concentration of B in the bulk (mol/cm^3)

C_{Na} = C_{Na2CO3} = concentration of molten Na_2CO_3 (mol/cm^3)

$C_{Na,i}$ = concentration of Na_2CO_3 at the interface (mol/cm^3)

C_{NO} = $C_{NO,L}$ = concentration of NO in liquid film (mol/cm^3)

$\cosh x = \frac{e^x + e^{-x}}{2}$

d_b = bubble diameter (cm)

D_A = $D_{NO/He}$ = diffusivity of NO in Helium (m^2/s)

D_{Na} = diffusivity of Na_2CO_3 in Na_2CO_3 (m^2/s)

D_{NO} = $D_{NO/Na}$ = diffusivity of NO in Na_2CO_3 (m^2/s)

D_t = outside diameter of purge tube (m)

Ea = activation energy (J/mol)

f (kT/e_{AB}) = collision function (= 0.31) (Treybal, p. 32)

g = gravitational constant = (9.81 m/s)

H_{NO} = $1/K_H$ = phase distribution coefficient ($atm\ cm^3/mol$)

J_{NO} = rate of absorption per unit surface area ($mol/\ cm^2\ s$)

k = second-order rate constant ($cm^3/mol\ s$)

k_0 = pre-exponential factor (1/s)

k_1 = pseudo first-order rate constant (1/s)

k_2 = undetermined rate constant (1/s)

k_g = gas film mass transfer coefficient ($mol/cm^2\ atm\ s$) = $\frac{RT}{zD_{NO,He}}$

k_L = liquid phase mass transfer coefficient (cm/s)

K_H = Henry's Law constant ($mol/cm^3\ atm$)

m = order of reaction with respect to A

m_{Na} = mass of Na_2CO_3 (g)

$\sqrt{M_A}$ = Hatta number

$M_1 = k_L\, C_{NO,i}$ (mol/cm^2 s)

M_i = molecular weight of species, i

n = order of reaction with respect to B

N = Avogadro's number = (6.022×10^{23})

N_{NO} = moles of NO (mol)

$[NO]_f$ = exit concentration of NO (ppm)

$[NO]_i$ = inlet concentration of NO (ppm)

$P_{He,m}$ = log mean pressure of helium (atm)

P_{NO} = partial pressure of NO (atm)

P_t = total pressure (atm)

r = molecular radius (m)

$r' = -r_{NO}$ = rate of depletion of NO based on volume of liquid (mol/cm^3 s)

r'' = rate of reaction based on surface area (mol/ cm^2 s)

$r_{NO/He}$ = molecular separation at collision (nm)

R = universal gas constant = (8.314 m^3 J/mol K)

R_c = radius of column = (0.02 m)

$R_o = \sqrt{kC_{Na}D_{NO}}\; C_{NO,i}$ (mol/ cm^2 s)

$R_2 = k\, C_{NO,i}\, C_{Na,L}\, \varphi/a$ (mol/cm^2 s)

$\sinh x = \frac{e^x - e^{-x}}{2}$

t = time (s)

T = absolute temperature (K)

U_{br} = bubble rise velocity (m/s)

U_{gs} = superficial gas velocity (m/s)

V = flow rate of gas (cm^3/s)

V_g = flow rate of gas (m^3/s)

$V_L = V_l$ = volume of molten salt (cm^3)

w_i = rate of diffusion of species i (mol/ cm^2 s)

x = linear dimension perpendicular to gas liquid interface (cm)

x_L = thickness of liquid film (cm)

X = percent conversion of NO

$X = R_o/M_1$ (dimensionless parameter used in the derivation of Eq. 51)

z = film thickness = (10^{-4} m) (estimated)

α = correlation factor (assumed 30)

ε = gas holdup

ϕ = association factor for solvent = 1

φ = liquid holdup = 1-ε

v_{NO} = solute molal volume at boiling point (= 0.0236 m^3/kmol)

$\Psi = P_{NO,f}/P_{NO,i} = [NO]_f/[NO]_i$

APPENDIX 2: MECHANISM FOR SELECTIVE NONCATALYTIC REDUCTION (SNCR) OF NO BY REACTION WITH AMMONIA[48]
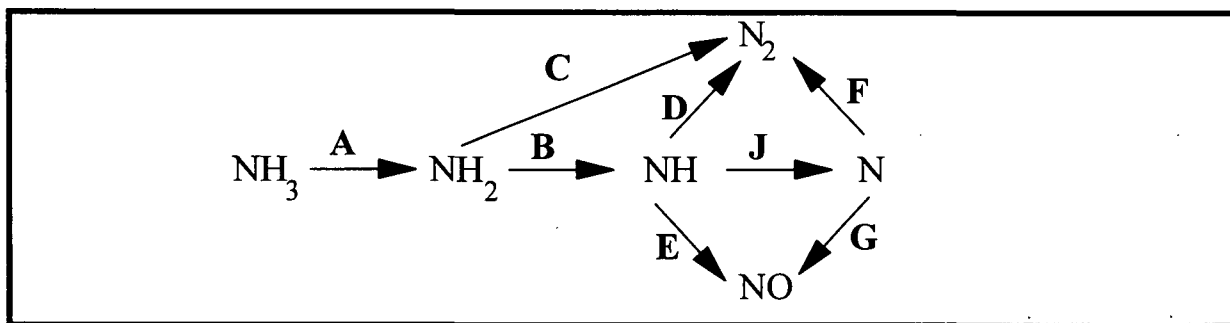
Path	Reactions	Path	Reactions
A	$NH_3 + H \leftrightarrow NH_2 + H_2$	E	$NH + O \leftrightarrow NO + H$
	$NH_3 + O \leftrightarrow NH_2 + OH$		$NH + OH \leftrightarrow NO + H_2$
	$NH_3 + OH \leftrightarrow NH_2 + H_2O$		
B	$NH_2 + H \leftrightarrow NH + H_2$	F	$N + N + M \leftrightarrow N_2 + M$
	$NH_2 + O \leftrightarrow NH + OH$		$N + NO \leftrightarrow N_2 + O$
			$N + NH \leftrightarrow N_2 + H$
C	$NH_2 + NO \leftrightarrow N_2 + H_2O$	G	$N + O_2 \leftrightarrow NO + O$
			$N + OH \leftrightarrow NO + H$
D	$NH + NO \leftrightarrow N_2 + OH$	J	$NH + OH \leftrightarrow N + H_2O$
	$NH + N \leftrightarrow N_2 + H$		$NH + O \leftrightarrow N + OH$
	$NH + NH \leftrightarrow N_2 + H_2$		$NH + H \leftrightarrow N + H_2$

APPENDIX 3: EXPERIMENTAL APPARATUS AND CALIBRATION METHODS

While the experimental apparatus has been described previously, additional information

is presented in this section regarding calibration methods, the furnace temperature profile, and a

list of suppliers or manufacturers for the individual components that comprise the apparatus.

CALIBRATION METHODS

Mass Flow Meters

The mass flow meters were calibrated by the manufacturer in the Spring of 1989. The

meters were checked periodically against each other and consistently gave the same readings for

flow rates in the range of 0 to 1.0 L/min as air at STP. While the meters were calibrated for air,

other gases are measured by using a calibration factor supplied by the manufacturer. For helium

the conversion factor is 1.43. It was assumed that the low concentration of NO or N_2/O_2 in the

gas mixtures (< 1.0%) did not affect the conversion factor.

NO_x Analyzer

The NO_x analyzer was calibrated using a certified gas mixture of NO in helium. A one

point calibration was used in accordance with instructions provided by the manufacturer. The

settings on the analyzer for all experiments are reported below.

Reaction Chamber Pressure = -30 inches Hg   Sample Bypass Flow = 1 to 2 SCFH
Sample Pressure = -5 inches Hg   Converter Temperature = 650°C
Oxygen Pressure = 2 psig

Gas Chromatograph

Calibration methods and settings for the GC are described in detail in the article entitled,

"Depletion of NO by Reaction with Molten Sodium Salts."

Thermocouple

The thermocouple used to measure the temperature of the molten salts was calibrated against an NBS certified thermocouple over the temperature range T = 1607 to 1742°F (878.3 to 949.4°C).

FURNACE TEMPERATURE PROFILE

To investigate the axial temperature profile in the apparatus, temperature measurments were made by inserting the thermocouple in the well and raising the thermocuople at approximately 0.5 cm intervals. During the measurments, gas was purged through the system at 1.0 L/min as air at STP. The bottom of the thermocouple well is approximately 0.5 cm from the bottom of the crucible. Measurements were also made for the furnace only with no reaction vessel present. The results of these measurements are shown below for the furnace only and for 35.0 grams of Na_2CO_3 in the reaction vessel.

Profile of Furnace Only

Profile of Reaction
Vessel Containing
35.0 g of Na_2CO_3
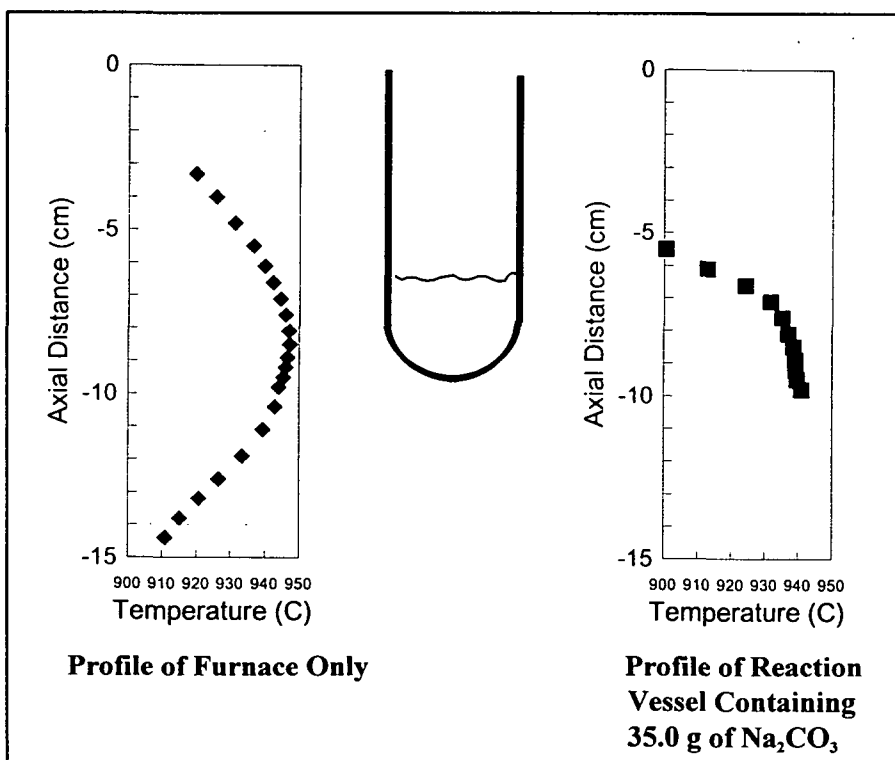
The temperature profile of the furnace reveals a large temperature gradient over the length of the furnace. However, the crucible is situated so that the melt is contained within the hottest section of the furnace. The profile of the temperature of the melt shows a gradient of almost 10°C with the largest drop in temperature near the surface of the melt. The majority of the melt has a fairly flat temperature profile.

Because the thermocouple well extends approximately one inch above the insulation on the top of the furnace, there will be an extreme temperature gradient along the walls of the well. It is therefore suspected that the temperature of the well may have an influence on the measured values for the temperature of the melt, especially as the thermocouple moves up the well. This idea is supported by the sharp gradient between 5 and 7 cm for the measurements in the salt. Measurements taken in the empty furnace at the same location showed less of a gradient It is therefor assumed that the temperature measured at the bottom of the well is an adequate representation of the temperature of the melt.

List of Major Components in Experimental Apparatus

Item	Supplier or Manufacturer	Model or Description
NO_x Analyzer	Thermo Environmental Instruments, Inc.	Model 10 AR
Gas Chromatograph	Carle	Basic GC Model 8000
GC Column	Supelco, Inc.	15' x 1/8" S.S. 60/80 Carboxen 1000
GC Sample Valve	Supelco, Inc.	Six Port Sampling Valve for 1/8" Fittings
Rotameter	Brooks Instruments, Inc.	Tube Size R - 215 - D
Integrator	Hewlett-Packard	Model 3392A
Computer	Swan	XT - 10
Data Acquisition Software	Laboratory Technologies Corp.	Labtech Acquire, Version 1.0
A/D Board		DT2808
Tube Furnace	Applied Test Systems	Series 3110
Temperature Controller	Omega Engineering, Inc.	Model 4001 AKC
Mass Flow Meters	Teledyne - Hastings - Raydist	NALL - 10K & NALL - 1K
NBS Standard Thermocouple	Omega Engineering, Inc.	3/16" Type K
Thermocouple	Omega Engineering, Inc.	1/16" Type K
Purge Tube & Thermocouple Well	Coors Ceramics	Alumina Cast Tubing 0.25" OD
Gasket	Seal Tech	1/16" Graph-Lock Flexible Gasketing
Helium	Air Products	Ultra High Purity
Nitric Oxide in Helium	Holox	Certified Gas Mixture
Helium (GC Carrier Gas)	Air Products	Chromatographic Grade
Oxygen and Nitrogen in Helium	Holox	Certified Gas Mixture
Tubing	AIN Plastics, Inc.	3/16 " ID .03 " Wall Teflon Tubing

APPENDIX 4: DETERMINATION OF THE ACTIVATION ENERGY FOR THE DEPLETION OF NO BY REACTION WITH Na_2CO_3/Na_2S MIXTURES BASED ON AN INFINITELY SLOW REACTION MODEL

For a pseudo first-order reaction, the rate of reaction can be written as:

$$-r_{NO} = -\frac{\delta C_{NO}}{\delta t} = k_1 C_{NO}.$$

Separation of variables and integration gives:

$$-\ln(\frac{C_{NO,f}}{C_{NO,i}}) = k_1 t.$$

By substituting, $C_{NO} = H_{NO} P_{NO}$, the pseudo first-order rate constant can be written as:

$$k_1 = \frac{-\ln\left(\frac{P_{NO,f}}{P_{NO,i}}\right)}{t}.$$

The rate constant can also be written as:

$$k_1 = k_o \exp(-E_a/RT) \text{ or } \ln(k_1) = \ln(k_o) - E_a/RT$$

To solve for the activation energy, Ea, data are plotted as $\ln(k1)$ vs $1/T$. Thus, the slope of the

line represents $-E_a/R$ and the intercept represents $\ln(k_o)$.

Infinitely Slow Reaction, Reaction Rate Controlled by Kinetics Only (lnk vs 1/T)

Exp 114

Regression Output:

Constant	18.162
Std Err of Y Est	0.038
R Squared	0.971
No. of Observations	17
Degrees of Freedom	15

X Coefficient(s)	-18203	
Std Err of Coef.	809.7	

Exp 123

Regression Output:

Constant	14.641
Std Err of Y Est	0.029
R Squared	0.948
No. of Observations	26
Degrees of Freedom	24

X Coefficient(s)	-14142	
Std Err of Coef.	674.9	

Exp 117

Regression Output:

Constant	19.981
Std Err of Y Est	0.058
R Squared	0.961
No. of Observations	15
Degrees of Freedom	13

X Coefficient(s)	-20354	
Std Err of Coef.	1134.3	

Exp 125

Regression Output:

Constant	18.843
Std Err of Y Est	0.053
R Squared	0.902
No. of Observations	26
Degrees of Freedom	24

X Coefficient(s)	-18802	
Std Err of Coef.	1263.9	

Exp 119

Regression Output:

Constant	14.482
Std Err of Y Est	0.028
R Squared	0.961
No. of Observations	25
Degrees of Freedom	23

X Coefficient(s)	-13842	
Std Err of Coef.	578.7	

Exp 127

Regression Output:

Constant	18.729
Std Err of Y Est	0.095
R Squared	0.911
No. of Observations	30
Degrees of Freedom	28

X Coefficient(s)	-18822	
Std Err of Coef.	1114.3	

Exp 121

Regression Output:

Constant	19.137
Std Err of Y Est	0.061
R Squared	0.888
No. of Observations	27
Degrees of Freedom	25

X Coefficient(s)	-19369	
Std Err of Coef.	1378.9	

Exp 129

Regression Output:

Constant	12.268
Std Err of Y Est	0.107
R Squared	0.607
No. of Observations	31
Degrees of Freedom	29

X Coefficient(s)	-11415	
Std Err of Coef.	1704.8	

The X Coefficient corresponds to -Ea/R.   The Constant corresponds to ln(ko).

APPENDIX 5: A COMPARISON OF EXPERIMENTALLY DETERMINED AND CALCULATED VALUES FOR THE GAS FILM MASS TRANSFER COEFFICIENT

For instantaneous reactions controlled by mass transfer through the gas film, the rate of reaction can be written as:

$$-r_{NO} = -\frac{1}{V_L}\frac{\delta N_{NO}}{\delta t} = ak_g P_{NO}.$$

By substituting $N_{NO}/V_L = C_{NO} = P_{NO}/H_{NO}$, the rate expression can be written as:

$$-\frac{\delta P_{NO}}{\delta t}\frac{1}{H_{NO}} = ak_g P_{NO} \quad or \quad -\frac{\delta P_{NO}}{P_{NO}} = ak_g H_{NO}\delta t.$$

Integrating both sides and rearranging terms gives:

$$k_g = \frac{-\ln(\frac{P_{NO,f}}{P_{NO,i}})}{aH_{NO}t}.$$

Experimentally determined values were calculated from the expression above.

By definition, $k_g = \frac{D_{NO/He}}{RTz}$. This definition was used in solving for the calculated values of k_g.

Both experimentally determined and calculated values for k_g for several experiments are included in the following tables.

Instantaneous Chemical Reaction, Reaction Controlled by Mass Transfer Only

Experiment 114

Temperature (C)	Experimental Kg (mol /cm^2 atm s)	Calculated Kg (mol /cm^2 atm s)	Exp/Calc
887.8	3.00E-05	7.35E-03	0.0041
887.8	3.20E-05	7.35E-03	0.0044
888.3	3.31E-05	7.36E-03	0.0045
888.3	3.41E-05	7.36E-03	0.0046
902.8	4.05E-05	7.40E-03	0.0055
905.0	4.11E-05	7.41E-03	0.0055
905.6	4.13E-05	7.41E-03	0.0056
906.1	4.12E-05	7.41E-03	0.0056
916.1	5.07E-05	7.44E-03	0.0068
916.1	4.94E-05	7.44E-03	0.0066
917.2	4.88E-05	7.45E-03	0.0066
916.7	4.84E-05	7.44E-03	0.0065
916.7	4.81E-05	7.44E-03	0.0065
932.2	6.57E-05	7.49E-03	0.0088
932.2	6.24E-05	7.49E-03	0.0083
932.8	5.91E-05	7.49E-03	0.0079
932.2	5.83E-05	7.49E-03	0.0078

Experiment 117

Temperature (C)	Experimental Kg (mol /cm^2 atm s)	Calculated Kg (mol /cm^2 atm s)	Exp/Calc
862.8	1.85E-05	7.27E-03	0.0025
862.2	2.01E-05	7.27E-03	0.0028
861.1	2.15E-05	7.27E-03	0.0030
879.4	2.72E-05	7.33E-03	0.0037
881.7	2.63E-05	7.33E-03	0.0036
882.8	2.66E-05	7.34E-03	0.0036
883.3	2.70E-05	7.34E-03	0.0037
892.2	3.54E-05	7.37E-03	0.0048
893.3	3.59E-05	7.37E-03	0.0049
895.0	3.62E-05	7.38E-03	0.0049
894.4	3.72E-05	7.37E-03	0.0050
911.1	4.50E-05	7.43E-03	0.0061
912.2	4.56E-05	7.43E-03	0.0061
913.3	4.58E-05	7.43E-03	0.0062
913.3	4.67E-05	7.43E-03	0.0063

Experiment 119

Temperature (C)	Experimental Kg (mol /cm^2 atm s)	Calculated Kg (mol /cm^2 atm s)	Exp/Calc
877.8	3.01E-05	7.32E-03	0.0041
878.3	2.92E-05	7.32E-03	0.0040
879.4	2.96E-05	7.33E-03	0.0040
880.0	3.11E-05	7.33E-03	0.0042
879.4	3.10E-05	7.33E-03	0.0042
889.4	3.46E-05	7.36E-03	0.0047
888.9	3.59E-05	7.36E-03	0.0049
888.9	3.64E-05	7.36E-03	0.0050
888.3	3.61E-05	7.36E-03	0.0049
888.9	3.62E-05	7.36E-03	0.0049
894.4	3.72E-05	7.37E-03	0.0050
896.1	3.79E-05	7.38E-03	0.0051
896.1	3.84E-05	7.38E-03	0.0052
896.1	3.89E-05	7.38E-03	0.0053
896.7	3.89E-05	7.38E-03	0.0053
905.0	4.26E-05	7.41E-03	0.0058
905.0	4.30E-05	7.41E-03	0.0058
905.6	4.34E-05	7.41E-03	0.0059
906.1	4.22E-05	7.41E-03	0.0057
906.1	4.19E-05	7.41E-03	0.0056
916.1	4.94E-05	7.44E-03	0.0066
916.7	4.85E-05	7.44E-03	0.0065
917.2	4.79E-05	7.45E-03	0.0064
917.8	4.70E-05	7.45E-03	0.0063
917.8	4.71E-05	7.45E-03	0.0063

Experiment 121

Temperature (C)	Experimental Kg (mol /cm^2 atm s)	Calculated Kg (mol /cm^2 atm s)	Exp/Calc
881.7	2.73E-05	7.33E-03	0.0037
881.7	2.77E-05	7.33E-03	0.0038
882.2	2.93E-05	7.34E-03	0.0040
882.2	3.00E-05	7.34E-03	0.0041
882.8	3.04E-05	7.34E-03	0.0041
891.7	4.13E-05	7.37E-03	0.0056
892.8	4.18E-05	7.37E-03	0.0057
893.3	4.05E-05	7.37E-03	0.0055
893.3	4.01E-05	7.37E-03	0.0054
893.3	3.89E-05	7.37E-03	0.0053
900.0	4.28E-05	7.39E-03	0.0058
900.6	4.32E-05	7.39E-03	0.0058
901.1	4.30E-05	7.40E-03	0.0058
901.1	4.34E-05	7.40E-03	0.0059
900.6	4.32E-05	7.39E-03	0.0058
906.1	4.51E-05	7.41E-03	0.0061
907.2	4.63E-05	7.41E-03	0.0062
907.2	4.58E-05	7.41E-03	0.0062
907.8	4.59E-05	7.42E-03	0.0062
907.8	4.56E-05	7.42E-03	0.0061
907.2	4.53E-05	7.41E-03	0.0061
915.0	5.15E-05	7.44E-03	0.0069
915.6	5.14E-05	7.44E-03	0.0069
915.6	5.06E-05	7.44E-03	0.0068
916.1	5.07E-05	7.44E-03	0.0068
916.1	5.27E-05	7.44E-03	0.0071
916.7	5.17E-05	7.44E-03	0.0069

Tables are continued on the next page.

Instantaneous Chemical Reaction, Reaction Controlled by Mass Transfer Only

Experiment 123

Temperature (C)	Experimental Kg (mol /cm^2 atm s)	Calculated Kg (mol /cm^2 atm s)	Exp/Calc
878.9	3.10E-05	7.33E-03	0.0042
880.0	2.98E-05	7.33E-03	0.0041
880.0	3.05E-05	7.33E-03	0.0042
880.0	3.02E-05	7.33E-03	0.0041
880.6	3.06E-05	7.33E-03	0.0042
888.9	3.67E-05	7.36E-03	0.0050
889.4	3.62E-05	7.36E-03	0.0049
890.0	3.60E-05	7.36E-03	0.0049
889.4	3.43E-05	7.36E-03	0.0047
888.9	3.48E-05	7.36E-03	0.0047
889.4	3.52E-05	7.36E-03	0.0048
896.7	3.96E-05	7.38E-03	0.0054
897.2	3.92E-05	7.38E-03	0.0053
897.2	3.92E-05	7.38E-03	0.0053
897.8	3.80E-05	7.39E-03	0.0052
897.8	3.86E-05	7.39E-03	0.0052
905.0	4.48E-05	7.41E-03	0.0060
905.6	4.28E-05	7.41E-03	0.0058
905.6	4.29E-05	7.41E-03	0.0058
905.6	4.27E-05	7.41E-03	0.0058
905.6	4.21E-05	7.41E-03	0.0057
912.8	4.58E-05	7.43E-03	0.0062
912.8	4.60E-05	7.43E-03	0.0062
913.3	4.54E-05	7.43E-03	0.0061
913.3	4.46E-05	7.43E-03	0.0060
913.9	4.46E-05	7.44E-03	0.0060

Experiment 125

Temperature (C)	Experimental Kg (mol /cm^2 atm s)	Calculated Kg (mol /cm^2 atm s)	Exp/Calc
883.9	3.56E-05	7.34E-03	0.0048
883.3	3.24E-05	7.34E-03	0.0044
883.3	3.42E-05	7.34E-03	0.0047
882.2	3.42E-05	7.34E-03	0.0047
882.2	3.54E-05	7.34E-03	0.0048
882.8	3.61E-05	7.34E-03	0.0049
889.4	4.19E-05	7.36E-03	0.0057
889.4	4.14E-05	7.36E-03	0.0056
889.4	4.14E-05	7.36E-03	0.0056
890.6	4.18E-05	7.36E-03	0.0057
890.0	4.25E-05	7.36E-03	0.0058
897.8	5.01E-05	7.39E-03	0.0068
897.8	4.84E-05	7.39E-03	0.0066
897.8	4.82E-05	7.39E-03	0.0065
897.8	4.81E-05	7.39E-03	0.0065
898.3	4.75E-05	7.39E-03	0.0064
903.9	5.39E-05	7.40E-03	0.0073
904.4	5.20E-05	7.41E-03	0.0070
904.4	5.17E-05	7.41E-03	0.0070
904.4	5.08E-05	7.41E-03	0.0069
905.0	5.09E-05	7.41E-03	0.0069
913.9	5.70E-05	7.44E-03	0.0077
915.0	5.82E-05	7.44E-03	0.0078
915.0	5.66E-05	7.44E-03	0.0076
915.0	5.59E-05	7.44E-03	0.0075
915.0	5.53E-05	7.44E-03	0.0074

Tables are continued on the next page.

Instantaneous Chemical Reaction, Reaction Controlled by Mass Transfer Only

Experiment 127

Temperature (C)	Experimental Kg (mol /cm^2 atm s)	Calculated Kg (mol /cm^2 atm s)	Exp/Calc
864.4	1.87E-05	7.28E-03	0.0026
864.4	1.90E-05	7.28E-03	0.0026
865.0	2.16E-05	7.28E-03	0.0030
865.0	2.26E-05	7.28E-03	0.0031
866.1	2.43E-05	7.28E-03	0.0033
878.9	3.08E-05	7.33E-03	0.0042
878.3	3.20E-05	7.32E-03	0.0044
878.3	3.25E-05	7.32E-03	0.0044
878.9	3.36E-05	7.33E-03	0.0046
879.4	3.44E-05	7.33E-03	0.0047
892.2	4.03E-05	7.37E-03	0.0055
892.2	3.96E-05	7.37E-03	0.0054
892.8	4.05E-05	7.37E-03	0.0055
892.8	4.00E-05	7.37E-03	0.0054
892.8	4.03E-05	7.37E-03	0.0055
904.4	4.79E-05	7.41E-03	0.0065
904.4	4.84E-05	7.41E-03	0.0065
905.0	4.63E-05	7.41E-03	0.0063
904.4	4.68E-05	7.41E-03	0.0063
905.0	4.62E-05	7.41E-03	0.0062
915.6	5.45E-05	7.44E-03	0.0073
915.0	5.26E-05	7.44E-03	0.0071
915.6	5.23E-05	7.44E-03	0.0070
916.1	5.23E-05	7.44E-03	0.0070
915.6	5.13E-05	7.44E-03	0.0069
927.2	5.94E-05	7.48E-03	0.0079
927.2	5.71E-05	7.48E-03	0.0076
927.8	5.70E-05	7.48E-03	0.0076
927.8	5.66E-05	7.48E-03	0.0076
927.8	5.70E-05	7.48E-03	0.0076

Experiment 129

Temperature (C)	Experimental Kg (mol /cm^2 atm s)	Calculated Kg (mol /cm^2 atm s)	Exp/Calc
872.2	2.36E-05	7.30E-03	0.0032
870.6	2.59E-05	7.30E-03	0.0036
870.6	2.80E-05	7.30E-03	0.0038
870.6	2.80E-05	7.30E-03	0.0038
870.6	2.74E-05	7.30E-03	0.0038
870.6	2.74E-05	7.30E-03	0.0038
881.1	3.16E-05	7.33E-03	0.0043
881.1	3.17E-05	7.33E-03	0.0043
881.1	3.07E-05	7.33E-03	0.0042
881.1	3.10E-05	7.33E-03	0.0042
885.6	3.03E-05	7.35E-03	0.0041
886.7	2.98E-05	7.35E-03	0.0041
886.7	3.04E-05	7.35E-03	0.0041
895.6	3.47E-05	7.38E-03	0.0047
896.1	3.44E-05	7.38E-03	0.0047
896.7	3.40E-05	7.38E-03	0.0046
892.2	3.47E-05	7.37E-03	0.0047
892.8	3.47E-05	7.37E-03	0.0047
893.3	3.39E-05	7.37E-03	0.0046
903.9	4.05E-05	7.40E-03	0.0055
903.3	3.95E-05	7.40E-03	0.0053
903.3	3.88E-05	7.40E-03	0.0052
905.0	3.78E-05	7.41E-03	0.0051
906.1	3.75E-05	7.41E-03	0.0051
906.7	3.74E-05	7.41E-03	0.0050
915.0	4.22E-05	7.44E-03	0.0057
915.6	4.15E-05	7.44E-03	0.0056
915.6	4.13E-05	7.44E-03	0.0055
913.9	4.35E-05	7.44E-03	0.0059
912.8	4.39E-05	7.43E-03	0.0059
913.3	4.31E-05	7.43E-03	0.0058

APPENDIX 6: CALCULATION OF THE PSEUDO FIRST ORDER RATE CONSTANT

Several calculation are required to determine the pseudo first order rate constant, k_1, as a function of flow rate, temperature, inlet concentration and the mass of salt. A sample set of calculations is given below for the following conditions taken from Experiment 24.

$m_{Na2CO3} = 35.0$ g $\qquad$ $[NO]_{in} = 1857$ ppm

$T = 934.0\,°C = 1207.1\,°K$ $\qquad$ $[NO]_{out} = 1670$ ppm

$V' = 1.00$ L/min as air at STP

$V = 1.43\ V'\ T/298 = 5.79$ L/min as He at 934 °C $= 9.65 \times 10^{-5}\,m^3/s$

Physical properties of the molten sodium carbonate at $T = 934$ °C are calculated based on correlations derived by Janz et al. as follows:

μ_{Na2CO3} = viscosity of molten $Na_2CO_3 = 3.832 \times 10^{-8} \exp(13215/T) = 2.18 \times 10^{-3}$ kg/m s

ρ = density of molten $Na_2CO_3 = 1000(2.4797 - 0.4487 \times 10^{-3}\ T) = 1938$ kg/m^3

γ = surface tension of $Na_2CO_3 = (254.8 - 0.0502t')/1000 = 0.208$ kg/s^2

t' = temperature (°C) = 934.0 °C

The derivation of the pseudo first order rate expression begins on page 54. At the end of the derivation it was shown that the rate constant, k_1, can be calculated by Eq. 51 as follows:

$$k_1 = \left(\frac{1}{\frac{at}{-\ln\Psi} - \frac{1}{H_A k_g}} \right)^2 \times \frac{1}{(D_{NO/Na})}$$

The following values are substituted to determine $k_1 = 2.21 \times 10^6$ s^{-1}

$H_A = 1.19 \times 10^6\,m^3$ Pa/mol $\qquad$ $a = 31.7\,m^{-1}$ $\qquad$ $t = 0.23$ s

$k_g = 7.38 \times 10^{-4}$ mol/m^2 Pa s $\qquad$ $D_{NO/Na} = 6.33 \times 10^{-9}\,m^2/s$ $\qquad$ $\Psi = 0.42$

By definition,

$\Psi = P_{NOf}/P_{NOi} = [NO]_f/[NO]_i = 0.42$

Janz, G.J., Dampier, F.W., Lakshminarayanan, G.R., Lorenz, P.K. and Tomkins, R.P.T., Molten Salts: Volume 1, Electrical Conductance, Density and Viscosity Data, National Standard Reference Data Series-National Bureau of Standards, October, 1968.
Janz, G.J., Lakshminarayanan, G.R., Tomkins, R.P.T., and Wong, J., Molten Salts: Volume 2: Surface Tension Data, National Standard Reference Data Series-National Bureau of Standards, August, 1969.

The diffusivity of NO in sodium carbonate is calculated according to the Wilke Chang equation (Treybal p. 35).

$$D_{NO/Na} = \frac{117.3 \times 10^{-18} (\varphi M_{Na_2CO_3})^{0.5} T}{\mu_{Na_2CO_3} (v)^{0.6}} = 6.33 \times 10^{-9} \ m^2/s$$

where, φ = association factor for solvent = 1 (assumed)

T = absolute temperature = 1207.1

μ_{Na2CO3} = viscosity of molten Na_2CO_3 = 2.18 x 10^{-3} kg/m s

M_{Na2CO3} = molecular weight of solvent = 106 g/mol

v = molal volume of NO at normal boiling point = 0.0236 m^3 (From Treybal p. 33)

The phase separation constant is determined from the Uhlig-Blander equation (Andreson).

$$K_H = \frac{\exp(-4\Pi N r^2 \gamma / 8.314T)}{82.06T} = 8.37 \times 10^{-7} \ mol/m^3 \ Pa$$

where, N = Avogadro's number = 6.022 x 10^{23}

r = molecular radius of NO = 1.26 x 10^{-10} m

γ = surface tension of Na_2CO_3 = 0.208 kg/s^2

T = absolute temperature = 1207.1 °K

H_A = 1/K_H = 1.19 x 10^6 m^3 Pa/mol

The gas film mass transfer coefficient is defined as (Treybal p.49):

$$k_g = D_{NO/He}/RTz = 7.38 \times 10^{-4} \ mol/m^2 \ Pa \ s$$

where, R = Universal gas constant = 8.314 m^3 Pa/mol °K

z = gas film thickness = 10^{-4} m (assumed)

T = absolute temperature = 1145.4 °K

$D_{NO/He}$ = diffusivity of NO in helium = 7.41 x 10^{-4} m^2/s

Treybal, R.E., Mass Transfer Operations, 3rd Edition, McGraw-Hill Book Company, New York, 1980.
Andreson, R.E., J. Electrochemical Society, 328-334(1979).

The diffusivity of NO in helium is calculated from the Wilke-Lee modification of the Hirschfelder-Bird-Spotz method (Treybal, p. 31).

$$D_{NO/He} = \frac{10^{-4}\left(1.084-0.249\sqrt{1/M_{NO}+1/M_{He}}\right)T^{1.5}\sqrt{1/M_{NO}+1/M_{He}}}{P_t(r_{NO/He})^2 f(kT/\varepsilon_{NO/He})} = 7.41 \times 10^{-4}\,m^2/s$$

where, M_{NO} = molecular weight of NO = 30 g/mol

M_{He} = molecular weight of He = 4 g/mol

P_t = absolute pressure = 101325 Pa

$r_{NO/He}$ = molecular separation at collision = $(r_{NO} + r_{He})/2$ = (0.3492 + 0.2551)/2 = 0.302 nm

T = absolute temperature = 1207.1 °K

$\varepsilon_{NO/He}$ = energy of molecular attraction = $\sqrt{\varepsilon_{NO}\varepsilon_{He}}$
$= \sqrt{116.7(10.22)}$ = 34.5 (Table 2.2, Treybal, p. 33)

$f(kT/\varepsilon_{NO/He})$ = collision function = 0.31 (Given by Figure 2.5, Treybal, p. 32)

The surface to volume ratio is calculated as (Treybal, p. 144):

$$a = 6\varepsilon/d_b, = 31.7\ m^{-1}$$

where, ε = gas holdup = 0.185

d_b = diameter of gas bubble (m) = 0.035 m

The bubble diameter is calculated as (Cheremisinoff, p. 228) :

$$d_b = \left[\left(\frac{\alpha\gamma D_t}{\rho g}\right)^2 + 9.5\left(\frac{V^2 D_t}{g}\right)^{0.867}\right]^{0.167} = 0.031\,m^{-1}$$

where, α = correlation factor = 30 (assumed)

D_t = outside diameter of purge tube = 0.25 in = 6.64 x 10^{-3} m

ρ = density of molten Na_2CO_3 = 1966 kg/m³

g = acceleration due to gravity = 9.81 m/s²

V = volumetric flow rate of gas in purge tube = 9.65 x 10^{-5} m³/s

Cheremisinoff, N.P., Encyclopedia of Fluid Mechanics, Volume 3: Gas-Liquid Flows, Gulf Publishing Company, Houston, 1986.

The gas holdup is calculated as (Cheremisinoff, p. 1199) :

$$\varepsilon = 0.5\left(\frac{U_{br}}{\sqrt{gR_c}}\right)^{0.4}\left(\frac{U_{gs}}{U_{br}}\right)^{0.8} = 0.143$$

where, U_{br} = bubble rise velocity = 0.16 m/s

R_c = radius of crucible = 0.02 m

U_{gs} = superficial gas velocity = $V/(\Pi R_c^2)$ = 0.077 m/s

g = acceleration due to gravity = 9.81 m/s^2

The bubble rise velocity is determined based on a correlation of the Reynold's number as a function of the dimensionless parameters, E_o and M. The Reynold's number is determined from a plot of log(M) vs. E_o (Hestroni, p. 1-206).

$E_o = g \rho d_b^2/\gamma = 112$ $M = g \mu^4/\rho\gamma^3 = 1.27 \times 10^{-11}$ $\log(M) = -10.9$

$Re = \rho d_b U_{br}/\mu = 5000$ Thus, $U_{br} = 0.16$ m/s.

where, g = acceleration due to gravity = 9.81 m/s^2

ρ = density of molten Na_2CO_3 = 1938 kg/m^3

d_b = diameter of bubble = 0.035 m

γ = surface tension of Na_2CO_3 = 0.208 kg/s^2

μ = viscosity of Na_2CO_3 = 2.18 x 10^{-3} kg/m s

The contact time is calculated based on the expanded liquid volume and volumetric flow rate:

$$t = \frac{V_L}{V(1-\varepsilon)} = \frac{m}{\rho V(1-\varepsilon)} = 0.23 \text{ s}$$

where, V = volumetric flow rate = 9.65 x 10^{-5} m^3/s

V_L = volume of molten Na_2CO_3 = m/ρ = 1.81 x 10^{-5} m^3

ρ = density of molten Na_2CO_3 = 1938 kg/m^3

m = mass of Na_2CO_3 = 0.035 kg

ε = gas holdup = 0.185

Hestroni, G., Handbook of Multiphase Systems, McGraw-Hill Book Company, New York, 1982.

APPENDIX 7: DETERMINATION OF THE PSEUDO FIRST ORDER RATE CONSTANT FOR THE DEPLETION OF NO BY REACTION WITH MOLTEN SODIUM CARBONATE

This appendix includes tables of raw data that was used to determine the pseudo first order rate constant for the depletion of NO by reaction with molten sodium carbonate. Data tables for the following experiments are included:

Experiment 24	Experiment 33
Experiment 27	Experiment 34
Experiment 28	Experiment 75
Experiment 29	Experiment 77

A plot of $\ln(k_1)$ vs $1/T$ for data from the above experiments is also included along with the regression output and confidence intervals for the activation energy, E_a, and pre-exponential constant, k_o.

Depletion of NO by Na₂CO₃
Experiment 24

[NO]ᵢₙ (ppm)	Mass of Na₂CO₃ (g)	Temperature (°C)	V in (L/min as air)	[NO]ₒᵤₜ (ppm)
1857	35.0	872:4	0.74	1670
1857	35.0	936.4	0.75	691
1857	35.0	957.4	0.75	576
1857	35.0	911.6	0.76	932
1857	35.0	893.6	0.74	1333
1857	35.0	889.7	0.98	1412
1857	35.0	956.1	0.99	639
1857	35.0	905.9	0.99	1082
1857	35.0	934.0	0.98	789

Depletion of NO by Na₂CO₃
Experiment 27

[NO]ᵢₙ (ppm)	Mass of Na₂CO₃ (g)	Temperature (°C)	V in (L/min as air)	[NO]ₒᵤₜ (ppm)
1857	35.0	914.2	0.76	924
1857	35.0	926.9	0.75	599
1857	35.0	877.2	0.76	1508
1857	35.0	892.2	0.76	1277
1857	35.0	947.2	0.75	477
1857	35.0	889.3	0.99	1287
1857	35.0	946.9	0.98	575
1857	35.0	913.5	0.99	1011
1857	35.0	926.9	0.97	725

Depletion of NO by Na$_2$CO$_3$
Experiment 28

[NO]$_{in}$ (ppm)	Mass of Na$_2$CO$_3$ (g)	Temperature (°C)	V in (L/min as air)	[NO]$_{out}$ (ppm)
1857	17.5	917.3	0.75	868
1857	17.5	875.7	0.75	1177
1857	17.5	897.7	0.75	1013
1857	17.5	957.2	0.76	609
1857	17.5	936.0	0.77	684
1857	17.5	897.9	0.99	1115
1857	17.5	917.2	1.00	956
1857	17.5	936.0	0.99	803
1857	17.5	957.1	0.98	679

Depletion of NO by Na$_2$CO$_3$
Experiment 29

[NO]$_{in}$ (ppm)	Mass of Na$_2$CO$_3$ (g)	Temperature (°C)	V in (L/min as air)	[NO]$_{out}$ (ppm)
1857	17.5	915.9	0.74	913
1857	17.5	881.0	0.75	1232
1857	17.5	957.2	0.75	757
1857	17.5	899.1	0.75	1073
1857	17.5	935.7	0.76	835
1857	17.5	915.5	0.99	1066
1857	17.5	956.7	1.00	825
1857	17.5	897.8	1.01	1272
1857	17.5	935.8	1.01	949

Depletion of NO by Na$_2$CO$_3$
Experiment 33

[NO]$_{in}$ (ppm)	Mass of Na$_2$CO$_3$ (g)	Temperature (°C)	V in (L/min as air)	[NO]$_{out}$ (ppm)
1,857	17.5	919.2	0.75	1179
1857	17.5	889.1	0.76	1346
1857	17.5	871.4	0.76	1559
1857	17.5	908.1	0.76	1260
1857	17.5	943.0	0.76	967
1857	17.5	958.9	0.76	861
1857	17.5	931.3	0.76	1113
1857	17.5	954.7	0.77	889
1857	17.5	944.0	0.96	1014
1857	17.5	922.2	0.96	1152
1857	17.5	933.1	0.96	1088
1857	17.5	909.8	0.98	1251
1857	17.5	954.1	0.99	946
1857	17.5	890.0	0.99	1379
1857	17.5	960.1	0.99	913

Depletion of NO by Na$_2$CO$_3$
Experiment 34

[NO]$_{in}$ (ppm)	Mass of Na$_2$CO$_3$ (g)	Temperature (°C)	V in (L/min as air)	[NO]$_{out}$ (ppm)
1857	35.0	955.1	0.76	620
1857	35.0	944.7	0.76	683
1857	35.0	933.2	0.76	794
1857	35.0	924.8	0.76	917
1857	35.0	960.0	0.77	604
1857	35.0	875.3	0.77	1857
1857	35.0	895.0	0.77	1309
1857	35.0	877.7	0.77	1507
1857	35.0	912.1	0.77	1117
1857	35.0	953.4	0.93	1858
1857	35.0	912.5	0.98	1126
1857	35.0	924.6	0.98	999
1857	35.0	945.2	0.99	777
1857	35.0	954.9	0.99	699
1857	35.0	959.2	0.99	664
1857	35.0	886.9	0.99	1274
1857	35.0	934.1	0.99	873

Depletion of NO by Na_2CO_3
Experiment 75

[NO]$_{in}$ (ppm)	Mass of Na$_2$CO$_3$ (g)	Temperature (°C)	V in (L/min as air)	[NO]$_{out}$ (ppm)
8400	25.0	888.9	0.64	6227
8400	25.0	907.2	0.65	5075
8400	25.0	864.4	0.65	7151
8400	25.0	945.3	0.65	2726
8400	25.0	944.4	0.65	2682
8400	25.0	967.8	0.65	2241
8400	25.0	925.8	0.65	3820
8400	25.0	968.9	0.65	2215
8400	25.0	926.1	0.65	3575
8400	25.0	943.9	0.65	2947
8400	25.0	907.2	0.79	5384
8400	25.0	925.0	0.79	4202
8400	25.0	967.5	0.80	2611
8400	25.0	888.3	0.80	6549
8400	25.0	945.0	0.80	3308
8400	25.0	968.9	0.80	2697
8400	25.0	945.0	0.80	3194
8400	25.0	908.3	0.80	5286
8400	25.0	926.1	0.80	4105
8400	25.0	862.8	0.85	7434
8400	25.0	865.6	0.94	7255
8400	25.0	887.8	0.95	6325
8400	25.0	907.2	0.95	5098
8400	25.0	888.9	0.95	6485
8400	25.0	907.8	0.95	5449
8400	25.0	859.4	0.95	7666
8400	25.0	925.6	0.95	4198
8400	25.0	945.3	0.95	3241
8400	25.0	944.4	0.95	3716
8400	25.0	926.4	0.95	4412
8400	25.0	968.6	0.95	2682

Depletion of NO by Na$_2$CO$_3$
Experiment 77

[NO]$_{in}$ (ppm)	Mass of Na$_2$CO$_3$ (g)	Temperature (°C)	V in (L/min as air)	[NO]$_{out}$ (ppm)
8400	25.0	867.2	0.65	7402
8400	25.0	947.2	0.65	2677
8400	25.0	869.4	0.65	7200
8400	25.0	891.1	0.65	5800
8400	25.0	948.3	0.65	2868
8400	25.0	910.6	0.65	4800
8400	25.0	910.0	0.65	3904
8400	25.0	972.8	0.65	2113
8400	25.0	971.1	0.65	2227
8400	25.0	930.0	0.65	3468
8400	25.0	970.6	0.80	2644
8400	25.0	972.8	0.80	2124
8400	25.0	867.8	0.80	7433
8400	25.0	948.3	0.80	3151
8400	25.0	910.6	0.80	5005
8400	25.0	890.6	0.80	6247
8400	25.0	890.0	0.80	6531
8400	25.0	928.9	0.80	3970
8400	25.0	910.6	0.80	5063
8400	25.0	927.8	0.80	4067
8400	25.0	947.8	0.80	3252
8400	25.0	870.6	0.80	7225
8400	25.0	927.8	0.95	4140
8400	25.0	871.1	0.95	7239
8400	25.0	889.4	0.95	6490
8400	25.0	890.6	0.95	6598
8400	25.0	928.9	0.95	4402
8400	25.0	948.3	0.95	3489
8400	25.0	910.6	0.95	5287
8400	25.0	971.1	0.95	2944
8400	25.0	970.6	0.95	3063

The preceeding data was used to calculate the rate constant for the depletion of NO by reaction with sodium carbonate as published in "Kinetics of NO Depletion by Reaction with Molten Sodium Carbonate." The table below correlates laboratory notebook page identification with experiment number identification as published in the paper.

Published Experiment #	Gas Flow Rate (L/min as air)	Lab Notebook ID by Page #
1A	0.75	28
1B	1.00	28
2A	0.65	75
2B	0.80	75
2C	0.95	75
3A	0.65	77
3B	0.80	77
3C	0.95	77
4A	0.75	24
4B	1.00	24
5A	0.75	27
5B	1.00	27
6A	0.75	34
6B	1.00	34
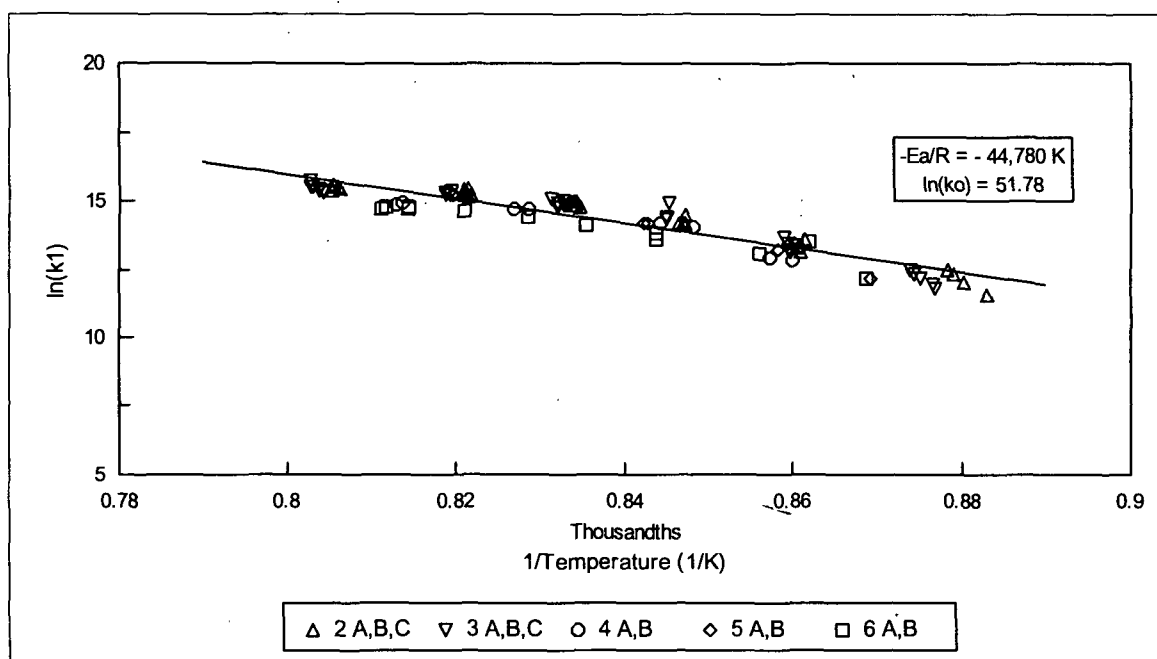
Determination of the Activation Energy for the Depletion of NO by Na₂CO₃
(as published in "Kinetics of NO Depletion by Reaction with Molten Sodium Carbonate").

Regression Output:	
Constant (ln(k₀))	51.78
Std Err of Y Est	0.39
R Squared	0.87
No. of Observations	95
Degrees of Freedom	93
X Coefficient(s) (-Eₐ/R)	-44,777
Std Err of Coef.	1,785

To determine the confidence intervals for the activation energy, Ea, and the pre-exponential constant, the standard error is multiplied by the "t" value for the appropriate confidence level as shown below:

Parameter	Std Error	$t_{90\%}$	$t_{95\%}$	90 % Conf Int	95 % Conf Int
Eₐ/R	1785	1.66	1.98	± 2963	± 3534
ln(k₀)	0.39	1.66	1.98	± 0.65	± 0.77

$E_a/R = 44780 \pm 2963$ $\ln(k_o) = 51.78 \pm .65$ at a 90 % confidence level.

APPENDIX 8: DEPLETION OF NO AT VARIOUS INLET CONCENTRATIONS

This appendix includes data for experiments in which NO was fed to the reaction system at various inlet concentrations. Data were plotted as conversion as a function of concentration to show that the reaction is first order with respect to [NO]. Experiments were conducted for both Na_2CO_3 and Na_2CO_3/Na_2S mixtures.

Experiments included in this section are:

Experiment 73	Experiment 74
Experiment 132	Experiment 133

Depletion of NO by Na₂CO₃ at Various Inlet Concentrations
Experiment 73 $m_{Na2CO3} = 35.0$ g

	Temp. (°C)	V_{He} (L/min as air)	V_{NO} (L/min as air)	Total Flow (L/min as air)	$[NO]_{in}$ (ppm)	$[NO]_{out}$ (ppm)	Conversion (%)
	863.9	0.00	0.91	0.91	8,259	7,545	8.6
	868.3	0.31	0.60	0.91	5,427	4,946	8.9
	868.9	0.46	0.45	0.91	4,079	3,627	11.1
	870.0	0.61	0.29	0.90	2,689	2,330	13.3
Average	867.8			0.91			10.5
Std. Dev.	2.3			0.00			1.9
	906.1	0.61	0.30	0.91	2,750	1,568	43.0
	906.7	0.46	0.45	0.92	4,099	2,557	37.6
	907.2	0.31	0.60	0.91	5,471	3,651	33.3
	907.8	0.00	0.90	0.90	8,262	5,900	28.6
Average	906.9			0.91			35.6
Std. Dev.	0.6			0.00			5.3
	943.9	0.00	0.90	0.90	8,270	3,675	55.6
	945.0	0.47	0.45	0.91	4,044	1,736	57.1
	945.0	0.31	0.59	0.90	5,409	2,493	53.9
	945.6	0.61	0.31	0.91	2,779	1,175	57.7
Average	944.9			0.91			56.1
Std. Dev.	0.6			0.01			1.5

Depletion of NO by Na$_2$CO$_3$ at Various Inlet Concentrations
Experiment 74   m$_{Na2CO3}$ = 35.0 g

	Temp. (°C)	V$_{He}$ (L/min as air)	V$_{NO}$ (L/min as air)	Total Flow (L/min as air)	[NO]$_{in}$ (ppm)	[NO]$_{out}$ (ppm)	Conversion (%)
	867.8	0.60	0.30	0.90	2,759	2,299	16.7
	869.4	0.46	0.45	0.91	4,125	3,503	15.1
	870.6	0.32	0.60	0.92	5,467	4,750	13.1
	871.7	0.00	0.90	0.90	8,350	7,289	12.7
Average	869.9			0.91			14.4
Std. Dev.	1.4			0.01			1.6
	916.7	0.00	0.90	0.90	8,350	4,970	40.5
	917.2	0.61	0.30	0.92	2,765	1,605	42.0
	917.2	0.46	0.45	0.91	4,125	2,503	39.3
	917.2	0.31	0.59	0.91	5,456	3,471	36.4
Average	917.1			0.91			39.5
Std. Dev.	0.2			0.01			2.0
	953.3	0.61	0.30	0.90	2,756	911	66.9
	953.9	0.46	0.45	0.91	4,143	1,488	64.1
	953.9	0.31	0.60	0.92	5,494	2,052	62.6
	953.7	0.00	0.90	0.90	8,350	3,191	61.8
Average	953.7			0.91			63.9
Std. Dev.	0.2			0.01			2.0

Depletion of NO by Na₂CO₃ at Various Inlet Concentrations
Experiments 73 and 74

Constant Conversion Shows Depletion Behaves as First Order with Respect to [NO]

Depletion of NO by Na$_2$CO$_3$/Na$_2$S Mixtures at Various Inlet Concentrations
Experiment 132   m$_{Na2CO3}$ = 38.0 g   m$_{Na2S}$ = 2.0 g

	Temp. (°C)	V$_{He}$ (L/min as air)	V$_{NO}$ (L/min as air)	Total Flow (L/min as air)	[NO]$_{in}$ (ppm)	[NO]$_{out}$ (ppm)	Conversion (%)
	890.0	0.00	0.89	0.89	9,420	388	95.9
	888.3	0.31	0.60	0.91	6,194	271	95.6
	887.8	0.47	0.45	0.92	4,612	170	96.3
	887.8	0.62	0.30	0.92	3,062	95	96.9
	888.3	0.46	0.45	0.91	4,679	136	97.1
	889.4	0.31	0.60	0.91	6,176	178	97.1
	890.6	0.15	0.75	0.90	7,850	221	97.2
	894.4	0.00	0.90	0.90	9,420	188	98.0
Average	889.6			0.91			96.8
Std. Dev.	2.1			0.01			0.7

Depletion of NO by Na$_2$CO$_3$/Na$_2$S Mixtures at Various Inlet Concentrations
Experiment 133A   m$_{Na2CO3}$ = 38.0 g   m$_{Na2S}$ = 2.0 g

	Temp. (°C)	V$_{He}$ (L/min as air)	V$_{NO}$ (L/min as air)	Total Flow (L/min as air)	[NO]$_{in}$ (ppm)	[NO]$_{out}$ (ppm)	Conversion (%)
	895.0	0.70	0.20	0.90	2,063	18	99.1
	895.0	0.56	0.35	0.91	3,654	40	98.9
	895.6	0.71	0.20	0.91	2,065	19	99.1
	896.1	0.55	0.35	0.91	3,654	39	98.9
	896.1	0.46	0.45	0.91	4,684	53	98.9
	896.1	0.35	0.55	0.90	5,734	74	98.7
	896.1	0.46	0.45	0.90	4,663	61	98.7
	895.6	0.37	0.55	0.92	5,652	81	98.6
	895.6	0.23	0.70	0.93	7,121	109	98.5
	898.3	0.00	0.90	0.90	9,420	125	98.7
	896.7	0.22	0.70	0.92	7,124	114	98.4
	898.3	0.00	0.90	0.90	9,420	132	98.6
Average	896.2			0.91			98.8
Std. Dev.	1.1			0.01			0.2

Table is continued on next page.

Table is continued from preceeding page.

Depletion of NO by Na₂CO₃/Na₂S Mixtures at Various Inlet Concentrations
Experiment 133B m_{Na2CO3} = 38.0 g m_{Na2S} = 2.0 g

	Temp. (°C)	V_{He} (L/min as air)	V_{NO} (L/min as air)	Total Flow (L/min as air)	[NO]$_{in}$ (ppm)	[NO]$_{out}$ (ppm)	Conversion (%)
	909.4	0.71	0.20	0.91	2,030	13	99.4
	910.0	0.56	0.36	0.91	3,675	26	99.3
	910.0	0.71	0.20	0.91	2,079	14	99.3
	910.0	0.55	0.35	0.90	3,691	27	99.3
	910.6	0.46	0.45	0.91	4,684	37	99.2
	911.1	0.34	0.55	0.89	5,821	44	99.2
	911.7	0.45	0.45	0.90	4,705	35	99.3
	911.7	0.36	0.55	0.91	5,693	50	99.1
	912.2	0.22	0.70	0.92	7,154	66	99.1
	911.7	0.00	0.90	0.90	9,420	80	99.2
	910.0	0.22	0.69	0.91	7,168	76	98.9
	911.1	0.00	0.91	0.91	9,420	82	99.1
Average	910.8			0.91			99.2
Std. Dev.	0.9			0.01			0.1

Tav= 889.6, Xav=96.8   Tav = 896.2, Xav=98.8   Tav = 910.8, Xav=99.2
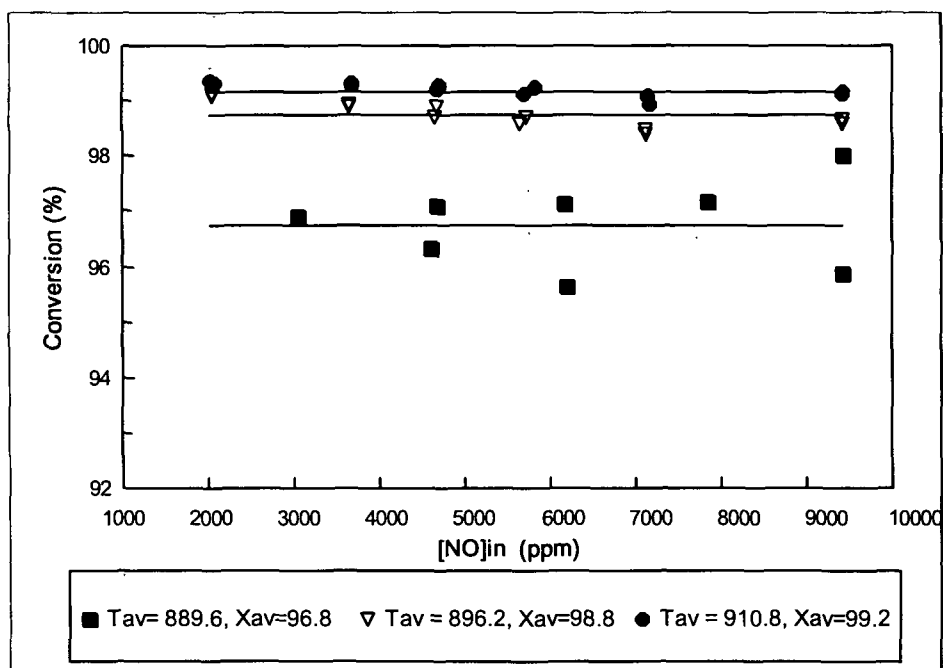
APPENDIX 9: DEPLETION OF NO BY REACTION WITH Na_2CO_3 AND Na_2CO_3/Na_2S MIXTURES; RATE DATA AND GAS ANALYSIS BY GC

This appendix includes data tables for the depletion of NO by reaction with Na_2CO_3 with gas analysis by GC. Experiments included in this section are:

Experiment 85	Experiment 86
Experiment 97	Experiment 98
Experiment 100	Experiment 112

This appendix also includes data tables for the depletion of NO by reaction with Na_2CO_3/Na_2S mixtures with gas analysis by GC. Experiments included in this section are:

Experiment 114	Experiment 117
Experiment 119	Experiment 123
Experiment 127	

Three additional experiments were conducted without gas analysis, simply to acquire more rate data. These experiments include:

Experiment 121	Experiment 125
Experiment 129	

A plot of $\ln(k_1)$ *vs* $1/T$ for data from the above experiments with Na_2S is also included along with the regression output and confidence intervals for the activation energy, E_a, and pre-exponential constant, k_o.

Depletion of NO by Na₂CO₃ with Gas Analysis by GC
Experiment 85 $m_{Na2CO3} = 30.0$ g   [NO]$_{in}$ = 8400 ppm in Helium

Temp (C)	V	[NO]$_{out}$	GC Run	Area O$_2$	Area N$_2$	[O$_2$]	[N$_2$]	[O$_2$]/[N$_2$]	[NO]Depl.	% O$_2$ Rec	% N$_2$ Rec
887.2	0.80	6,860	89		4,155		442		1,540		57.4
888.3	0.79	6,673	90		5,835		621		1,727		71.9
888.3	0.79	6,520	91		8,550		910		1,880		96.8
889.4	0.80	6,179	92		10,383		1,105		2,221		99.5
891.1	0.80	5,931	93		10,007		1,065		2,469		86.2
891.1	0.80	5,669	94		13,358		1,421		2,731		104.1
913.9	0.79	4,493	96	3,048	17,024	1,790	1,811	0.99	3,907	91.6	92.7
915.6	0.78	4,266	97	4,745	20,892	1,962	2,223	0.88	4,134	94.9	107.5
916.1	0.78	4,103	98	4,631	22,206	1,897	2,362	0.80	4,297	88.3	110.0
916.1	0.78	3,852	99	5,771	23,618	1,983	2,513	0.79	4,548	87.2	110.5
916.7	0.78	3,711	100	4,809	22,990	1,804	2,446	0.74	4,689	76.9	104.3
916.7	0.78	3,621	101	7,398	22,886	2,144	2,435	0.88	4,779	89.7	101.9
937.2	0.77	3,044	102	10,436	25,057	2,401	2,666	0.90	5,356	89.7	99.5
937.2	0.77	2,955	103	10,495	26,815	2,383	2,853	0.84	5,445	87.5	104.8
937.2	0.77	2,895	104	10,657	29,486	2,388	3,137	0.76	5,505	86.7	114.0
937.8	0.77	2,765	105	11,358	28,379	2,448	3,019	0.81	5,635	86.9	107.2
938.3	0.77	2,727	106	11,580	27,939	2,468	2,972	0.83	5,673	87.0	104.8
959.4	0.78	2,238	107	8,747	23,569	1,918	2,507	0.76	6,162	62.3	81.4
959.4	0.77	2,427	108	14,302	30,552	2,764	3,250	0.85	5,973	92.5	108.8
959.4	0.76	2,348	109	17,781	31,180	3,234	3,317	0.97	6,052	106.9	109.6
960.0	0.76	2,281	110	14,393	29,118	2,733	3,098	0.88	6,119	89.3	101.2
960.6	0.76	2,231	111	14,579	29,691	2,744	3,159	0.87	6,169	89.0	102.4
960.6	0.76	2,194	112	15,479	30,421	2,861	3,236	0.88	6,206	92.2	104.3

All concentrations are reported as ppm.
Conversion of peak area to concentration based on Calibration Experiment 91.

Depletion of NO by Na$_2$CO$_3$ with Gas Analysis by GC
Experiment 86   m$_{Na2CO3}$ = 30.0 g   [NO]$_{in}$ = 8400 ppm in Helium

Temp (C)	V	[NO]$_{out}$	GC Run	Area O$_2$	Area N$_2$	[O$_2$]	[N$_2$]	[O$_2$]/[N$_2$]	[NO]Depl.	% O$_2$ Rec	% N$_2$ Rec
896.7	0.78	6,376	128		9,298		989		2,024		97.7
896.7	0.78	6,151	129		10,507		1,118		2,249		99.4
896.7	0.78	5,902	130		13,321		1,417		2,498		113.5
896.7	0.77	5,646	131		14,414		1,533		2,754		111.4
917.2	0.77	4,464	133	2,690	19,898	1,730	2,117	0.82	3,936	87.9	107.6
917.2	0.77	4,349	134	4,149	21,239	1,903	2,259	0.84	4,051	93.9	111.6
917.8	0.77	4,141	135	6,149	22,299	2,124	2,372	0.90	4,259	99.7	111.4
917.8	0.77	4,047	135	4,618	27,131	1,878	2,886	0.65	4,353	26.2	133.7
917.2	0.76	3,849	136	5,774	25,401	1,982	2,702	0.73	4,551	87.1	118.8
917.2	0.76	3,795	136	6,273	23,468	2,037	2,497	0.82	4,605	88.5	108.4
940.6	0.77	2,734	137	9,040	23,893	2,109	2,542	0.83	5,666	74.5	89.7
940.6	0.77	2,824	137	10,263	28,432	2,310	3,025	0.76	5,576	82.9	108.5
942.2	0.77	2,822	138	14,044	29,723	2,846	3,162	0.90	5,578	102.1	113.4
942.2	0.77	2,774	138	11,247	29,317	2,435	3,119	0.78	5,626	86.6	110.9

All concentrations are reported as ppm.
Conversion of peak area to concentration based on Calibration Experiment 91.

Table is continued from preceeding page.

Depletion of NO by Na$_2$CO$_3$ with Gas Analysis by GC
Experiment 86   m$_{Na2CO3}$ = 30.0 g   [NO]$_{in}$ = 8400 ppm in Helium

Temp (C)	V	[NO]$_{out}$	GC Run	Area O$_2$	Area N$_2$	[O$_2$]	[N$_2$]	[O$_2$]/[N$_2$]	[NO]Depl.	% O$_2$ Rec	% N$_2$ Rec
941.7	0.77	2,674	139	14,156	30,686	2,818	3,264	0.86	5,726	98.4	114.0
941.7	0.77	2,618	139	12,200	30,539	2,523	3,249	0.78	5,782	87.3	112.4
941.7	0.76	2,549	140	14,479	31,021	2,826	3,300	0.86	5,851	96.6	112.8
941.7	0.76	2,507	140	12,372	30,532	2,514	3,248	0.77	5,893	85.3	110.2
961.1	0.77	2,067	141	12,539	28,089	2,405	2,988	0.80	6,333	75.9	94.4
961.1	0.77	2,084	141	13,876	29,794	2,600	3,170	0.82	6,316	82.3	100.4
961.1	0.77	2,102	142	18,318	32,525	3,236	3,460	0.94	6,298	102.8	109.9
961.1	0.77	2,068	142	15,270	31,243	2,793	3,324	0.84	6,332	88.2	105.0
962.2	0.77	2,003	143	17,912	33,720	3,148	3,587	0.88	6,397	98.4	112.2
962.2	0.76	1,972	143	17,366	36,123	3,062	3,843	0.80	6,428	95.3	119.6
962.2	0.77	1,916	144	17,383	32,530	3,047	3,461	0.88	6,484	94.0	106.7
962.2	0.77	1,900	144	18,079	33,749	3,141	3,590	0.87	6,500	96.6	110.5

All concentrations are reported as ppm.
Conversion of peak area to concentration based on Calibration Experiment 91.

Depletion of NO by Na$_2$CO$_3$ with Gas Analysis by GC
Experiment 97   m$_{Na2CO3}$ = 40.0 g   [NO]$_{in}$ = 8400 ppm in Helium

Temp (C)	V	[NO]$_{out}$	GC Run	Area O$_2$	Area N$_2$	[O$_2$]	[N$_2$]	[O$_2$]/[N$_2$]	[NO]Depl.	% O$_2$ Rec	% N$_2$ Rec
893.9	0.75	6,787	370		4,763		551		1,613		68.3
895.6	0.74	6,773	371		5,096		589		1,627		72.4
896.7	0.74	6,556	372		6,130		709		1,844		76.9
899.4	0.73	6,283	373		7,560		874		2,117		82.6
921.1	0.74	4,723	376	2,379	15,240	2,067	1,762	1.17	3,677	112.4	95.9
920.0	0.74	4,591	377	3,660	16,534	2,192	1,912	1.15	3,809	115.1	100.4
921.7	0.74	4,433	378	5,178	18,562	2,341	2,147	1.09	3,967	118.0	108.2
922.8	0.74	4,156	379	6,113	19,424	2,366	2,246	1.05	4,244	111.5	105.9
922.8	0.73	3,928	380	7,744	21,356	2,504	2,470	1.01	4,472	112.0	110.5
936.7	0.74	2,968	382	10,447	23,097	2,519	2,671	0.94	5,432	92.7	98.3
937.8	0.73	3,001	383	11,925	24,462	2,732	2,829	0.97	5,399	101.2	104.8
937.8	0.73	2,936	384	12,262	25,057	2,754	2,898	0.95	5,464	100.8	106.1

All concentrations are reported as ppm.
Conversion of peak area to concentration based on Calibration Experiment 96.

Table is continued on next page.

Table is continued from preceeding page.

Depletion of NO by Na₂CO₃ with Gas Analysis by GC

Experiment 97 m_{Na2CO3} = 40.0 g $[NO]_{in}$ = 8400 ppm in Helium

Temp (C)	V	$[NO]_{out}$	GC Run	Area O₂	Area N₂	$[O_2]$	$[N_2]$	$[O_2]/[N_2]$	[NO]Depl.	% O₂ Rec	% N₂ Rec
938.3	0.73	2,853	385	13,796	26,111	2,933	3,020	0.97	5,547	105.7	108.9
948.9	0.72	2,383	386	13,268	25,028	2,687	2,894	0.93	6,017	89.3	96.2
951.7	0.75	2,449	387	15,330	28,085	2,993	3,248	0.92	5,951	100.6	109.2
950.0	0.74	2,373	388	16,258	26,626	3,091	3,079	1.00	6,027	102.6	102.2
952.2	0.74	2,322	389	16,259	27,930	3,072	3,230	0.95	6,078	101.1	106.3
952.8	0.74	2,292	390	16,310	28,258	3,068	3,268	0.94	6,108	100.5	107.0
965.0	0.74	2,066	392	17,555	28,873	3,155	3,339	0.94	6,334	99.6	105.4
965.6	0.74	2,015	393	17,915	28,971	3,185	3,350	0.95	6,385	99.8	104.9
966.1	0.74	1,966	394	19,674	30,798	3,406	3,562	0.96	6,434	105.9	110.7
966.1	0.74	1,908	395	19,281	30,029	3,332	3,473	0.96	6,492	102.6	107.0
966.1	0.73	1,898	396	19,024	30,148	3,293	3,487	0.94	6,502	101.3	107.2

All concentrations are reported as ppm.

Conversion of peak area to concentration based on Calibration Experiment 96.

Depletion of NO by Na₂CO₃ with Gas Analysis by GC
Experiment 98 m_{Na2CO3} = 40.0 g [NO]$_{in}$ = 8400 ppm in Helium

Temp (C)	V	[NO]$_{out}$	GC Run	Area O₂	Area N₂	[O₂]	[N₂]	[O₂]/[N₂]	[NO]Depl.	% O₂ Rec	% N₂ Rec
905.6	0.75	6,085	405		8,235		952		2,315		82.3
910.6	0.73	5,747	406		10,631		1,229		2,653		92.7
911.1	0.73	5,366	407	1,166	12,813	2,138	1,482	1.44	3,034	141.0	97.7
912.2	0.75	5,048	408	2,517	15,211	2,205	1,759	1.25	3,352	131.6	105.0
913.3	0.75	4,655	409	3,649	17,583	2,215	2,033	1.09	3,745	118.3	108.6
914.4	0.74	4,342	410	5,972	19,646	2,416	2,272	1.06	4,058	119.1	112.0
927.8	0.73	2,890	411	4,765	18,059	1,715	2,088	0.82	5,510	62.3	75.8
927.8	0.73	3,319	412	8,373	21,997	2,365	2,544	0.93	5,081	93.1	100.1
928.3	0.73	3,391	413	10,297	25,334	2,654	2,930	0.91	5,009	106.0	117.0
928.9	0.73	3,259	414	10,825	25,094	2,677	2,902	0.92	5,141	104.2	112.9
928.9	0.73	3,105	415	10,768	25,279	2,613	2,923	0.89	5,295	98.7	110.4
938.9	0.73	2,526	416	10,525	24,208	2,366	2,800	0.85	5,874	80.6	95.3

All concentrations are reported as ppm.
Conversion of peak area to concentration based on Calibration Experiment 96.

Table is continued on next page.

Table is continued from preceeding page.

Depletion of NO by Na$_2$CO$_3$ with Gas Analysis by GC
Experiment 98   m$_{Na2CO3}$ = 40.0 g   [NO]$_{in}$ = 8400 ppm in Helium

Temp (C)	V	[NO]$_{out}$	GC Run	Area O$_2$	Area N$_2$	[O$_2$]	[N$_2$]	[O$_2$]/[N$_2$]	[NO]Depl.	% O$_2$ Rec	% N$_2$ Rec
940.0	0.73	2,653	417	12,500	26,117	2,682	3,020	0.89	5,747	93.3	105.1
940.0	0.73	2,617	418	13,891	27,666	2,858	3,200	0.89	5,783	98.9	110.7
940.6	0.72	2,479	419	15,175	29,397	2,983	3,400	0.88	5,921	100.7	114.8
940.0	0.72	2,403	420	15,090	28,926	2,943	3,345	0.88	5,997	98.1	111.6
951.7	0.73	2,027	421	13,612	26,280	2,603	3,039	0.86	6,373	81.7	95.4
951.1	0.72	2,126	422	16,527	29,820	3,037	3,449	0.88	6,274	96.8	109.9
952.2	0.73	2,085	423	17,008	31,524	3,087	3,646	0.85	6,315	97.8	115.5
952.2	0.72	2,013	424	17,140	30,426	3,078	3,519	0.87	6,387	96.4	110.2
952.8	0.73	1,947	425	17,224	31,446	3,066	3,637	0.84	6,453	95.0	112.7
961.1	0.73	1,765	426	17,127	29,838	2,985	3,451	0.87	6,635	90.0	104.0
961.1	0.73	1,781	427	19,312	32,540	3,289	3,763	0.87	6,619	99.4	113.7
961.7	0.72	1,740	428	20,030	33,344	3,372	3,856	0.87	6,660	101.2	115.8
962.2	0.72	1,700	429	20,680	32,801	3,445	3,793	0.91	6,700	102.8	113.2
962.2	0.72	1,668	430	20,482	32,907	3,407	3,806	0.90	6,732	101.2	113.1

All concentrations are reported as ppm.
Conversion of peak area to concentration based on Calibration Experiment 96.

Depletion of NO by Na$_2$CO$_3$ with Gas Analysis by GC

Experiment 100 m$_{Na2CO3}$ = 25.0 g [NO]$_{in}$ = 8400 ppm in Helium

Temp (C)	V	[NO]$_{out}$	GC Run	Area O$_2$	Area N$_2$	[O$_2$]	[N$_2$]	[O$_2$]/[N$_2$]	[NO]Depl.	% O$_2$ Rec	% N$_2$ Rec
910.0	0.84	6,302	433		9,243		1,069		2,098		96.1
910.0	0.84	6,033	434	1,196	11,361	2,389	1,314	1.82	2,367	166.7	104.7
910.0	0.83	5,719	435	1,944	12,729	2,375	1,472	1.61	2,681	144.9	103.6
911.1	0.82	5,452	436	2,940	15,083	2,412	1,744	1.38	2,948	133.2	111.6
911.1	0.83	5,230	437	3,230	15,308	2,370	1,770	1.34	3,170	117.2	105.4
910.6	0.82	5,011	438	4,028	16,069	2,397	1,858	1.29	3,389	109.4	103.5
923.3	0.83	4,395	439	6,082	17,020	2,450	1,968	1.24	4,005	82.3	92.7
923.9	0.82	4,445	440	6,561	18,250	2,534	2,111	1.20	3,955	92.4	100.7
923.9	0.82	4,322	441	7,482	20,184	2,614	2,334	1.12	4,078	96.6	108.0
923.9	0.82	4,160	442	7,716	20,003	2,586	2,313	1.12	4,240	93.2	102.9
923.9	0.82	4,008	443	9,027	21,238	2,709	2,456	1.10	4,392	94.7	105.5
934.4	0.83	3,488	444	9,598	19,665	2,595	2,274	1.14	4,912	81.8	87.4
934.4	0.82	3,600	445	10,782	22,137	2,797	2,560	1.09	4,800	90.1	100.6
935.0	0.82	3,540	446	12,368	23,492	2,991	2,717	1.10	4,860	95.8	105.5
935.0	0.82	3,443	447	12,345	23,876	2,953	2,761	1.07	4,957	92.3	105.1
935.0	0.82	3,355	448	13,095	25,071	3,022	2,899	1.04	5,045	93.3	108.4
945.6	0.82	2,867	449	12,874	22,511	2,812	2,603	1.08	5,533	81.7	88.8
946.1	0.82	2,976	450	15,376	25,779	3,193	2,981	1.07	5,424	94.3	103.7
946.1	0.81	2,925	451	15,418	25,974	3,180	3,004	1.06	5,475	93.3	103.5

All concentrations are reported as ppm.
Conversion of peak area to concentration based on Calibration Experiment 96.

Depletion of NO by Na_2CO_3 with Gas Analysis by GC

Experiment 112 m_{Na2CO3} = 40.0 g $[NO]_{in}$ = 9600 ppm in Helium

Temp (C)	V	[NO]$_{out}$	GC Run	Area O$_2$	Area N$_2$	[O$_2$]	[N$_2$]	[O$_2$]/[N$_2$]	[NO]Depl.	% O$_2$ Rec	% N$_2$ Rec
891.7	0.89	7,267	556		9,032		1,073		2,333		92.02
891.7	0.89	6,982	557		11,683		1,389		2,618		106.07
892.2	0.90	6,730	558	1,381	12,778	1,629	1,519	1.07	2,870	113.54	105.83
904.4	0.90	5,780	560	3,757	15,507	1,739	1,843	0.94	3,820	91.03	96.49
905.0	0.90	5,786	561	4,695	16,380	1,864	1,947	0.96	3,814	97.73	102.08
905.0	0.90	5,528	562	6,365	19,126	2,029	2,273	0.89	4,072	99.64	111.65
904.4	0.90	5,287	563	7,597	19,269	2,140	2,290	0.93	4,313	99.21	106.2
917.8	0.90	4,233	565	11,206	22,358	2,389	2,657	0.90	5,367	89.04	99.02
918.3	0.90	4,305	566	14,223	23,457	2,803	2,788	1.01	5,295	105.87	105.3
917.8	0.89	4,165	567	13,145	24,747	2,631	2,941	0.89	5,435	96.8	108.23
918.3	0.89	3,982	568	13,469	24,629	2,634	2,927	0.90	5,618	93.77	104.21
931.7	0.89	3,278	570	16,725	25,594	2,912	3,042	0.96	6,322	92.14	96.23
932.2	0.89	3,309	571	17,011	26,532	2,957	3,153	0.94	6,291	94.0	100.25
932.2	0.89	3,197	572	17,630	27,920	3,015	3,318	0.91	6,403	94.16	103.65
932.8	0.89	3,081	573	18,491	28,296	3,103	3,363	0.92	6,519	95.21	103.17
950.0	0.89	2,530	575	21,044	30,299	3,322	3,601	0.92	7,070	93.97	101.87
950.6	0.89	2,468	576	21,404	30,636	3,356	3,641	0.92	7,132	94.11	102.11
951.1	0.89	2,393	577	24,022	31,347	3,685	3,726	0.99	7,207	102.27	103.39
951.1	0.89	2,344	578	23,598	31,688	3,619	3,766	0.96	7,256	99.75	103.81

All concentrations are reported as ppm.
Conversion of peak area to concentration based on Calibration Experiment 111.

Depletion of NO by Na$_2$CO$_3$/Na$_2$S Mixture with Gas Analysis by GC
Experiment 114   m$_{Na2CO3}$ = 40.0 g   m$_{Na2S}$=1.5 g   [NO]$_{in}$ = 9600 ppm in Helium

Temp (C)	V	[NO]$_{out}$	GC Run	Area O$_2$	Area N$_2$	[O$_2$]	[N$_2$]	[O$_2$]/[N$_2$]	[NO]Depl.	% O$_2$ Rec	% N$_2$ Rec
887.8	0.89	349	606		34,725		4,217		9,251		91.2
887.8	0.88	278	607		33,093		4,019		9,322		86.2
888.3	0.88	247	608		32,267		3,919		9,353		83.8
888.3	0.88	219	609		32,605		3,960		9,381		84.4
902.8	0.88	125	610		35,405		4,300		9,475		90.8
905.0	0.88	119	611		36,352		4,415		9,481		93.1
905.6	0.88	117	612		33,241		4,037		9,483		85.1
906.1	0.88	118	613		35,869		4,356		9,482		91.9
916.1	0.89	50	614		32,601		3,959		9,550		82.9
916.1	0.89	57	615		44,965		5,461		9,543		114.4
917.2	0.89	61	616		42,651		5,180		9,539		108.6
916.7	0.89	63	617		46,221		5,613		9,537		117.7

All concentrations are reported as ppm.
Conversion of peak area to concentration based on Calibration Experiment 113.

Table is continued from preceeding page.

Depletion of NO by Na₂CO₃/Na₂S Mixture with Gas Analysis by GC
Experiment 114   m$_{Na2CO3}$ = 40.0 g   m$_{Na2S}$=1.5 g   [NO]$_{in}$ = 9600 ppm in Helium

Temp (C)	V	[NO]$_{out}$	GC Run	Area O₂	Area N₂	[O₂]	[N₂]	[O₂]/[N₂]	[NO]Depl.	% O₂ Rec	% N₂ Rec
916.7	0.89	65	618		43,926		5,335		9,535		111.9
932.2	0.89	13	619		42,826		5,201		9,587		108.5
932.2	0.89	18	620		42,308		5,138		9,582		107.2
932.8	0.89	25	621		44,256		5,375		9,575		112.3
932.2	0.88	27	622		42,308		5,138		9,573		107.3
					- Oxygen is Detected Upon Consumption of Na₂S -						
932.8	0.88	4,909	623	6,835	18,827	2,216	2,241	0.99	4,691	94.5	95.6
932.8	0.88	4,601	624	9,374	23,279	2,436	2,827	0.86	4,999	97.5	113.1
933.9	0.88	4,218	625	12,095	25,294	2,658	3,072	0.87	5,382	98.8	114.2
933.3	0.88	3,875	626	14,428	27,691	2,843	3,363	0.85	5,725	99.3	117.5
933.3	0.88	3,631	627	15,699	29,071	2,928	3,531	0.83	5,969	98.1	118.3
933.3	0.88	3,365	628	18,184	31,218	3,154	3,791	0.83	6,235	101.2	121.6

All concentrations are reported as ppm.
Conversion of peak area to concentration based on Calibration Experiment 113.

Depletion of NO by Na$_2$CO$_3$/Na$_2$S Mixture with Gas Analysis by GC

Experiment 117   m$_{Na2CO3}$ = 40.0 g   m$_{Na2S}$=1.5 g   [NO]$_{in}$ = 9600 ppm in Helium

Temp (C)	V	[NO]$_{out}$	GC Run	Area O$_2$	Area N$_2$	[O$_2$]	[N$_2$]	[O$_2$]/[N$_2$]	[NO]Depl.	% O$_2$ Rec	% N$_2$ Rec
862.8	0.89	1,108	667		41,369		4,523		8,492		106.5
862.2	0.88	909	668		41,421		4,529		8,691		104.2
861.1	0.88	764	669		41,731		4,563		8,836		103.3
879.4	0.89	450	670		42,818		4,682		9,150		102.3
881.7	0.88	503	671		43,011		4,703		9,097		103.4
882.8	0.88	490	672		43,538		4,760		9,110		104.5
883.3	0.88	468	673		43,445		4,750		9,132		104.0
892.2	0.88	198	674		46,170		5,048		9,402		107.4
893.3	0.88	189	675		44,630		4,880		9,411		103.7
895.0	0.88	184	676		44,900		4,909		9,416		104.3
894.4	0.88	164	677		45,260		4,949		9,436		104.9
911.1	0.88	84	678		44,516		4,867		9,516		102.3
912.2	0.88	79	679		44,684		4,886		9,521		102.6
913.3	0.88	78	680		45,427		4,967		9,522		104.3
913.3	0.88	71	682		45,456		4,970		9,529		104.3
- Oxygen is Detected Upon Consumption of Na$_2$S -											
913.3	0.88	5,422	683	4,258	17,832	1,785	1,950	0.92	4,178	85.5	93.3
913.3	0.88	5,051	684	7,325	22,223	2,052	2,430	0.84	4,549	90.2	106.8
913.3	0.88	4,731	685	10,669	24,044	2,362	2,629	0.9	4,869	97	108.
914.4	0.88	3,450	687	18,966	32,820	3,017	3,588	0.84	6,150	98.1	116.7
913.9	0.88	3,140	688	18,700	29,816	2,912	3,260	0.89	6,460	90.2	100.9

All concentrations are reported as ppm. Conversion of peak area to concentration based on Calibration Experiment 116.

Depletion of NO by Na₂CO₃/Na₂S Mixture with Gas Analysis by GC
Experiment 119 m_{Na2CO3} = 40.0 g m_{Na2S}=1.5 g $[NO]_{in}$ = 9600 ppm in Helium

Temp (C)	V	[NO]$_{out}$	GC Run	Area O₂	Area N₂	[O₂]	[N₂]	[O₂]/[N₂]	[NO]Depl.	% O₂ Rec	% N₂ Rec
877.8	0.89	324	720		43,290		4,536		9,276		97.8
878.3	0.89	358	721		44,384		4,651		9,242		100.6
879.4	0.89	343	722		43,014		4,507		9,257		97.4
880.0	0.89	292	723		43,632		4,572		9,308		98.2
879.4	0.89	294	724		44,518		4,665		9,306		100.3
889.4	0.89	217	725		45,710		4,790		9,383		102.1
888.9	0.89	185	726		44,564		4,670		9,415		99.2
888.9	0.89	174	727		48,283		5,060		9,426		107.4
888.3	0.89	180	728		45,166		4,733		9,420		100.5
888.9	0.89	178	729		44,410		4,654		9,422		98.8
894.4	0.89	169	730		46,320		4,854		9,431		102.9
896.1	0.89	158	731		45,835		4,803		9,442		101.7
896.1	0.89	149	732		46,477		4,870		9,451		103.1
896.1	0.89	142	733		45,600		4,778		9,458		101
896.7	0.89	142	734		45,674		4,786		9,458		101.2

All concentrations are reported as ppm.
Conversion of peak area to concentration based on Calibration Experiment 118.

Table is continued from preceeding page.

Depletion of NO by Na$_2$CO$_3$/Na$_2$S Mixture with Gas Analysis by GC

Experiment 119 m$_{Na2CO3}$ = 40.0 g m$_{Na2S}$=1.5 g [NO]$_{in}$ = 9600 ppm in Helium

Temp (C)	V	[NO]$_{out}$	GC Run	Area O$_2$	Area N$_2$	[O$_2$]	[N$_2$]	[O$_2$]/[N$_2$]	[NO]Depl.	% O$_2$ Rec	% N$_2$ Rec
905.0	0.89	104	735		45,150		4,731		9,496		99.6
905.0	0.89	99	736		47,041		4,929		9,501		103.8
905.6	0.89	95	737		46,738		4,898		9,505		103.1
906.1	0.89	108	738		45,950		4,815		9,492		101.5
906.1	0.88	112	739						9,488		
916.1	0.89	57	740		47,188		4,945		9,543		103.6
916.7	0.89	62	741		47,379		4,965		9,538		104.1
917.2	0.88	66	742		47,116		4,937		9,534		103.6
917.8	0.88	73	743		46,297		4,851		9,527		101.8
917.8	0.88	72	744		46,609		4,884		9,528		102.5
- Oxygen is Detected Upon Consumption of Na$_2$S -											
917.8	0.88	4,809	745	9,392	25,083	2,547	2,628	0.97	4,791	106.3	109.7
917.2	0.88	4,483	746	12,220	27,005	2,810	2,830	0.99	5,117	109.8	110.6
917.2	0.88	4,165	747	13,561	28,867	2,889	3,025	0.95	5,435	106.3	111.3
917.2	0.88	3,880	748	15,261	29,019	3,022	3,041	0.99	5,720	105.7	106.3
917.8	0.88	3,684	749	16,667	30,825	3,143	3,230	0.97	5,916	106.3	109.2

All concentrations are reported as ppm.

Conversion of peak area to concentration based on Calibration Experiment 118.

Depletion of NO by Na$_2$CO$_3$/Na$_2$S Mixture with Gas Analysis by GC
Experiment 123   m$_{Na2CO3}$ = 35.0 g   m$_{Na2S}$=1.30 g   [NO]$_{in}$ = 9600 ppm in Helium

Temp (C)	V	[NO]$_{out}$	GC Run	Area O$_2$	Area N$_2$	[O$_2$]	[N$_2$]	[O$_2$]/[N$_2$]	[NO]Depl.	% O$_2$ Rec	% N$_2$ Rec
878.9	0.70	311	793						9,289		
880.0	0.70	360	794						9,240		
880.0	0.70	333	795						9,267		
880.0	0.69	338	796						9,262		
880.6	0.69	324	797						9,276		
888.9	0.70	179	803						9,421		
889.4	0.69	189	804						9,411		
890.0	0.71	202	805						9,398		
889.4	0.70	239	806						9,361		
888.9	0.70	225	807						9,375		
889.4	0.70	216	808						9,384		
896.7	0.71	145	810		46,061		5,021		9,455		106.2
897.2	0.70	151	811		48,392		5,275		9,449		111.6
897.2	0.70	150	812		46,611		5,081		9,450		107.5
897.8	0.70	170	813		46,692		5,089		9,430		107.9
897.8	0.70	160	814		46,838		5,105		9,440		108.1

All concentrations are reported as ppm.
Conversion of peak area to concentration based on Calibration Experiment 122.

Table is continued on next page.

Table is continued from preceeding page.

Depletion of NO by Na$_2$CO$_3$/Na$_2$S Mixture with Gas Analysis by GC
Experiment 123   m$_{Na2CO3}$ = 35.0 g   m$_{Na2S}$=1.30 g   [NO]$_{in}$ = 9600 ppm in Helium

Temp (C)	V	[NO]$_{out}$	GC Run	Area O$_2$	Area N$_2$	[O$_2$]	[N$_2$]	[O$_2$]/[N$_2$]	[NO]Depl.	% O$_2$ Rec	% N$_2$ Rec
905.0	0.70	90	815		47,237		5,149		9,510		108.2
905.6	0.70	110	816		46,842		5,106		9,490		107.6
905.6	0.70	109	817		46,703		5,091		9,491		107.2
905.6	0.70	111	818		48,020		5,234		9,489		110.3
905.6	0.70	120	819		48,107		5,244		9,480		110.6
912.8	0.71	88	821		48,872		5,327		9,512		112.1
912.8	0.70	86	822		47,929		5,224		9,514		109.8
913.3	0.70	92	823		46,733		5,094		9,508		107.1
913.9	0.70	99	825		30,521		3,327		9,501		70.1
- Oxygen is Detected Upon Consumption of Na$_2$S -											
910.6	0.70	3,790	827	16,727	30,521	2,751	3,327	0.83	5,810	94.71	114.5
911.1	0.70	3,598	828	18,154	34,675	2,876	3,780	0.76	6,002	95.83	125.9
911.1	0.70	3,436	829	18,072	33,228	2,832	3,622	0.78	6,164	91.88	117.5
910.6	0.70	3,295	830	18,313	33,579	2,829	3,660	0.77	6,305	89.75	116.1
911.1	0.70	3,191	831	20,172	35,401	3,023	3,859	0.78	6,409	94.33	120.4

All concentrations are reported as ppm.
Conversion of peak area to concentration based on Calibration Experiment 122.

Depletion of NO by Na$_2$CO$_3$/Na$_2$S Mixture with Gas Analysis by GC
Experiment 127   m$_{Na2CO3}$ = 30.0 g   m$_{Na2S}$= 2.00 g   [NO]$_{in}$ = 9600 ppm in Helium

Temp (C)	V	[NO]$_{out}$	GC Run	Area O$_2$	Area N$_2$	[O$_2$]	[N$_2$]	[O$_2$]/[N$_2$]	[NO]Depl.	% O$_2$ Rec	% N$_2$ Rec
864.4	0.80	1,720	897		38,275		3,674		7,880		93.3
864.4	0.79	1,673	898		40,819		3,919		7,927		98.9
865.0	0.80	1,327	899		41,426		3,977		8,273		96.1
865.0	0.79	1,197	900		41,807		4,013		8,403		95.5
866.1	0.80	1,034	901		44,267		4,250		8,566		99.2
878.9	0.80	622	902		44,753		4,296		8,978		95.7
878.3	0.80	554	903		46,306		4,445		9,046		98.3
878.3	0.79	528	904		46,851		4,498		9,072		99.2
878.9	0.79	478	905		47,633		4,573		9,122		100.3
879.4	0.79	446	906						9,154		
892.2	0.80	295	907		48,272		4,634		9,305		99.6
892.2	0.80	313	908		46,967		4,509		9,287		97.1
892.8	0.79	291	909		46,455		4,460		9,309		95.8
892.8	0.79	303	910		47,148		4,526		9,297		97.4
892.8	0.79	294	911						9,306		

All concentrations are reported as ppm.
Conversion of peak area to concentration based on Calibration Experiment 128.

Table is continued from preceeding page.

Depletion of NO by Na₂CO₃/Na₂S Mixture with Gas Analysis by GC

Experiment 127 $m_{Na2CO3} = 30.0$ g $m_{Na2S} = 2.00$ g $[NO]_{in} = 9600$ ppm in Helium

Temp (C)	V	[NO]out	GC Run	Area O₂	Area N₂	[O₂]	[N₂]	[O₂]/[N₂]	[NO]Depl.	% O₂ Rec	% N₂ Rec
904.4	0.80	170	912		48,714		4,677		9,430		99.2
904.4	0.80	165	913		47,732		4,582		9,435		97.1
905.0	0.80	196	914		48,725		4,678		9,404		99.5
904.4	0.80	186	916		46,081		4,424		9,414		94.0
905.0	0.79	197	917						9,403		
915.6	0.80	110	918		46,963		4,508		9,490		95.0
915.0	0.80	127	919		48,570		4,663		9,473		98.4
915.6	0.80	130	920		48,562		4,662		9,470		98.5
916.1	0.79	130	921		48,253		4,632		9,470		97.8
915.6	0.80	143	922		48,307		4,637		9,457		98.1
927.2	0.81	84	923		47,818		4,591		9,516		96.5
927.2	0.80	100	924		48,673		4,673		9,500		98.4
927.8	0.80	101	925		47,423		4,553		9,499		95.9
927.8	0.80	104	926		47,547		4,565		9,496		96.1
927.8	0.80	100	927		49,321		4,735		9,500		99.7

All concentrations are reported as ppm.
Conversion of peak area to concentration based on Calibration Experiment 128.

Depletion of NO by Na$_2$CO$_3$/Na$_2$S Mixture
Experiment 121
m$_{Na2CO3}$ = 35.0 g   ṁ$_{Na2S}$ = 1.29 g   [NO]$_{in}$ = 9600 ppm in Helium

Temperature (C)	V in (L/min as air)	[NO] out (ppm)	[NO] Depleted (ppm)
881.7	0.70	481	9,119
881.7	0.70	458	9,142
882.2	0.71	394	9,206
882.2	0.71	363	9,237
882.8	0.71	349	9,251
891.7	0.70	114	9,486
892.8	0.70	109	9,491
893.3	0.70	125	9,475
893.3	0.70	130	9,470
893.3	0.70	149	9,451
900.0	0.70	105	9,495
900.6	0.70	101	9,499
901.1	0.70	104	9,496
901.1	0.70	99	9,501
900.6	0.70	101	9,499
906.1	0.70	88	9,512
907.2	0.70	78	9,522
907.2	0.70	82	9,518
907.8	0.70	81	9,519
907.8	0.70	84	9,516
907.2	0.70	86	9,514
915.0	0.70	50	9,550
915.6	0.70	50	9,550
915.6	0.70	54	9,546
916.1	0.70	55	9,545
916.1	0.70	45	9,555
916.7	0.70	50	9,550

Depletion of NO by Na₂CO₃/Na₂S Mixture
Experiment 125
$m_{Na2CO3} = 30.0$ g $m_{Na2S} = 2.00$ g $[NO]_{in} = 9600$ ppm in Helium

Temperature (C)	V in (L/min as air)	[NO] out (ppm)	[NO] Depleted (ppm)
883.9	0.79	418	9,182
883.3	0.80	551	9,049
883.3	0.80	476	9,124
882.2	0.80	469	9,131
882.2	0.80	421	9,179
882.8	0.80	399	9,201
889.4	0.80	253	9,347
889.4	0.80	263	9,337
889.4	0.79	262	9,338
890.6	0.81	263	9,337
890.0	0.81	245	9,355
897.8	0.81	137	9,463
897.8	0.81	158	9,442
897.8	0.80	160	9,440
897.8	0.80	160	9,440
898.3	0.80	170	9,430
903.9	0.80	104	9,496
904.4	0.80	122	9,478
904.4	0.80	125	9,475
904.4	0.80	134	9,466
905.0	0.80	134	9,466
913.9	0.80	88	9,512
915.0	0.80	80	9,520
915.0	0.80	91	9,509
915.0	0.80	96	9,504
915.0	0.79	101	9,499

Depletion of NO by Na₂CO₃/Na₂S Mixture

Experiment 129

$m_{Na2CO3} = 37.0$ g $m_{Na2S} = 3.00$ g $[NO]_{in} = 9600$ ppm in Helium

Temperature (C)	V in (L/min as air)	[NO] out (ppm)	[NO] Depleted (ppm)
870.6	0.65	226	9,374
870.6	0.65	296	9,304
872.2	0.64	408	9,192
885.6	0.65	191	9,409
886.7	0.65	192	9,408
886.7	0.64	202	9,398
895.6	0.65	122	9,478
896.1	0.65	127	9,473
896.7	0.65	132	9,468
905.0	0.65	88	9,512
906.1	0.65	92	9,508
906.7	0.65	94	9,506
915.0	0.65	58	9,542
915.6	0.65	64	9,536
915.6	0.65	65	9,535
870.6	0.90	394	9,206
870.6	0.90	422	9,178
870.6	0.90	420	9,180
881.1	0.89	298	9,302
881.1	0.89	309	9,291
881.1	0.89	280	9,320
881.1	0.90	284	9,316
892.2	0.90	219	9,381
892.8	0.90	221	9,379
893.3	0.89	240	9,360
903.3	0.90	144	9,456
903.3	0.90	156	9,444
903.9	0.90	131	9,469
912.8	0.91	102	9,498
913.3	0.91	111	9,489
913.9	0.91	107	9,493
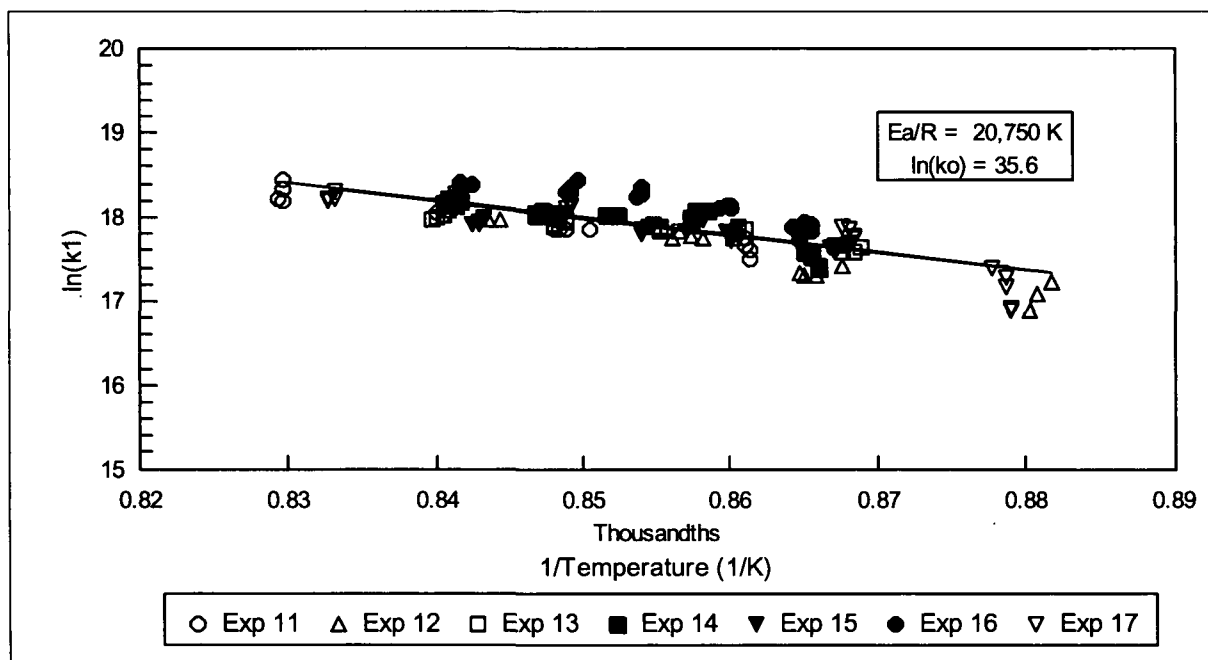
Determination of the Activation Energy for the Depleiton of NO by Na$_2$CO$_3$/Na$_2$S Mixtures (as published in"The Rate of Depletion of NO by Reaction with Molten Sodium Salts").

Regression Output:	
Constant	35.63
Std Err of Y Est	0.18
R Squared	0.83
No. of Observations	166
Degrees of Freedom	164
X Coefficient(s)	-20,749
Std Err of Coef.	1,241

Parameter	Std Error	$t_{90\%}$	$t_{95\%}$	90 % Conf. Int	95 % Conf Int
E$_a$/R	1,241	1.655	1.976	± 2054	± 2452
ln(k$_o$)	0.18	1.655	1.976	± 0.30	± 0.36

Confidence intervals for the activation energy and pre-exponential factor.

$E_a/R = 20750 \pm 2054$ $\ln(k_o) = 35.63 \pm 0.30$ at a 90 % confidence level.

APPENDIX 10: GC CALIBRATION DATA

This appendix includes all of the calibration data for experiments with gas analysis by GC. Data tables are included for:

Experiment 91	Experiment 96
Experiment 111	Experiment 113
Experiment 116	Experiment 118
Experiment 122	Experiment 128

GC Calibration
Experiment 91

RUN	[N₂]	[O₂]	[NO]	Area O₂	Area N₂
237	3,833	3,878	2,012	24,019	34,119
238	3,830	3,876	2,016	25,986	37,401
240	3,830	3,876	2,016	23,474	35,245
241	3,830	3,876	2,016	23,808	35,788
242	2,515	2,545	4,208	8,428	23,843
243	2,515	2,545	4,208	7,052	23,070
244	2,520	2,550	4,200	7,859	23,624
246	2,525	2,555	4,192	7,894	24,599
248	3,028	3,064	3,353	14,991	29,750
249	3,028	3,064	3,353	12,478	28,035
250	3,032	3,068	3,347	12,456	27,650
251	3,032	3,068	3,347	11,733	27,195
252	1,915	1,938	5,208	4,238	18,113
253	1,921	1,944	5,198	9,981	25,370
254	1,921	1,944	5,198	3,516	17,061
255	1,921	1,944	5,198	5,175	19,461
256	1,921	1,944	5,198	3,445	17,701
257	5,040	5,100	0	34,516	46,635
258	5,040	5,100	0	41,376	53,450
259	5,040	5,100	0	37,013	46,194
260	5,040	5,100	0	37,724	45,989
261	5,040	5,100	0	38,874	45,272
262	5,040	5,100	0	39,508	46,560
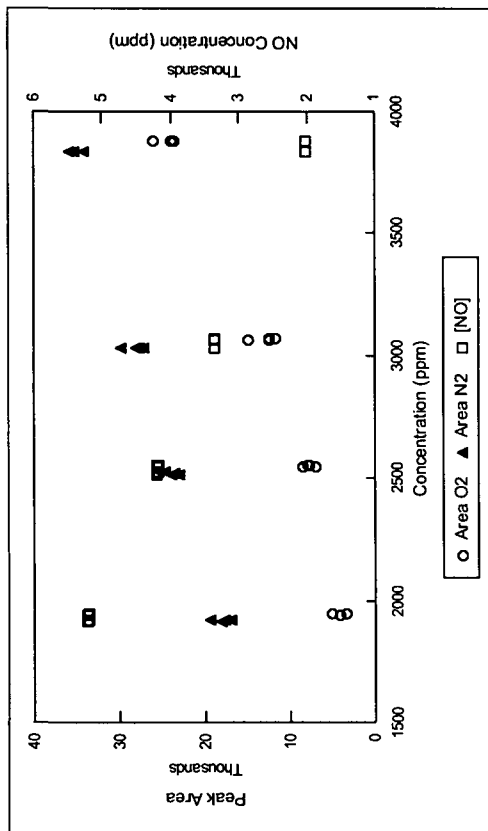
Regression Output:

	Oxygen	Nitrogen
Constant	0.00	0.00
Std Err of Y	129.7	1067.7
R Squared	0.953	0.975
No of Obs.	16	18
Deg. of Free	14	17

	[NO]	[O2]	[N2]
X Coefficient	-2.131	7.050	9.406
Std Err of X	0.219	0.288	0.085

Based on Regression: [O2] = 0.302[NO] + 0.142(Area)
N2] = 0.106(Area)

All concentrations are reported as ppm.

GC Calibration
Experiment 96

Chart: Peak Area (Thousands) vs. Concentration (ppm), with [NO] (ppm) secondary axis (Thousands). Legend: ◆ Area O2 ▲ Area N2 -- O2 Regression — N2 Regression

Regression Output:

	Oxygen	Nitrogen
Constant	0.00	0.0
Std Err of Y	129.7	652.5
R Squared	0.984	0.987
No of Obs.	20	20
Deg. of Free	18	19

	[NO]	[O2]	[N2]
X Coefficient	-2.713	7.353	8.647
Std Err of X	0.129	0.137	0.046

Based on linear regression: $[O_2] = 0.369[NO] + 0.136(Area)$
$[N_2] = 0.116(Area)$

Run	[N₂]	[O₂]	[NO]	Area O₂	Area N₂
350	4,034	4,082	1,677	26,776	35,290
351	4,036	4,084	1,673	26,692	35,869
352	4,036	4,084	1,673	26,345	36,216
353	4,036	4,084	1,673	25,467	34,683
354	3,024	3,060	3,360	13,612	26,349
355	3,024	3,060	3,360	12,701	25,926
356	3,024	3,060	3,360	12,099	26,098
357	3,024	3,060	3,360	12,513	25,993
358	2,307	2,335	4,554	5,405	19,206
359	2,307	2,335	4,554	6,238	19,847
360	2,307	2,335	4,554	5,444	18,885
361	2,262	2,289	4,630	5,226	18,488
362	2,726	2,759	3,856	8,908	22,816
363	2,726	2,759	3,856	9,712	23,775
364	2,731	2,763	3,849	9,569	23,823
365	2,731	2,763	3,849	10,162	23,925
366	3,531	3,573	2,515	18,346	30,812
367	3,534	3,576	2,510	18,668	30,755
368	3,537	3,579	2,505	18,627	30,601
369	3,537	3,579	2,505	18,045	29,420

All concentrations are reported as ppm.

GC Calibration
Experiment 111

RUN	[N₂]	[O₂]	[NO]	Area O₂	Area N₂
533	4,032	4,080	1,920	29,402	34,314
534	4,032	4,080	1,920	29,101	34,391
535	4,032	4,080	1,920	28,921	34,037
536	3,629	3,672	2,688	21,633	29,341
537	3,629	3,672	2,688	22,585	30,441
538	3,629	3,672	2,688	22,970	30,039
539	3,226	3,264	3,456	18,083	27,459
540	3,226	3,264	3,456	19,351	26,743
541	3,226	3,264	3,456	18,518	27,180
542	2,822	2,856	4,224	14,767	24,597
543	2,822	2,856	4,224	14,336	24,274
544	2,822	2,856	4,224	14,818	23,807
545	2,419	2,448	4,992	11,982	21,112
546	2,419	2,448	4,992	10,626	22,411
547	2,419	2,448	4,992	9,878	20,519
548	4,435	4,488	1,152	32,102	37,567
549	4,435	4,488	1,152	31,161	36,551
550	4,435	4,488	1,152	31,814	35,924
551	5,040	5,100	0	36,573	39,524
552	5,040	5,100	0	38,590	40,024
553	5,040	5,100	0	38,011	38,678

All concentrations are reported as ppm.

Regression Output:

	Oxygen	Nitrogen
Constant	0	0
Std Err of Y	976.7	794.6
R Squared	0.985	0.979
No of Observations	18	18
Deg. of Freedom	16	17

	[NO]	[O2]	[N2]
X Coefficient	-1.623	7.558	8.414
Std Erro of X	0.122	0.115	0.054

Based on Regression: $[O2] = 0.215[NO] + 0.132(Area)$
$[N2] = 0.119(Area)$

GC Calibration
Experiment 113

RUN	[N₂]	[O₂]	[NO]	Area O₂	Area N₂
587	4,532	4,586	968	36,244	38,337
588	4,532	4,586	968	36,910	38,407
589	4,532	4,586	968	36,086	37,923
590	4,193	4,243	1,613	30,904	34,771
591	4,193	4,243	1,613	30,617	34,516
592	4,193	4,243	1,613	30,937	35,003
593	3,854	3,900	2,259	27,045	32,354
594	3,854	3,900	2,259	25,066	30,515
595	3,854	3,900	2,259	26,087	31,406
596	3,515	3,557	2,904	22,337	28,620
597	3,515	3,557	2,904	21,688	28,641
598	3,515	3,557	2,904	23,176	29,081
599	3,176	3,214	3,550	19,422	26,755
600	3,176	3,214	3,550	18,191	25,622
601	3,176	3,214	3,550	19,190	26,236
602	5,040	5,100	0	38,904	41,867
603	5,040	5,100	0	38,116	40,402
604	5,040	5,100	0	38,698	40,134

Regression Output:

	Oxygen	Nitrogen
Constant	0	0
Std Err of Y	905.9	725.5
R Squared	0.981	0.981
No of Observations	15	18
Deg. of Freedom	13	17
	[NO]	[O2]	[N2]
X Coefficient	-2.335	8.256	8.234
Std Erro of X	0.197	0.122	0.042

Based on Regression: [O2] = 0.283[NO] + 0.121(Area)
                     [N2] = 0.121(Area)

All concentrations are reported as ppm.

GC Calibration
Experiment 116

RUN	[N₂]	[O₂]	[NO]	Area O₂	Area N₂
645	4,637	4,692	768	39,156	42,784
646	4,637	4,692	768	39,281	42,153
647	4,637	4,692	768	38,661	41,778
648	4,234	4,284	1,536	36,250	39,586
649	4,234	4,284	1,536	33,696	38,578
650	4,234	4,284	1,536	33,156	38,232
651	3,730	3,774	2,496	28,123	35,499
652	3,730	3,774	2,496	26,491	33,958
653	3,730	3,774	2,496	26,498	32,927
654	3,226	3,264	3,456	20,338	30,025
655	3,226	3,264	3,456	20,036	28,745
656	3,226	3,264	3,456	20,098	28,977
657	2,722	2,754	4,416	16,367	25,449
658	2,722	2,754	4,416	15,288	24,288
659	2,722	2,754	4,416	14,795	24,756
660	5,040	5,100	0	39,264	44,906
661	5,040	5,100	0	40,351	45,276
662	5,040	5,100	0	40,372	44,726
663	5,040	5,100	0	44,118	47,720

Regression Output:

	Oxygen	Nitrogen
Constant	0	0
Std Err of Y	1058.9	795.9
R Squared	0.987	0.990
No of Observations	15	19
Deg. of Freedom	13	18

	[NO]	[O2]	[N2]
X Coefficient	-2.060	8.641	9.146
Std Erro of X	0.157	0.117	0.033

Based on Regression: [O2] = 0.238[NO] + 0.116(Area)
[N2] = 0.109(Area)

All concentrations are reported as ppm.

GC Calibration
Experiment 118

RUN	[N₂]	[O₂]	[NO]	Area O₂	Area N₂
696	4,032	4,080	1,920	33,481	37,943
697	4,032	4,080	1,920	31,740	38,525
698	4,032	4,080	1,920	34,148	38,721
699	3,528	3,570	2,880	25,349	33,683
700	3,528	3,570	2,880	24,259	32,184
702	3,024	3,060	3,840	18,467	29,415
703	3,024	3,060	3,840	19,310	29,237
704	3,024	3,060	3,840	19,871	29,073
705	2,520	2,550	4,800	14,859	25,791
706	2,520	2,550	4,800	13,989	24,027
707	2,520	2,550	4,800	13,369	23,865
708	5,040	5,100	0	43,347	48,679
709	5,040	5,100	0	40,349	47,109
710	5,040	5,100	0	41,436	46,040
711	5,040	5,100	0	42,579	48,282
712	3,528	3,570	2,880	27,968	35,774
713	3,528	3,570	2,880	27,021	34,386
714	5,040	5,100	0	41,837	47,987
715	5,040	5,100	0	42,396	47,970
716	5,040	5,100	0	41,812	47,323

Regression Output:

	Oxygen	Nitrogen
Constant	0	0
Std Err of Y	906.3	1019.0
R Squared	0.989	0.989
No of Observations	10	18
Deg. of Freedom	8	17

	[NO]	[O2]	[N2]
X Coefficient	-2.256	7.947	9.542
Std Erro of X	0.195	0.098	0.059

Based on Regression: [O2] = 0.284[NO] + 0.126(Area)
[N2] = 0.105(Area)

All concentrations are reported as ppm.

GC Calibration
Experiment 122

Run	[N₂]	[O₂]	[NO]	Area O₂	Area N₂
774	4,435	4,488	1,152	37,361	41,050
775	4,435	4,488	1,152	35,507	39,738
776	4,435	4,488	1,152	37,087	41,139
777	3,830	3,876	2,304	30,546	36,252
778	3,830	3,876	2,304	29,382	34,870
779	3,830	3,876	2,304	28,185	34,617
780	3,226	3,264	3,456	21,703	29,146
781	3,226	3,264	3,456	21,620	29,633
782	3,226	3,264	3,456	21,361	30,054
783	2,621	2,652	4,608	15,360	24,456
784	2,621	2,652	4,608	14,065	24,474
785	2,621	2,652	4,608	14,112	23,647
790	5,040	5,100	0	42,155	47,371
791	5,040	5,100	0	42,227	45,469
792	5,040	5,100	0	41,340	43,970
834	5,040	5,100	0	42,315	48,309
835	5,040	5,100	0	42,219	46,187
836	5,040	5,100	0	41,785	46,190
837	5,040	5,100	0	42,816	47,942

Regression Output:

	Oxygen	Nitrogen
Constant	0	0
Std Err of Y	788.8	989.0
R Squared	0.993	0.987
No of Observations	12	19
Deg. of Freedom	10	18

	[NO]	[O2]	[N2]
X Coefficient	-1.852	8.643	9.207
Std Erro of X	0.126	0.109	0.054

Based on Regression: $[O2] = 0.214[NO] + 0.116(Area)$
$[N2] = 0.109(Area)$

All concentrations are reported as ppm.

GC Calibration
Experiment 128

Run	[N₂]	[O₂]	[NO]	Area O₂	Area N₂
929	5,040	5,100	0	47,719	53,213
930	5,040	5,100	0	50,041	55,666
931	5,040	5,100	0	48,617	52,518
932	4,637	4,692	768	43,432	48,359
933	4,637	4,692	768	43,112	48,118
934	4,637	4,692	768	44,102	49,646
935	4,234	4,284	1,536	37,185	44,112
936	4,234	4,284	1,536	37,869	43,701
937	4,234	4,284	1,536	36,338	42,338
938	3,830	3,876	2,304	30,752	39,757
939	3,830	3,876	2,304	32,705	39,765
940	3,830	3,876	2,304	30,703	39,792
941	3,226	3,264	3,456	23,904	33,219
942	3,226	3,264	3,456	23,895	36,845
943	3,226	3,264	3,456	22,987	34,233
944	5,040	5,100	0	45,656	52,705
945	5,040	5,100	0	44,083	50,697
946	5,040	5,100	0	46,049	52,092
947	5,040	5,100	0	47,514	51,876
948	5,040	5,100	0	46,658	52,483

Regression Output:

	Oxygen	Nitrogen
Constant	0	0
Std Err of Y	1417.1	1261.0
R Squared	0.976	0.967
No of Observations	20	18
Deg. of Freedom	18	17

	[NO]	[O2]	[N2]
X Coefficient	-1.901	9.303	10.449
Std Erro of X	0.224	0.086	0.063

Based on Regression: $[O2] = 0.204[NO] + 0.107(Area)$
$[N2] = 0.096(Area)$

All concentrations are reported as ppm.

APPENDIX 11: A COMPARISON OF PREDICTED AND MEASURED VALUES FOR THE EXIT CONCENTRATION OF NO

This appendix includes graphs showing the predicted and measured values for the concentration of NO in the exit gas. Results are shown for both Na_2CO_3 and Na_2CO_3/Na_2S mixtures.
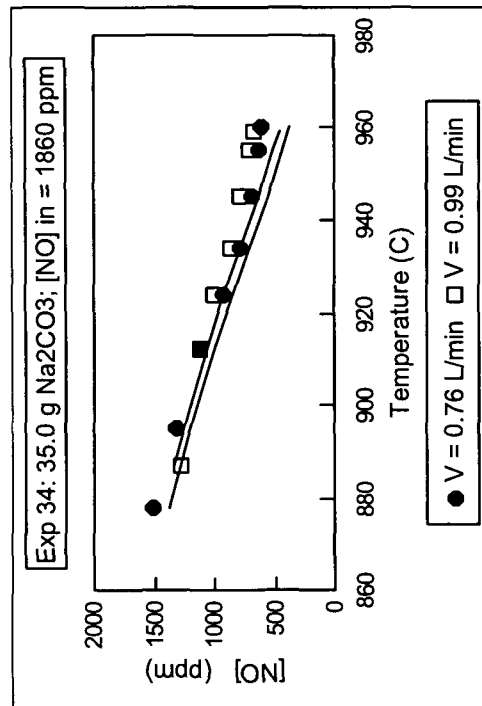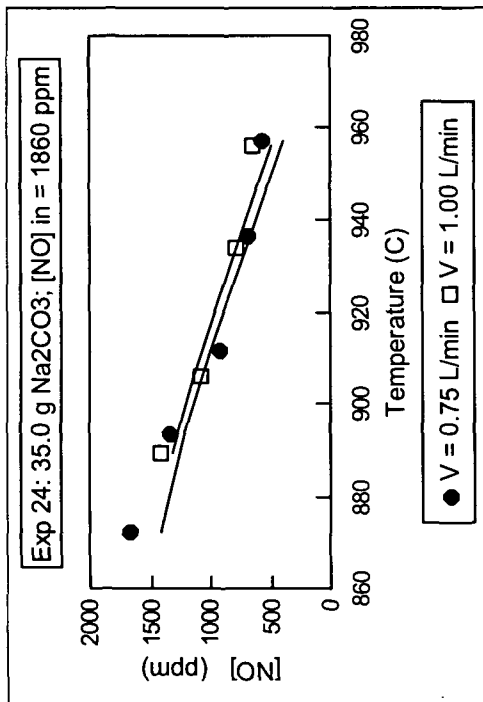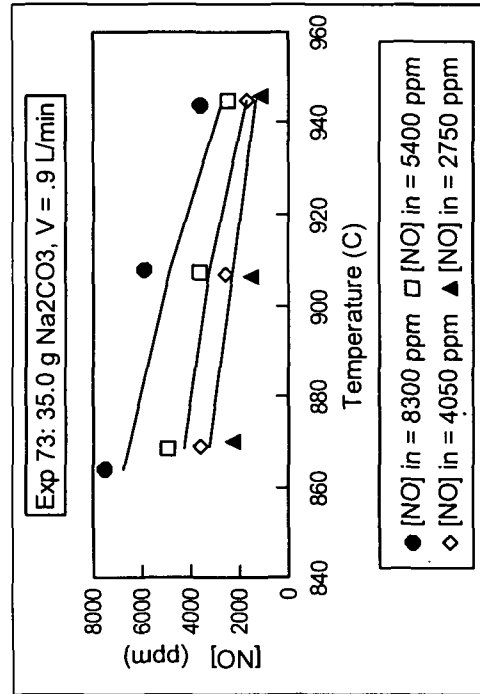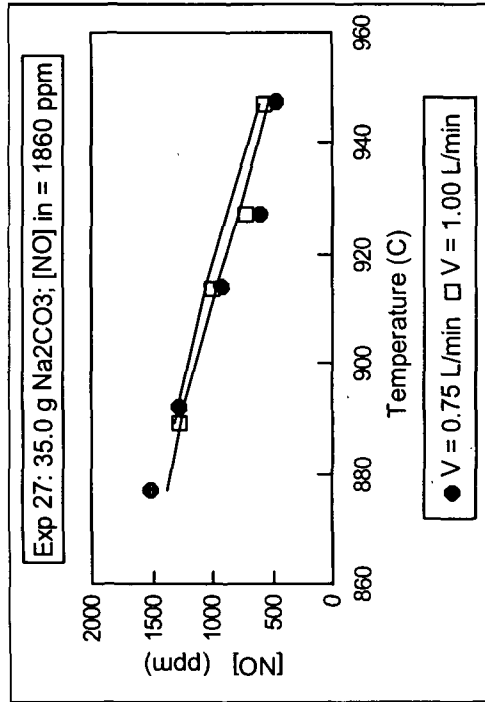
Experiments for depletion of NO by Na_2CO_3 include:
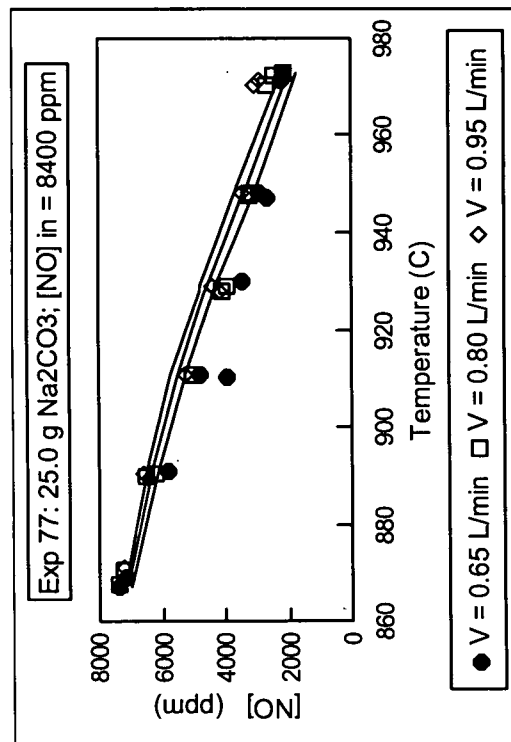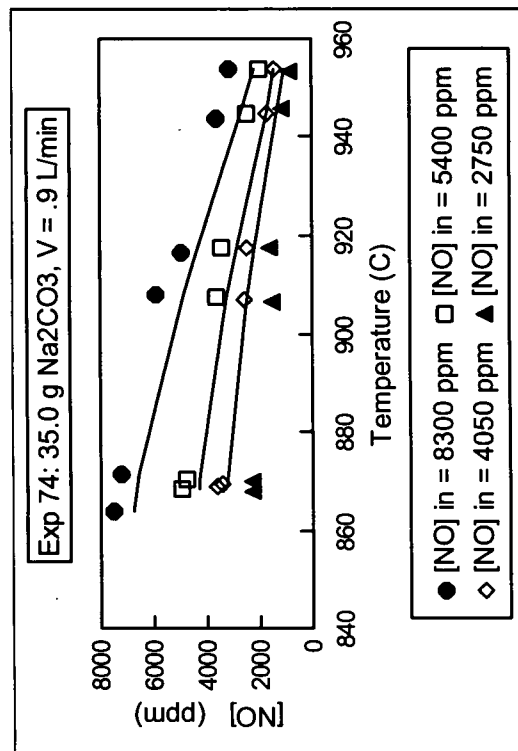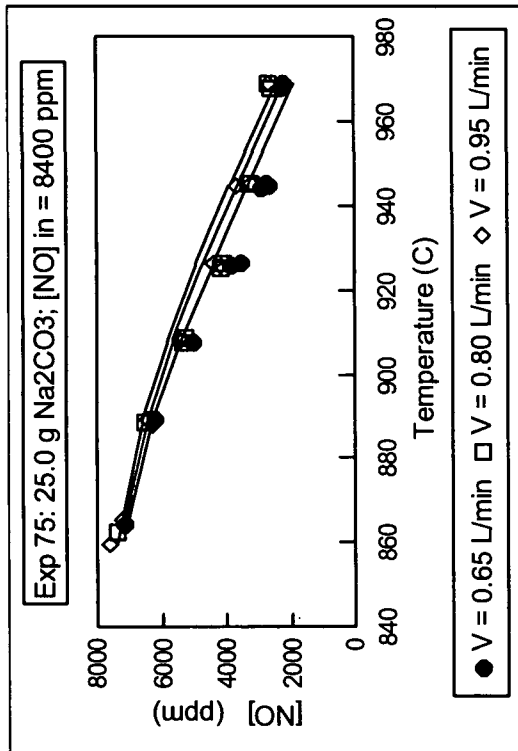
Experiment 24   Experiment 27

Experiment 34   Experiment 73
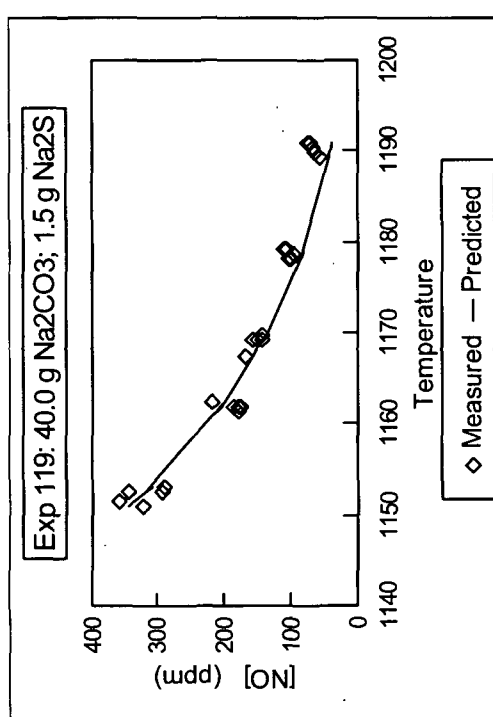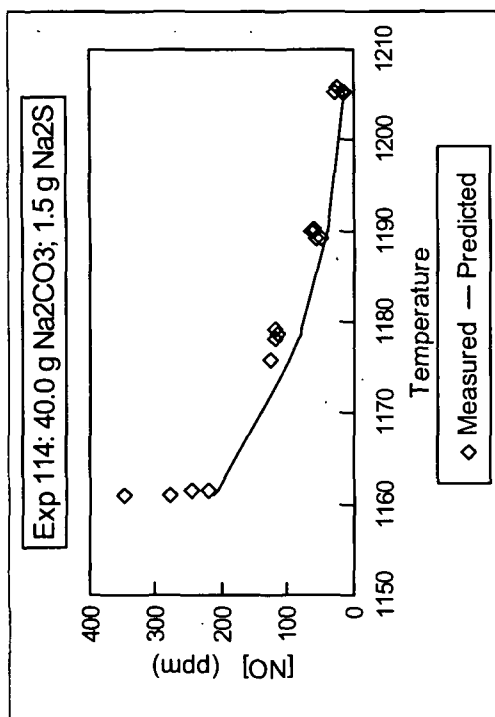
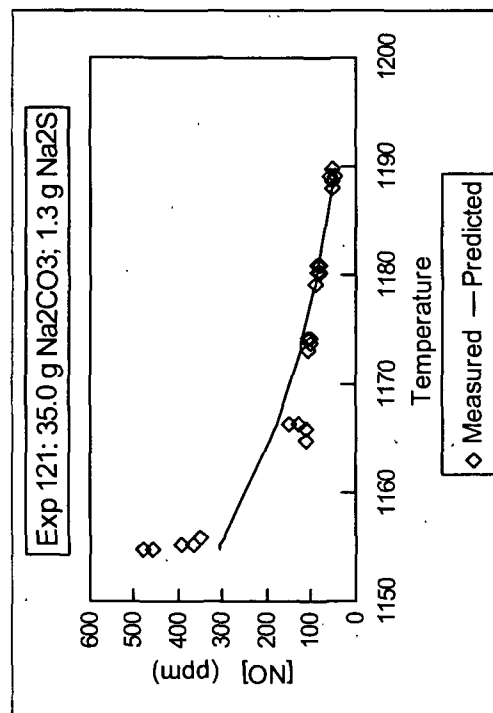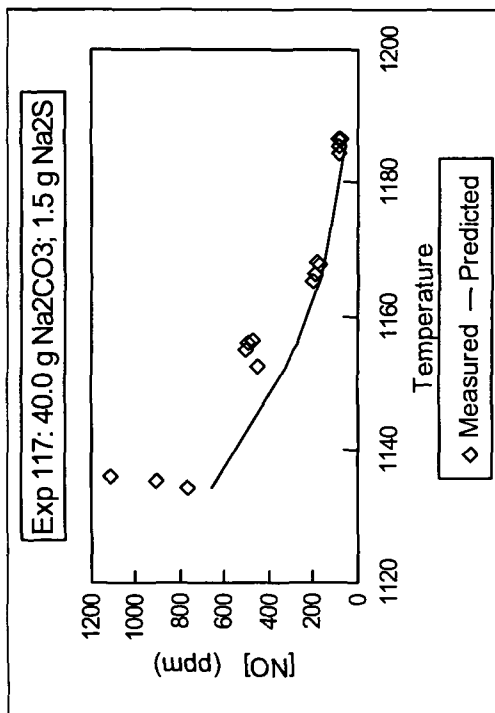Experiment 74   Experiment 75

Experiment 77

Experiments for depletion of NO by Na_2CO_3/Na_2S mixtures include:

Experiment 114   Experiment 117

Experiment 119   Experiment 121

Experiment 123   Experiment 125

Experiment 127   Experiment 129

Exp 27: 35.0 g Na2CO3; [NO] in = 1860 ppm

● V = 0.75 L/min □ V = 1.00 L/min

Exp 73: 35.0 g Na2CO3, V = .9 L/min

● [NO] in = 8300 ppm □ [NO] in = 5400 ppm
◇ [NO] in = 4050 ppm ▲ [NO] in = 2750 ppm

Exp 24: 35.0 g Na2CO3; [NO] in = 1860 ppm

● V = 0.75 L/min □ V = 1.00 L/min

Exp 34: 35.0 g Na2CO3; [NO] in = 1860 ppm

● V = 0.76 L/min □ V = 0.99 L/min

Exp 75: 25.0 g Na2CO3; [NO] in = 8400 ppm

● V = 0.65 L/min □ V = 0.80 L/min ◇ V = 0.95 L/min

Exp 74: 35.0 g Na2CO3, V = .9 L/min

● [NO] in = 8300 ppm □ [NO] in = 5400 ppm
◇ [NO] in = 4050 ppm ▲ [NO] in = 2750 ppm

Exp 77: 25.0 g Na2CO3; [NO] in = 8400 ppm

● V = 0.65 L/min □ V = 0.80 L/min ◇ V = 0.95 L/min

Exp 114: 40.0 g Na2CO3; 1.5 g Na2S
◇ Measured — Predicted

Exp 117: 40.0 g Na2CO3; 1.5 g Na2S
◇ Measured — Predicted

Exp 119: 40.0 g Na2CO3; 1.5 g Na2S
◇ Measured — Predicted

Exp 121: 35.0 g Na2CO3; 1.3 g Na2S
◇ Measured — Predicted

Exp 125: 30.0 g Na2CO3; 2.0 g Na2S

Exp 129: 37.0 g Na2CO3; 3.0 g Na2S

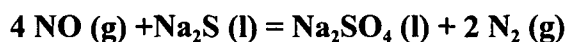Exp 123: 35.0 g Na2CO3; 1.3 g Na2S

Exp 127: 30.0 g Na2CO3; 2.0 g Na2S

APPENDIX 12: ENTHALPY AND GIBBS FREE ENERGY OF REACTION FOR PROPOSED DEPLETION REACTIONS

The tables below include values for ΔH_{rxn} and ΔG_{rxn} for the proposed overall depletion reactions. These calculations were made using the thermodynamic software program, HSC.

$4 \text{ NO (g) } + \text{Na}_2\text{S (l) } = \text{Na}_2\text{SO}_4 \text{ (l) } + 2 \text{ N}_2 \text{ (g)}$

Temperature (°C)	Enthalpy Change ΔH_{rxn} (kJ/mol)	Free Energy of Reaction ΔG_{rxn} (kJ/mol)
850	-1,345.8	-956.6
875	-1,344.9	-947.9
900	-1,344.1	-939.3
925	-1,343.3	-930.7
950	-1,342.4	-922.1
975	-1,341.6	-913.5
1,000	-1,340.8	-904.9
1,025	-1,339.9	-896.4
1,050	-1,339.2	-887.8
1,075	-1,338.4	-879.3
1,100	-1,337.6	-870.8
1,125	-1,336.8	-862.3
1,150	-1,335.9	-853.8

$\text{NO (g) } = 1/2 \text{ N}_2 \text{ (g) } + 1/2 \text{ O}_2 \text{ (g)}$
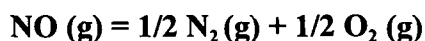
Temperature (°C)	Enthalpy Change ΔH_{rxn} (kJ/mol)	Free Energy of Reaction ΔG_{rxn} (kJ/mol)
850	-90.67	-76.14
875	-90.68	-75.82
900	-90.70	-75.49
925	-90.71	-75.17
950	-90.73	-74.84
975	-90.74	-74.52
1,000	-90.76	-74.19
1,025	-90.77	-73.87
1,050	-90.79	-73.54
1,075	-90.80	-73.22
1,100	-90.81	-72.89
1,125	-90.83	-72.56
1,150	-90.84	-72.24

HSC-Software For Thermodynamic Calculations, Developed by Outokumpu Oy, Metallurgical Research Centre, Pori, Finland.